

University of Montana

ScholarWorks at University of Montana

Graduate Student Theses, Dissertations, &
Professional Papers

Graduate School

2000

In situ chemical sensor measurements in a freshwater lake: An analysis of the short-term and seasonal effects of ice cover ice out and turnover on carbon dioxide and oxygen

Matthew M. Baehr
The University of Montana

Follow this and additional works at: <https://scholarworks.umt.edu/etd>

Let us know how access to this document benefits you.

Recommended Citation

Baehr, Matthew M., "In situ chemical sensor measurements in a freshwater lake: An analysis of the short-term and seasonal effects of ice cover ice out and turnover on carbon dioxide and oxygen" (2000). *Graduate Student Theses, Dissertations, & Professional Papers*. 10617.
<https://scholarworks.umt.edu/etd/10617>

This Dissertation is brought to you for free and open access by the Graduate School at ScholarWorks at University of Montana. It has been accepted for inclusion in Graduate Student Theses, Dissertations, & Professional Papers by an authorized administrator of ScholarWorks at University of Montana. For more information, please contact scholarworks@mso.umt.edu.

INFORMATION TO USERS

This manuscript has been reproduced from the microfilm master. UMI films the text directly from the original or copy submitted. Thus, some thesis and dissertation copies are in typewriter face, while others may be from any type of computer printer.

The quality of this reproduction is dependent upon the quality of the copy submitted. Broken or indistinct print, colored or poor quality illustrations and photographs, print bleedthrough, substandard margins, and improper alignment can adversely affect reproduction.

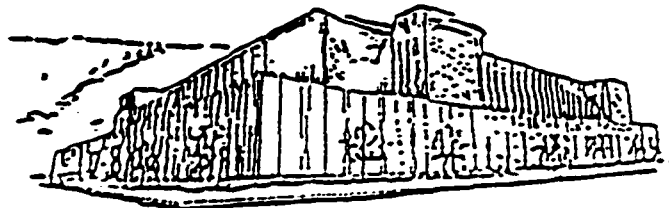
In the unlikely event that the author did not send UMI a complete manuscript and there are missing pages, these will be noted. Also, if unauthorized copyright material had to be removed, a note will indicate the deletion.

Oversize materials (e.g., maps, drawings, charts) are reproduced by sectioning the original, beginning at the upper left-hand corner and continuing from left to right in equal sections with small overlaps.

Photographs included in the original manuscript have been reproduced xerographically in this copy. Higher quality 6" x 9" black and white photographic prints are available for any photographs or illustrations appearing in this copy for an additional charge. Contact UMI directly to order.

Bell & Howell Information and Learning
300 North Zeeb Road, Ann Arbor, MI 48106-1346 USA
800-521-0600

UMI[®]



Maureen and Mike
MANSFIELD LIBRARY

The University of **MONTANA**

Permission is granted by the author to reproduce this material in its entirety,
provided that this material is used for scholarly purposes and is properly cited in
published works and reports.

*** Please check "Yes" or "No" and provide signature ***

Yes, I grant permission _____
No, I do not grant permission _____

Author's Signature Matthew M. Baeh

Date 12-26-00

Any copying for commercial purposes or financial gain may be undertaken only with
the author's explicit consent.

***In Situ* Chemical Sensor Measurements in a Freshwater Lake:
An Analysis of the Short-term and Seasonal Effects of Ice
Cover, Ice Out, and Turnover on CO₂ and O₂**

by

Matthew M. Baehr

B.S., University of Wisconsin-River Falls, 1993

presented in partial fulfillment of the requirements


for the degree of

Doctor of Philosophy

The University of Montana

2000

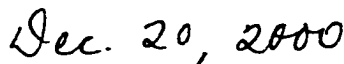
Approved by:



Chairperson, Board of Examiners



Dean, Graduate School



Date

UMI Number: 9996589

UMI[®]

UMI Microform 9996589

Copyright 2001 by Bell & Howell Information and Learning Company.

All rights reserved. This microform edition is protected against
unauthorized copying under Title 17, United States Code.

Bell & Howell Information and Learning Company

300 North Zeeb Road

P.O. Box 1346

Ann Arbor, MI 48106-1346

In situ Chemical Sensor Measurements in a Freshwater Lake: An Analysis of the Short-term and Seasonal Effects of Ice Cover, Ice Out, and Turnover on CO₂ and O₂Director: Michael D. DeGrandpre *MD*

Several autonomous, *in situ* sensors were deployed on a subsurface mooring in Placid Lake, Montana USA, a dimictic, freshwater lake, to measure the partial pressure of CO₂ (*p*CO₂), dissolved O₂ (DO), temperature and several other variables. These high temporal resolution time-series were obtained over six different deployments from winter 1997 to summer 1999. Data from periodic profile measurements and local and regional meteorology were obtained to aid the interpretation of the *in situ* data. Emphasis is placed on the analysis of the short-term and seasonal biogeochemical variability during the 1997 and 1998 under-ice deployments and the 1999 deployment from ice cover to summer stratification.

Gas variability on diel or shorter time scales was small or undetectable during most of the ice-covered periods, only becoming significant prior to ice-out when runoff and light penetration increased, promoting convective currents, vertical mixing, and biological production. A surprising 7.6 d period oscillation, believed to be driven by a baroclinic seiche, dominated the short-term variability during the first year. Increasing *p*CO₂ and decreasing DO, as a result of microbial metabolism, characterized the long-term variability.

Vertically distributed sensors within the water column during 1999 showed that convective currents led to lake turnover and complete mixing under ice. A one-dimensional (vertical) physical mixed-layer model for the upper ocean was adapted for use in freshwater. The model simulated the thermal structure of the lake exceptionally well in both ice-covered and ice-free conditions. Simple two-box biogeochemical models were developed for *p*CO₂ and DO and were coupled to the mixed-layer depth output from the physical model. The biogeochemical models were used to quantify the relative importance of biology, air-water gas exchange, mixing, and heating and cooling on *p*CO₂ and DO. Net community production dominated the average daily variability of *p*CO₂ (78%) and DO (98%) under ice. After ice out, net community production, gas exchange, mixing, and heating and cooling each contributed 33, 30, 14, and 23%, respectively, to *p*CO₂ variability in the surface mixed-layer. These same processes contributed 36, 45, 19 and 0% to the DO.

Acknowledgements

Many people have aided me in my mission to advance my education. I am deeply indebted to my mentor, Mike DeGrandpre, for his guidance and continual support during the course of this work. I owe many thanks to my fellow lab mates for their camaraderie and for their insistence that I be their sounding board for which I have benefited immensely. I would especially like to thank Jeff Carr for his friendship and for helping me with several deployments and late night analyses.

I thank Ed Keller for his generosity in allowing me to use his Placid Lake cabin as a launching pad for my research activities. I am also indebted to Ed Keller and Dr. Dick Juday for their procurement of needed research equipment and for sharing their knowledge of Placid Lake and the surrounding area. Dr. Juday's medicinal and medieval anecdotes will surely be missed.

I acknowledge Mr. Kreitzberg for permitting me to deploy the meteorological station on his property and Richard Taylor for meteorological measurements at the Seeley Lake Ranger District Station.

I thank Terry Hammar (Woods Hole Oceanographic Institution) for his engineering expertise and his work on the atmospheric CO₂ system and Creighton Wirick (Brookhaven National Laboratories) for the use of his autonomous DO sensors. I also thank Jim Price (Woods Hole Oceanographic Institution) for providing the mixed-layer model and David Walsh (International Arctic Research Center) for helpful discussions. MONTS-EPSCoR (Grant 292144) and NSF-Ocean Sciences (OCE-9814388) provided funding.

I also want to express my appreciation to my committee members Richard Field, Nancy Hinman, Garon Smith, and Jack Stanford for generously donating their time.

Special thanks to Doug Kolwaite for confiding in me his "secret" elk and mule deer hunting spots where I have enjoyed much success.

To my parents, Patti and Greg Baehr, I extend my deepest respect and appreciation for their love and support. I am grateful for the generosity and love that my parents-in-law, Ray and Dorothy Nelson, have shown me and for making me a part of their family.

Finally, I thank my wife Karla, the love of my life, for postponing her teaching career and her enthusiastic acceptance of our Montana adventure. Words cannot express how much I appreciate her unwavering encouragement and understanding. To her I am eternally grateful for giving birth to my pride and joy, our beautiful son David.

Table of Contents

	page
Authorization to Submit Dissertation	i
Abstract	ii
Acknowledgements	iii
Table of Contents	iv
List of Tables	vii
List of Figures	viii
Chapter 1: Introduction	1
1.1 Dissertation overview.....	1
1.2 Introduction	1
1.3 Research objectives.....	5
1.4 Background.....	6
1.4.1 Processes that control CO ₂ and O ₂ variability in lakes.....	6
1.4.1.a Physical processes.....	7
1.4.1.b Biological processes.....	9
1.4.1.c Chemical processes	10
1.4.2 CO ₂ research.....	11
1.4.3 DO research.....	12
1.4.4 Biogeochemical models.....	12
1.5 Study Lake.....	13
Chapter 2: Methods	16
2.1 Mooring detail	16
2.2 <i>In situ</i> chemical measurements.....	16
2.2.1 The partial pressure of carbon dioxide (<i>p</i> CO ₂)	16
2.2.2 Dissolved oxygen (DO)	20
2.3 Other <i>in situ</i> measurements	21
2.3.1 Temperature	21
2.3.2 Photosynthetically active radiation (PAR).....	22
2.3.3 Chlorophyll- <i>a</i> fluorescence	22
2.3.4 Specific conductance	23
2.3.5 Depth.....	24
2.4 Periodic profile samples and measurements.....	24
2.4.1 DIC and pH	26
2.4.2 DO and temperature.....	29
2.4.3 Winkler DO titrations	29

2.4.4	Total alkalinity (TA)	29
2.4.5	Chlorophyll- <i>a</i>	30
2.4.6	Nutrients	30
2.4.7	Cations	31
2.4.8	Chromophoric dissolved organic matter (CDOM)	31
2.4.9	Photometry	32
2.4.10	Optical Transparency	32
2.5	Carbonate system calculations	33
2.6	Other supporting data	36
2.6.1	Regional meteorology and river discharge	36
2.6.2	Local meteorology	37
2.7	Physical and biogeochemical models	40
2.7.1	Air-water fluxes and meteorology	40
2.7.2	Physical model	45
2.7.3	Biogeochemical models	46
2.7.3.a	Air-water gas exchange	47
2.7.3.b	Photosynthesis and respiration	48
2.7.3.c	Entrainment	50
Chapter 3:	Under-Ice CO₂ and O₂ Variability in 1997 and 1998	53
3.1	Results	53
3.1.1	Conditions during winter 1997 and 1998	53
3.1.2	1997 and 1998 <i>in situ</i> time-series	54
3.2	Discussion	58
3.2.1	Temporal scales of variability	58
3.2.2	Year 1	59
3.2.3	Year 2	68
3.3	Chapter summary and conclusions	71
Chapter 4:	<i>In situ</i> Chemical Sensor Measurements in 1999: Comparisons between Observations and Results from Physical and Biogeochemical Modeling	72
4.1	Results and discussion	73
4.1.1	Figure overview	73
4.1.2	Time-series overview	73
4.1.3	Major features	78
4.1.3.a	Turnover	78
4.1.3.b	Post-turnover episodic deep-mixing events	79
4.1.3.c	Seasonal stratification	80
4.1.3.d	Biomass and nutrients	81
4.1.4	Thermal stratification and model comparisons	83
4.1.4.a	Under-ice period	83
4.1.4.b	Ice-free period	83
4.1.5	Dissolved gas observations and comparisons with model predictions	86

4.1.5.a Under-ice period	86
4.1.5.b Ice-free period.....	92
4.2 Chapter summary and conclusions	99
Chapter 5: Placid Lake Data Overview, Summary, and Conclusions.....	101
5.1 Temperature.....	101
5.2 Lake transparency	103
5.3 Autonomous <i>in situ</i> time-series	106
5.4 Profile measurements and total inventories.....	108
5.5 Conclusions	110
Appendix 1: SAMI-CO₂ Data Manipulation Program	112
Appendix 2: Profile Measurement Results	123
Appendix 3: <i>FreshH₂O</i> CO₂ – Carbonate System Calculations Program	140
Appendix 4: Meteorological Station Control Software.....	150
References.....	155

List of Tables

	page
Table 2.1: <i>In situ</i> instrumentation deployment summary	18
Table 2.2: Periodic profile measurements	25
Table 2.3: A summary of the Placid and Owl Creek data	38
Table 3.1: Meteorological conditions summary for winters 1997 and 1998	54
Table 4.1: A summary of important events in the 1999 study	74
Table 4.2: Average daily contributions to dissolved gas variability	91

List of Figures

	page
Figure 1.1: Box model diagram illustrating DIC pathways in a stratified lake	8
Figure 1.2: Bathymetric map of Placid Lake, Montana	14
Figure 2.1: Photograph of the instrumented mooring	17
Figure 2.2: The 1999 measured and calculated $p\text{CO}_2$ at 2 m in Placid Lake	35
Figure 2.3: Photograph of the meteorological station and site	39
Figure 2.4: Profile measurements of DO and DIC.....	52
Figure 3.1: Under-ice <i>in situ</i> time-series collected during the winter 1997	55
Figure 3.2: Under-ice <i>in situ</i> time-series collected during the winter 1998	56
Figure 3.3: 1997 meteorological and discharge data.....	60
Figure 3.4: 1998 meteorological and discharge data.....	61
Figure 3.5: Under-ice temperature profiles during the 1997 study.....	63
Figure 3.6: Chemical profiles obtained under ice during 1997	64
Figure 3.7: 1997 contour plot of DIC.....	65
Figure 3.8: Expanded time-series for Figure 3.1	67
Figure 3.9: Expanded time-series for Figure 3.2	70
Figure 4.1: <i>In situ</i> time-series and profile measurements in 1999	75
Figure 4.2: Meteorological and biomass data.....	76
Figure 4.3: Measured and simulated water temperatures and mixed-layer depth	77
Figure 4.4: Profile measurements of nutrients and chlorophyll- α	82
Figure 4.5: An overview of the <i>in situ</i> and modeled $p\text{CO}_2$ and DO	85

Figure 4.6: Under-ice dissolved gas time-series and model simulations	87
Figure 4.7: Contributions of several processes to dissolved gas variability under ice....	88
Figure 4.8: Specific conductance	92
Figure 4.9: The dissolved gas time-series and model simulations after ice out	94
Figure 4.10: Contributions of several processes to dissolved gas variability after ice out.....	95
Figure 4.11: Profiles of major cations and total alkalinity	97
Figure 5.1: Temperature contour plot produced from all profile measurements.....	102
Figure 5.2: Extinction coefficients and Secchi Disk measurements.....	104
Figure 5.3: Swan River discharge for water years 1996 – 1999.....	105
Figure 5.4: <i>In situ</i> time-series of surface $p\text{CO}_2$, DO, and temperature spanning winter 1997 to summer 1999.....	107
Figure 5.5: Selected profile measurements made at the mid-lake mooring site and total inventory means of DO, DIC, and pH	109

Chapter 1

Introduction

1.1 Dissertation overview

This dissertation describes biogeochemical research conducted on a freshwater lake from November 1996 to July 1999. It is comprised of several chapters: 1) an introduction and background with a listing of research objectives and a description of the study lake, 2) a summary of the research methods, 3) a description and interpretation of data collected under ice in the winters of 1997 and 1998, 4) a description and interpretation of data collected in 1999 during the transitional period from ice cover to open water, and 5) a brief summary and overview of the biogeochemical data collected over the course of the research and concluding remarks. Chapters 3 and 4, which could be combined into one chapter, are introduced separately for clarity and because they are each based on manuscripts that are being submitted to refereed journals.

1.2 Introduction

Lakes undergo dramatic changes in physical forcing between ice-covered and ice-free periods with important consequences for short-term and seasonal biogeochemical cycles. Ice often insulates lakes from wind-generated mixing, gas and heat exchange, and light penetration (Matthews and Heaney 1987; Bolsenga and Vanderploeg 1992; Agbeti and Smol 1995) and the duration of ice-cover, coupled with microbial metabolism, has been shown to be important in determining seasonal dissolved O₂ (DO) levels (e.g.,

Mathias and Barica 1980; Babin and Prepas 1985; Baird et al. 1987; Livingstone 1993), carbon dioxide (CO₂) supersaturation (Coyne and Kelley 1974; Hesslein et al. 1991; Cole et al. 1994; Striegl and Michmerhuizen 1998), and water column pH (Kratz et al. 1987). The insulating properties of ice cover, however, are not absolute as light penetration and mixing in ice-covered lakes can be considerable, especially with the waning of the ice and snow cover in spring (Nebaeus 1984; Kling et al. 1992; Bengtsson 1996). Spring phytoplankton blooms are often a result of these physical processes (e.g., Wright 1964; Wetzel 1983). Furthermore, spring ice melt may contribute to phytoplankton blooms by releasing dry-fall nutrients that accumulate on the ice surface (J.A. Stanford, pers. comm. 2000). Lake turnover, which occurs during the transitional period of ice cover to open water, has a profound effect on the distribution and budgets of DO, organic and inorganic carbon, alkalinity, nutrients, biomass, and other materials within a lake (Effler and Perkins 1987; Kling et al. 1991). For example, if turnover is incomplete or its duration is so short that an equilibrium is not established between the DO and the atmosphere, anoxia and poor water quality may result (e.g., Effler and Perkins 1987). Turnover can cease abruptly with the warming of the surface waters by solar radiation and the subsequent mixing of the heat downward by wind action. This process of surface heating and wind mixing leads to the thermal stratification of the lake, which fundamentally influences its physical and biogeochemical cycles.

Dissolved CO₂ and O₂ are two of the most important biogeochemical parameters in lakes. The dissolved carbonate system is significant because it regulates the pH and the composition of natural waters. Increasing atmospheric concentrations of anthropogenically-produced greenhouse gases, including CO₂, appear to be changing the

earth's climatic system. This has led to a push to determine if lakes act either as sources or sinks for atmospheric CO₂. Dissolved O₂ is perhaps the most fundamental parameter used to describe water quality because its concentration determines redox conditions and is important in the solubility and availability of many nutrients (Wetzel 1983). Dissolved CO₂ and O₂ are also important in the respiratory metabolism of most aquatic organisms and are related through photosynthesis and respiration.

Dissolved gas concentrations can vary considerably on seasonal, daily, and even hourly time-scales in lakes (see Chapter 1.4). Therefore, frequent measurements are required to completely characterize the complex biogeochemical cycles of CO₂ and DO. While the seasonal trends of these dissolved gases in lakes have been well characterized, little is known about their short-term variability under ice and during the spring transitional period. Collecting samples for analysis in late winter/early spring can prove to be quite challenging or impossible due to, for example, harsh weather or unstable ice conditions. These difficulties, combined with the general assumption that biogeochemical variability is suppressed under ice cover, have limited winter biogeochemical data to typically monthly and, at most, biweekly intervals. Furthermore, measurements are often infrequent because researchers have time and/or financial constraints or they lack the necessary instrumentation to make more frequent measurements.

New autonomous *in situ* chemical sensor technologies are making it possible to record long-term, continuous, time-series measurements even in adverse conditions (e.g., Wallace and Wirick 1992; DeGrandpre et al. 1997, 1998). Studies that employ autonomous sensors, which are typically moored at the research site, are at a significant

advantage because environmental and time factors that plague traditional grab-sampling studies are not a concern. Considering that commercial O₂ instruments are widely available, it is curious that few long-term continuous time-series of O₂ in lakes were found in the literature (see Kelly et al. 1983, Van Duin and Lijklema 1989, Portielje et al. 1996, and Carignan 1998). These instruments have been used more extensively in oceanographic studies (e.g., McNeil and Farmer 1995) but their high cost probably limits their use in freshwater studies, which are usually less well funded. Sensors for CO₂ are not widely available. The submersible autonomous moored instrument for CO₂ or SAMI-CO₂, developed by my advisor, Dr. Michael DeGrandpre, is the only commercial *in situ* CO₂ instrument available and had been used exclusively in marine research prior to this study (DeGrandpre et al. 1995, 1997, 1998). It is autonomous, has low power draw, and measures the partial pressure of CO₂ ($p\text{CO}_2$) *in situ* with high temporal resolution for extended time periods.

To my knowledge, only Coyne and Kelley (1974), Sellers et al. (1995), and Carignan (1998) have performed continuous CO₂ measurements in lakes. In these studies, an infrared CO₂ gas analyzer was used to measure the $p\text{CO}_2$ at the lake surface in an equilibration chamber. Rafts were required to support the analyzer, power supply, and the *in situ* chamber. These systems were limited to monitoring the lake surface and are neither conducive to long-term studies nor useful during freeze-up or ice-out conditions.

The extensive temporal coverage provided by *in situ* sensors is important because it can lead to further insight into the sources and sinks of CO₂ and DO in lakes. Furthermore, the simultaneous measurement of CO₂ and DO helps elucidate the physical and biogeochemical processes that control their variability (Oudot 1989; DeGrandpre et

al. 1997, 1998; Carignan 1998). This study is the first to report long-term (multi-month), simultaneous, *in situ* chemical sensor measurements of both CO₂ and DO in a freshwater lake. Moreover, biogeochemical variability during the important transitional period from ice cover to summer stratification was characterized and analyzed.

1.3 Research objectives

Motivated by the desire to further our understanding of biogeochemical processes in freshwater lakes, a comprehensive study of a local freshwater lake was undertaken. There were several research objectives. The first objective was to characterize the short-term and seasonal biogeochemical variability in a freshwater lake during ice-covered and ice-free periods with autonomous *in situ* sensors. A further objective was to analyze the biogeochemical data to determine the processes that control CO₂ and DO variability with time. The primary goal of environmental science, in general, is to develop models that are able to describe and help us understand natural processes. With that in mind, another important objective was to develop biogeochemical models to describe the short-term and seasonal variability of *p*CO₂ and DO. These models could then be used to quantify the relative importance of biology, air-water gas exchange, mixing, and heating and cooling on CO₂ and DO.

The specific questions that accompany the objectives outlined above are: 1) What is the magnitude of CO₂ and DO variability on diel and longer time scales? 2) What physical, biological, or chemical processes control CO₂ and DO and their relationship? 3) What impact do the duration of ice cover and the extent of spring turnover have on the CO₂ and DO budgets? 4) To what extent does biological production contribute to the

dissolved gas variability in the spring? 5) What is the fate of CO₂ in the epilimnion and hypolimnion after seasonal stratification develops? and finally 6) Is the lake a net source or sink for atmospheric CO₂?

To accomplish these goals, several autonomous *in situ* sensors were deployed on a subsurface mooring in Placid Lake, Montana USA. High temporal resolution time-series of *p*CO₂, DO, temperature, and several other variables were obtained over six different deployments from winter 1997 to summer 1999. Data from periodic profile measurements and local and regional meteorology were also obtained to aid the interpretation of the *in situ* data. Emphasis is placed on the analysis of the short-term and seasonal biogeochemical variability during the 1997 and 1998 under-ice deployments (Chapter 3) and the 1999 deployment from ice cover to summer stratification (Chapter 4). The 1999 study was the most comprehensive in that autonomous sensors for *p*CO₂ and

carbon, or DIC, be used. The speciation of DIC is controlled by the set of equilibria given in the box model on the following page (Figure 1.1). In contrast, DO is relatively simple in that it only exists in one dissolved form.

The spatial and temporal distribution of DIC and DO in lakes is controlled by a number of physical, biological, and chemical processes. The primary autochthonous, or in-lake, physical processes affecting dissolved gas variability are air-water gas exchange, heating and cooling, mixing, and advection. Photosynthesis and respiration are very important mediators of DIC and DO. Also, chemical processes, such as the formation and dissolution of calcium carbonate (CaCO_3) and the photooxidation of organic matter to inorganic carbon, may influence dissolved gas variability. A brief description of how these processes affect DIC and DO will be presented in the paragraphs to follow. In addition to these autochthonous contributions to dissolved gas variability, a number of

gas transfer rate can be estimated from wind speed and air-water gas exchange contributions to CO₂ variability can be determined.

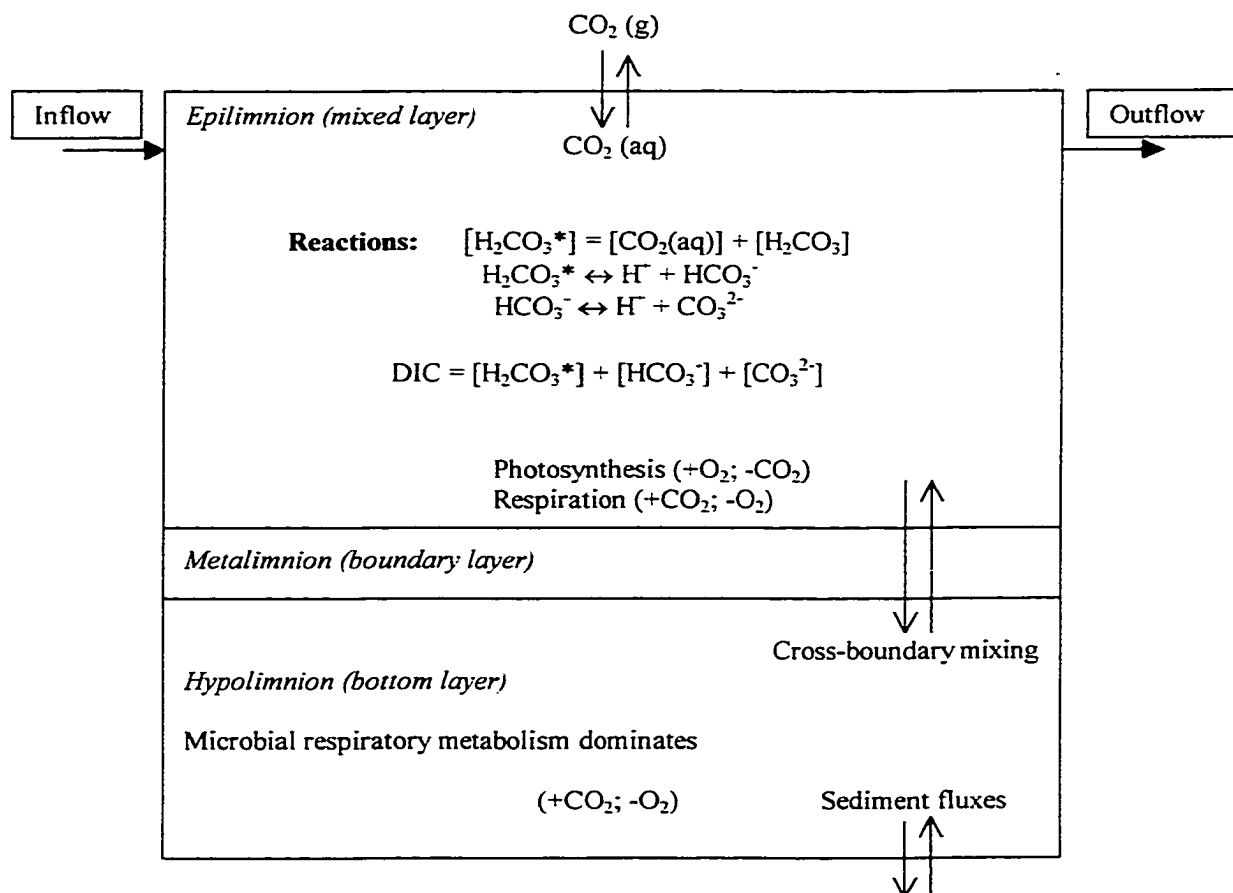


Figure 1.1: Box model of a thermally stratified lake. This box model illustrates the pathways of DIC into or out of the compartments within the system. Similar processes act on DO.

Heating and cooling: The absorption of solar radiation, and its dissipation as heat, controls the thermal structure and affects the circulation patterns of the lake, which, in turn, affects the distribution of dissolved gases. The solubility of CO₂ and DO are also temperature-dependent. The *p*CO₂ and DO % saturation both increase with increasing temperature. Over the temperature range 0 to 20 °C, DO solubility changes at an average

rate of 2.3% per degree. The $p\text{CO}_2$ is more complicated because it can be redistributed through the carbonate equilibria. It is related to the aqueous CO_2 as follows:



where K_{H} is the temperature-dependent Henry's law, which describes the equilibrium distribution of a volatile species between liquid and gaseous phases. Assuming a constant DIC and carbonate alkalinity (say 1100 μM and 1050 $\mu\text{equiv/L}$, respectively) the $p\text{CO}_2$ would change at an average rate of 3.5% per degree from 0 to 20 °C. In addition to its effect on solubility, temperature is of major importance in determining reaction rates, thermodynamic equilibria, and water density. Thermal stratification (density gradients) of the water column has a profound influence on physical and chemical cycles in lakes. Differential heating of the water mass leads to density driven currents, which have been shown to be important for mixing and transport in lakes (e.g., van Senden et al. 1990). An important metric of thermal stratification is the mixed-layer depth (MLD). Numerous models have been developed to estimate the MLD (Hanna 1990) and it is used as a variable in energy-flux models (e.g., Chapter 2.7.2).

1.4.1.b Biological processes

Primary productivity, which is the photosynthetic production of particulate and dissolved organic matter from inorganic carbon per unit time, plays a dominant role in the budgets of DIC and DO. Net community production (P_c), a term which is referred to frequently in Chapter 4, is defined as:

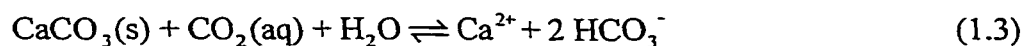
$$P_c = P_n - R_h \quad (1.2)$$

where P_n is the net primary production (gross primary production less autotrophic respiration) and R_h is the respiration of all heterotrophs. Aqueous CO_2 is the primary

source of carbon for photosynthesis by phytoplanktonic algae and macrophytic vegetation (Wetzel and Likens 1991). Photosynthetically available radiation (PAR) is required for primary production, thus light climate is a key factor in controlling the dynamics of phytoplankton (e.g., Bleiker and Schanz 1997) and determines the relationship of the rate of photosynthesis with depth (Fogg 1980). In lakes, the particulate organic matter that is photosynthetically produced in the euphotic zone settles out and accumulates in the hypolimnion (Figure 1.1). In addition to this autochthonous source of organic matter, a significant fraction of organic carbon to the system may come from terrestrial sources. Microbes consume DO and produce CO₂ in the metabolism of this organic carbon. These respiration processes may lead to anoxic conditions in the hypolimnion during winter and summer stratification when the hypolimnion is isolated from the surface waters. Metabolic activity can also alter the alkalinity (or acid neutralizing capacity) of a water mass through the uptake of inorganic nutrients or decomposition of organic matter. For example, the uptake of nitrate by phytoplankton generates an increase in alkalinity whereas oxidation of organic-N to nitrate during decomposition processes is associated with a decrease in alkalinity (see Equation 2.39) (Naumoski and Lehman 1984).

1.4.1.c Chemical processes

The dissolution and precipitation of CaCO₃ is controlled by the amount of free CO₂ in solution:



During intense photosynthesis, the concentrations of bicarbonate start to be reduced as a result of CO₂ drawdown. The constraint of charge balance causes additional bicarbonate to dissociate to carbonate until the solubility of CaCO₃ is exceeded and it starts to

precipitate. The net result is a decrease in alkalinity. Analogously, net respiration may lead to the dissolution of CaCO_3 and an increase in alkalinity.

Photooxidation of DOC to DIC may also be an important abiotic contributor to DIC and DO variability in lakes with high organic acid concentrations (Granéli et al. 1996). The main sources for dissolved organic substances in lakes are lignins, carbohydrates, and lipids. Approximately 20% of the dissolved organic matter in natural waters consists of identifiable compounds. The remaining 80% has been classified as humic substances consisting of hydrophobic (fulvic and humic acids) and hydrophilic acids (Leenheer 1994).

1.4.2 CO_2 research

Seasonal changes in the $p\text{CO}_2$ in lakes have been studied to calculate CO_2 budgets, which can be used to determine whether a lake is a net source or a sink for atmospheric CO_2 (Hesslein et al. 1991; Kling et al. 1992; Cole et al. 1994; McConnaughey et al. 1994; Striegl and Michmerhuizen 1998) and to show its effect on other variables such as lake pH (Herczeg and Hesslein 1984; Kratz et al. 1987). It is important to note that most lake $p\text{CO}_2$ studies are based upon periodic measurements (most a few times a year, some weekly). Short-term studies to characterize diel variation in aqueous CO_2 are less common, but have also been undertaken (Maberly 1996; Raymond et al. 1997). Sellers et al. (1995) have shown that for highly productive lakes with large diel changes of $p\text{CO}_2$, frequent measurements in water are necessary to accurately determine the magnitude and direction of gas fluxes. They also found that even if accurate estimates of net daily fluxes were determined from frequent discrete sampling in each 24-hour period, serious errors (from 25 to 181% of the actual flux)

could be expected if these short period flux estimates were extrapolated to longer periods (weeks). Lakes with low productivity, which show a small CO₂ gradient across the air-water interface, also require frequent measurements to accurately determine gas fluxes because of their sensitivity to small changes in CO₂ (Hesslein et al. 1991). The results from these studies reiterate the need for more frequent CO₂ measurements over longer periods.

1.4.3 DO research

Like CO₂, frequent measurements are required to completely characterize DO variability in lakes. Representative studies of DO in lakes include the relationship between DO and biological production (Wharton and Simmons 1986), the role of DO in nutrient cycling (Chapra and Canale 1991; Lehman and Branstrator 1994), the examination of winter DO depletion rates under ice-covered lakes (Barica 1984; Babin and Prepas 1985; Baird et al. 1987; Livingstone 1993), and the development of models to simulate DO profiles (Ginot and Hervé 1994). Stefan et al. (1995) describe a deterministic, one-dimensional model for DO that can successfully simulate summer DO conditions in a wide array of lakes in the north central U.S. They suggest that the assumption that DO varies spatially only in the vertical dimension is appropriate for many freshwater lakes because horizontal variations in concentration are often small when compared to other sources of variability.

1.4.4 Biogeochemical models

Numerous models have been developed for studying biogeochemical dynamics in lakes. Model complexity ranges from general steady state, input-output models to specific time-dependent multicomponent ecosystem models. Perhaps the most common

are simple box models in which each spatial compartment is considered to be homogeneous and is linked to adjacent compartments with a physical mixing mechanism. Many studies have shown that an accurate simulation of biogeochemistry in aquatic systems requires a coupling of biogeochemical and physical models (e.g., Riley and Stefan 1988; Karagounis et al. 1993; Kemp et al. 1994; McNeil and Farmer 1995; Jewell 1995; Kraines et al. 1996; Gnanadesikan 1996; Hamilton and Schladow 1997). Of the physical-biogeochemical model studies, relatively few have included *in situ* measurements for comparison (Van Duin and Lijklema 1989; Kemp et al. 1994; McNeil and Farmer 1995; Kraines et al. 1996). The ability to compare model results with *in situ* measurements becomes increasingly important when the time scale of biogeochemical variability is short. Many of the topics discussed above will be revisited in more detail later in the dissertation.

1.5 Study lake

Studies were conducted on Placid Lake (47°07' N, 113°31' W), 45 km NE of Missoula, Montana (Figure 1.2). Placid Lake was chosen for logistical reasons (proximity to Missoula and availability of a boat and cabin at the site) and because the lake has been studied in the past (Juday and Keller 1980, 1984). A bathymetric map of the lake was not available prior to this study. Figure 1.2 was constructed from lake depth measurements made along North-South and East-West transects of the lake in March 1974 by E.J. Keller and R.E. Juday of The University of Montana Department of Chemistry.

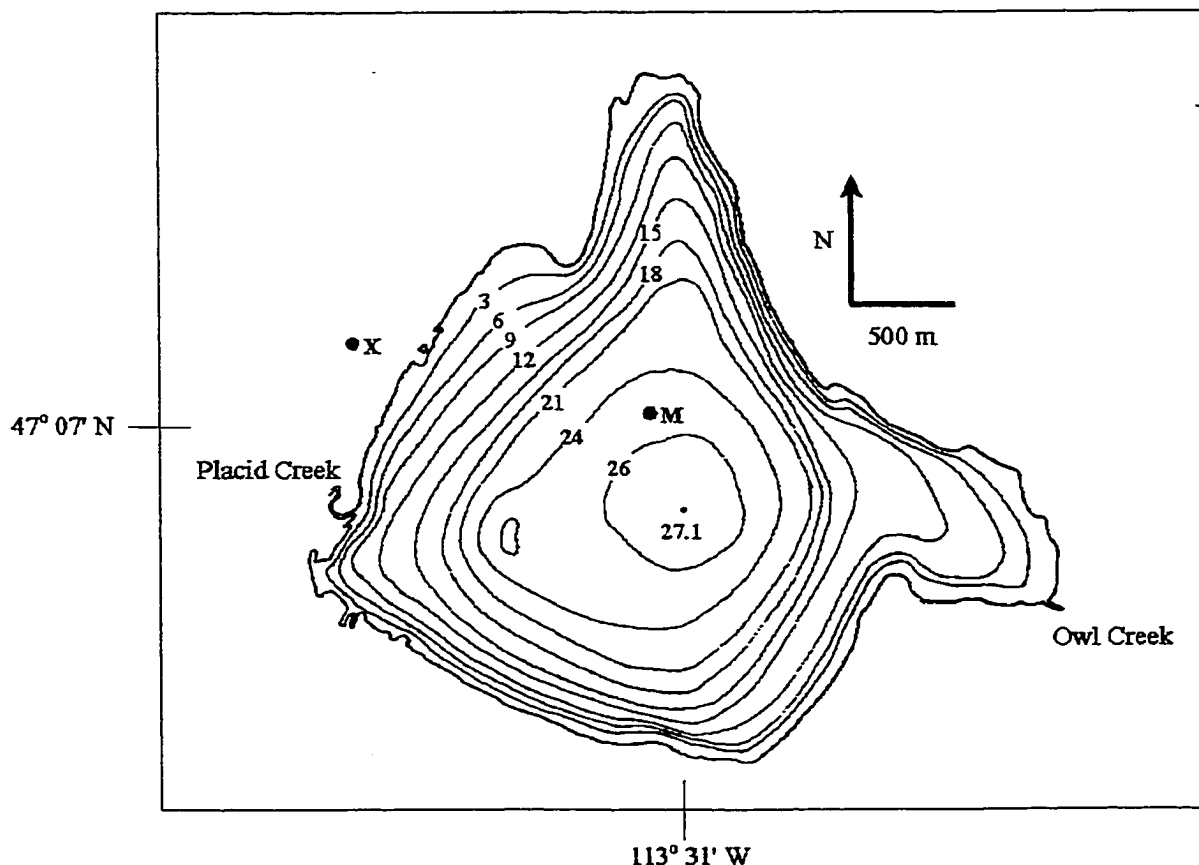


FIGURE 1.2: Bathymetric map of Placid Lake, Montana. **M** designates the location of the instrumented mooring(s) deployed in all studies. The meteorological station (**X**) in 1999 was deployed in a meadow 1.5 km northwest of the mid-lake mooring site. Contour intervals are in meters.

The lake has a surface area of $4.90 \times 10^6 \text{ m}^2$, volume of $7.33 \times 10^7 \text{ m}^3$, maximum depth of 27.1 m, and a mean depth of 15.0 m (Figure 1.2). Placid Lake is a dimictic, mesotrophic, kettle lake (Juday and Keller 1980) that resides in a sedimentary carbonate rock basin at an elevation of 1256 m (Streebin et al. 1973). Placid Creek, which drains an area of 180.3 km^2 (Streebin et al. 1973), is the lake's primary surface water source (Figure 1.2). The hydrologic residence time of the lake, determined from discharge measurements made on Placid Creek and the outlet stream, Owl Creek, is ~ 2 years.

Local groundwater input into the lake is considered negligible (Juday and Keller 1980) and is supported by discharge measurements (Chapter 2.6.1) and dissolved gas measurements near the lake bottom (Chapter 4.1.4.b).

Chapter 2

Methods

2.1 Mooring detail

A subsurface mooring was made from a surlyn foam float (Gilman Corp.), steel chain or cable, and anchor (Figure 2.1). The mooring was deployed either through the ice or from a small research boat during ice-free periods. The mooring was located near the center of the Placid Lake basin at ~25 m depth for all study years (Figure 1.2). *In situ* sensors for $p\text{CO}_2$, DO, photosynthetically active radiation (PAR), chlorophyll-*a* fluorescence, conductivity, temperature and depth, all described below, were deployed on the mooring. Biogeochemical instrumentation was located near the surface, the expected zone of greatest short-term variability, in all studies. Instrument availability prohibited more extensive spatial coverage in all but the 1999 study when additional sensors for $p\text{CO}_2$ and DO were deployed near the lake bottom. A thermistor chain mooring was deployed in summer/fall 1998 and included a DO sonde in the winter 1998 and 1999 deployments. The instrumentation deployment periods and depths are presented in Table 2.1.

2.2 *In situ* chemical measurements

2.2.1 The partial pressure of carbon dioxide ($p\text{CO}_2$)

The moored $p\text{CO}_2$ measurements were made using the Submersible Autonomous Moored Instrument for CO_2 (SAMI- CO_2). The SAMI- CO_2 operates by equilibration of

the ambient water $p\text{CO}_2$ with a pH indicator solution (5.51×10^{-5} M bromothymol blue with 4.20×10^{-5} M NaOH) contained within a tubular gas-permeable membrane. The equilibrated solution is then pumped into an optical cell where the absorbance of the indicator is measured at specific wavelengths. Exceptional long-term stability has been obtained by basing the instrumental response on the ratio of these absorbances and by renewing the pH indicator for each measurement. See DeGrandpre et al. (1999) for a thorough description of the SAMI-CO₂, its operating principle, and performance characteristics.

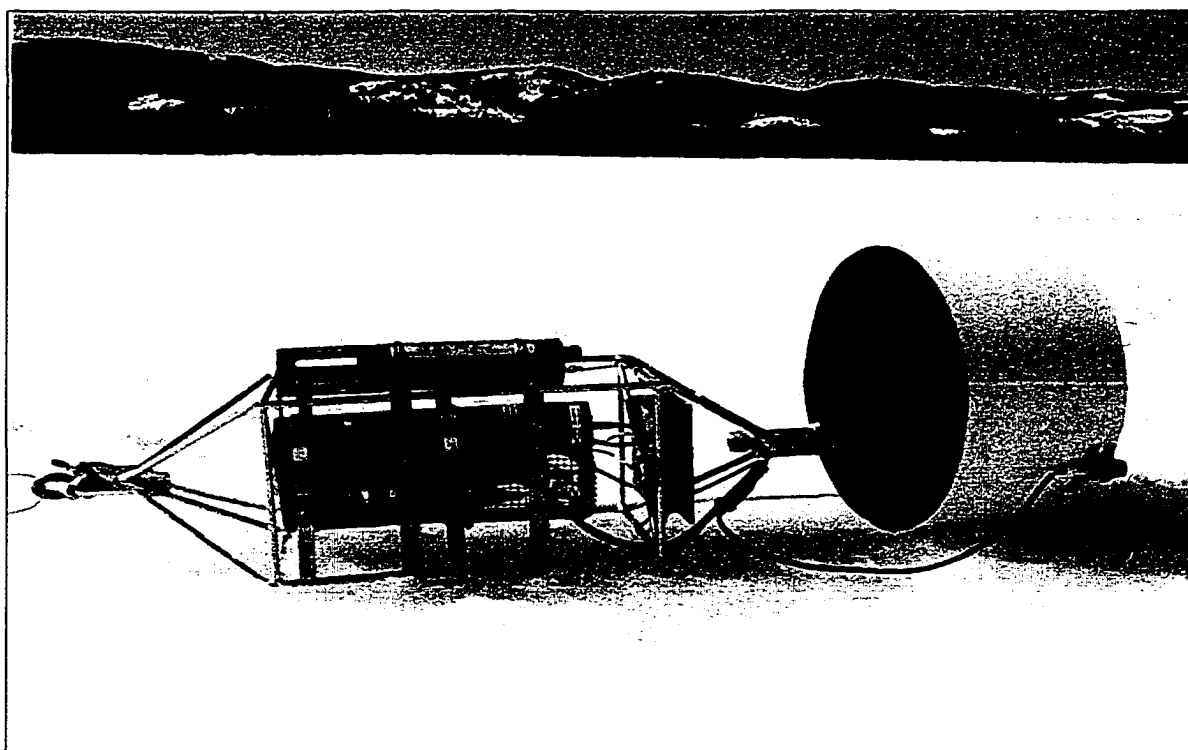


FIGURE 2.1: A photograph of the instrumented stainless steel mooring cage attached to the white mooring float. The cylindrical instrument furthest from the ice is a YSI Model 6000 DO sensor. The battery housing is the gray PVC cylinder below the DO sensor. The SAMI-CO₂ is partially hidden from view but lies closest to the ice with the sensing end covered by a copper mesh cage. The PAR sensor is attached to the side of the mooring float.

TABLE 2.1: *In situ* instrumentation deployed on a subsurface mooring at the mid-lake mooring site. Instrument descriptions are given in the text. The number of instruments deployed in a period is given in parentheses. The depth is the initial deployment depth.

Instrument	Parameter	Deployment Period	Depth (m)
SAMI-CO ₂	<i>p</i> CO ₂ , temperature	08 Jan – 29 May 1997 (1)	2.7
		19 Jun – 28 Aug 1997 (1)	1.7
		11 Sep – 14 Nov 1997 (1)	2.7
		26 Nov 1997 – 20 May 1998 (1)	3.2
		16 Jun – 30 Oct 1998 (1)	2.5
		18 Mar – 02 Jul 1999 (2)	1.7, 19.7
YSI Inc. Model 6000	O ₂ , temperature, conductivity, depth	08 Jan – 29 May 1997 (2)	2.9
		19 Jun – 28 Aug 1997 (2)	1.9
		11 Sep – 14 Nov 1997 (1)	2.9
		26 Nov 1997 – 20 May 1998 (1)	3.4
		14 Mar – 12 May 1998 (1)*	2.4
		16 Jun – 30 Oct 1998 (1)	2.7
		18 Mar – 02 Jul 1999 (2)	1.9, 19.9
18 Mar – 02 Jul 1999 (1)*	4.1		
Chelsea Instruments Model Minitracka II	Chlorophyll- <i>a</i> fluorescence	18 Mar – 02 Jul 1999 (1)	1.8
LI-COR Inc. Model LI-192SA	PAR	08 Jan – 29 May 1997 (1)	1.5
		19 Jun – 28 Aug 1997 (1)	0.7
		11 Sep – 14 Nov 1997 (1)	1.5
		26 Nov 1997 – 20 May 1998 (1)	2.0
		16 Jun – 30 Oct 1998 (1)	1.3
		18 Mar – 02 Jul 1999 (1)	0.7
Onset Computer Corp. Model WTA080537	Temperature	14 Mar – 12 May 1998 (5)*	1.0, 2.0, 3.0, 4.0, 5.0
		16 Jun – 30 Oct 1998 (5)*	1.9, 3.9, 5.9, 7.9, 9.9
		18 Mar – 02 Jul 1999 (5)*	0.7, 5.1, 6.1, 8.1, 10.1

*This instrument was deployed on a second subsurface mooring.

The SAMI-CO₂ was calibrated at The University of Montana prior to deployment in Placid Lake. The SAMI-CO₂ response was determined in a water-filled chamber thermostated near the expected average water temperature. The partial pressure of CO₂ within the calibration chamber was controlled with two mass flow controllers that were used to mix a 3000 ppm CO₂ gas standard with CO₂-free air. The gas concentrations in the chamber headspace were determined using a nondispersive infrared CO₂ analyzer (NDIR) (LI-6251, LI-COR, Inc.) calibrated with a 360 ± 1 ppm NIST traceable CO₂ gas standard. The NDIR measures the mole fraction of CO₂ on a wet basis or with water vapor present. Water vapor absorbs infrared radiation and thus the NDIR measurements had to be corrected for pressure broadening effects (see the LI-6251 instruction manual).

The SAMI-CO₂ response (R_{CO_2}) was plotted against the NDIR $p\text{CO}_2$ over the expected $p\text{CO}_2$ range to generate a calibration curve. The calibration curve fit used is of the form,

$$R_{\text{CO}_2} = a (\log p\text{CO}_2)^2 + b (\log p\text{CO}_2) + c. \quad (2.1)$$

The logarithmic form in Equation 2.1 was used rather than a second order polynomial because it provided a better fit through the points at the calibration extremes.

The response of the SAMI-CO₂ is temperature dependent (DeGrandpre et al. 1995, 1999). Therefore, differences between the *in situ* and calibration temperature had to be corrected for. Upon retrieval of the SAMI-CO₂ from the field, the data were downloaded from the data logger and manipulated with a QuickBasic program (Appendix 1) that calculates R_{CO_2} using the molar absorptivities of the indicator (DeGrandpre et al. 1999) and the stored absorbance and temperature data. The temperature-corrected R_{CO_2} is calculated with the equation:

$$R_{\text{CO}_2}(T_0) = (T - T_0) \cdot 0.0072 + R_{\text{CO}_2}(T) \quad (2.2)$$

where T and T_0 are the *in situ* and average calibration temperature in °C, respectively. The $p\text{CO}_2$ is calculated using the quadratic equation with the temperature-corrected R_{CO_2} and the calibration coefficients a , b , and c (Equation 2.1).

Measurement precision, estimated from the SAMI-CO₂ calibrations, is $\sim \pm 1 \mu\text{atm}$ at 360 μatm , $\pm 10 \mu\text{atm}$ at 1200 μatm , and $\pm 20 \mu\text{atm}$ at 1500 μatm . Accuracy is $\sim \pm 1-3 \mu\text{atm}$ at 360 μatm and is estimated to be similar to the precision at higher levels. The increasing uncertainty reflects the decrease in sensitivity with higher $p\text{CO}_2$ levels (DeGrandpre et al. 1999). We have shown that the original laboratory calibration remains accurate and that the SAMI-CO₂ measurements have very little long-term drift (DeGrandpre et al. 1999).

SAMI-CO₂ data quality was evaluated through periodic measurements of total dissolved inorganic carbon (DIC) and pH (Chapter 2.5) and through comparisons with complementary DO records.

2.2.2 Dissolved oxygen (DO)

DO was measured with commercially available autonomous sondes (YSI Inc., Model 6000). The reported sensor accuracy and resolution are ± 0.20 and $\pm 0.01 \text{ mg L}^{-1}$, respectively. Single-point DO calibrations were performed just prior to deployment in water-saturated air at a temperature near the expected lake temperature. The instrument calibrations were checked upon retrieval by placing the sensor in water-saturated air and comparing the measurement to the expected DO % atmospheric saturation value. The results of these checks showed that most instruments had little long-term drift. In four deployments, multiple DO sensors were deployed at the same depth to provide *in situ*

replicates (Table 2.1). These data along with comparisons to the *in situ* $p\text{CO}_2$ were used to evaluate the quality of the *in situ* DO measurements. Periods when the DO sensors were not performing well are not presented.

In the 1999 study (Chapter 4), discrete measurements of Winkler titration DO (Chapter 2.4.3) were used to check the calibration accuracy of the Model 6000 sensors. A comparison between the *in situ* and Winkler DO indicated that sensor drift was negligible but there were offsets between the *in situ* and cast measurements. Average offsets of $-16 \mu\text{mol L}^{-1}$ (-0.51 mg L^{-1}) and $-27 \mu\text{mol L}^{-1}$ (-0.85 mg L^{-1}) were applied to the surface and bottom DO time-series, respectively. The replicate sensor measurements at 4.1 m validated the surface sensor measurements and are not presented. The average offset between the two surface (1.9 and 4.1 m) DO sensors prior to stratification was $16 \pm 3 \mu\text{mol L}^{-1}$ ($0.21 \pm 0.19 \text{ mg L}^{-1}$) ($N=4219$). Notable differences between the two sensors did not develop until they were effectively separated by water column stratification.

2.3 Other *in situ* measurements

2.3.1 Temperature

Both the SAMI- CO_2 and Model 6000 measured temperature. The accuracy and resolution of the temperature sensors are ± 0.15 and ± 0.01 °C, respectively. The temperature records for both sensors agreed to within the accuracy of the measurement for all deployments. Therefore, only one of the two records is presented for each deployment.

Five underwater temperature loggers (Onset Computer Corp., Model WTA080537) were obtained in early 1998 and were used in subsequent deployments to

provide additional water column temperature measurements with the same sampling frequency as the *in situ* chemical measurements (Table 2.1). The accuracy and resolution of the temperature loggers are ± 0.20 and ± 0.15 °C, respectively.

2.3.2 Photosynthetically active radiation (PAR)

PAR (waveband 400 to 700 nm) was measured with an underwater quantum sensor (LI-COR Inc., Model LI-192SA) connected to an external sensor input on the SAMI-CO₂. The PAR sensor was attached to the side of the subsurface float to prevent shadowing (Figure 2.1; Table 2.1). The sensor produces a photocurrent that is proportional to the number of photons incident per unit time on the sensor surface. The calibrated output has units of $\mu\text{mol photons m}^{-2} \text{ s}^{-1}$, which are equivalent to $\mu\text{Einstein m}^{-2} \text{ s}^{-1}$. Depending on the level of diffuse light, 45-55 % of solar radiation is in the PAR waveband. PAR was taken as 46% of solar radiation for surface energy budget considerations (Chapter 2.7.1) (Bleiker and Schanz 1997). In the 1999 deployment (Chapter 4), the PAR sensor was deployed too shallow for the circuit resistor resulting in the loss of data when the voltage output exceeded the A/D convertor range during high light periods. Therefore, PAR signals that exceeded the saturation value, $150 \mu\text{E m}^{-2} \text{ s}^{-1}$, were estimated from the net solar insolation calculated at the lake surface (Chapter 2.7.1) and the extinction coefficient for the lake (Chapter 2.4.9).

2.3.3 Chlorophyll-*a* fluorescence

An *in situ* fluorometer (Chelsea Instruments, Minitracka II, Serial # 175044) was deployed at the surface during the 1999 study (Table 2.1). Prior to deployment, the fluorometer and PAR sensor cables were spliced together and were interfaced with an external 6-pin connector on the SAMI-CO₂. The fluorometer was controlled via the

SAMI-CO₂ data logger program. Chlorophyll-*a* fluorescence was observed to decrease during the day and increase at night throughout the study. Others (e.g., Marra 1997; Kiefer and Reynolds 1992) have reported that nonphotochemical quenching occurs at high irradiances and show field data with a trend similar to our data. Because of this quenching the daytime chlorophyll-*a* fluorescence was estimated by linearly interpolating the fluorescence between dawn and dusk. This procedure had an effect of smoothing out the diel variability in chlorophyll-*a* fluorescence but retained the longer-term gross features (Figure 4.2d).

The fluorometer response is known to vary linearly with chlorophyll-*a* concentration (Chelsea Instruments). Therefore, a linear calibration curve was generated from the *in situ* fluorescence and the chlorophyll-*a* measurements taken periodically at the depth of the instrument (Chapter 2.4.5). The calibrated *in situ* fluorometer and profile chlorophyll-*a* measurements agreed to within $1.2 \pm 1.0 \text{ mg m}^{-3}$ (Figure 4.2d).

2.3.4 Specific conductance

Conductivity was measured with the Model 6000 with a reported accuracy of $\pm 0.5\%$ of the reading and a resolution of $\pm 1 \text{ } \mu\text{S cm}^{-1}$. The sensors were calibrated in a calibration cup with a 1 mS cm^{-1} standard solution prepared from a 1000 mS cm^{-1} standard (YSI). The conductivity of solutions of ionic species is highly temperature dependent, therefore the temperature and raw conductivity (*C*) values were used to generate a specific conductance value compensated to $25 \text{ }^\circ\text{C}$ (*SC*):

$$SC = \left(\frac{C}{1 + 0.0191 \cdot (T - 25)} \right) \quad (2.3)$$

where T is the *in situ* temperature in °C. The YSI instruction manual for the Model 6000 states that the temperature coefficient varies with the nature of the ionic species and that the specific conductance determined with Equation 2.3 will provide a close approximation for seawater. Placid Lake is much more dilute than seawater ($\mu \sim 1.8$ mM versus ~ 0.7 M) so the specific conductance will be somewhat inaccurate. Nevertheless, assuming no significant change in ionic composition over time, trends in specific conductance are likely valid.

2.3.5 Depth

The Model 6000 has an internal pressure transducer that relates pressure to depth. The pressure transducer is sensitive to swings in barometric pressure and therefore the depth record had to be corrected for changes in barometric pressure. Barometric pressure was measured at a NOAA National Data Center site at Johnson-Bell Field in Missoula, MT. To correct the depth record for barometric pressure variability, the barometric pressure at the time of deployment was subtracted from the entire barometric pressure record. Then, using the fact that for every 1 m increase in depth there is a corresponding hydrostatic pressure increase of 0.0968 atm, the depth change resulting from variability in barometric pressure was calculated and subtracted from the original depth record. The resolution of the measurement is ± 0.001 m.

2.4 Periodic profile samples and measurements

Periodic profile samples and measurements were collected at Placid Lake on 31 occasions from 6 Nov 1996 to 28 Jun 1999 and are summarized in Table 2.2. The data collected from these sampling trips are tabulated in Appendix 2.

TABLE 2.2: Periodic profile measurements. The format used for reporting measurements is the number of discrete samples followed by the depth range (m) in parenthesis. The letters “a” and “b” represent measurements made by the YSI models 58 and 6000, respectively.

Profile Date	Temperature	DO (YSI)	DO (Winkler)	DIC & pH	TA	Chl- <i>a</i>	Nutrients	Cations	CDOM	Light Intensity	Secchi Disc Transparency
11/01/96	11 (1-25) a	6 (5-25) a	-	10 (5-25)	-	-	-	-	-	-	-
01/08/97	-	Problem b	-	10 (2-23.5)	-	-	-	-	-	-	-
02/03/97	6 (2-23) b	6 (2-23) b	-	10 (2-23)	-	-	-	-	-	11 (0-10)	-
02/23/97	6 (1-22) b	6 (1-22) b	-	10 (2-23)	-	-	-	-	-	11 (0-10)	-
03/17/97	6 (1-20) b	6 (1-20) b	-	10 (2-20)	-	-	-	-	-	11 (0-10)	-
05/29/97	-	Problem b	-	10 (2-20)	-	-	-	-	-	9 (0-13)	2.0 m
06/18/97	11 (2-20) a	11 (2-20) a	-	-	-	-	-	-	-	-	2.25 m
06/19/97	11 (2-22) a	11 (2-22) a	-	-	-	-	-	-	-	-	-
07/02/97	12 (2-22) a	12 (2-22) a	-	10 (2-20)	-	-	-	-	-	11 (0-10)	3.75 m
07/17/97	12 (2-22) a	12 (2-22) a	-	10 (2-20)	-	-	-	-	10 (2-20)	9 (0-8)	3.5 m
08/05/97	11 (2-21) a, b	11 (2-21) a, b	-	10 (2-20)	-	-	-	-	10 (2-20)	11 (0-10)	3.75 m
08/20/97	12 (2-22) a	12 (2-22) a	-	10 (2-20)	-	-	-	-	10 (2-20)	9 (0-8)	3.5 m
09/25/97	12 (1-20) a	12 (1-20) a	-	10 (2-20)	-	-	-	-	-	11 (0-10)	5.0 m
10/23/97	16 (1-20) a	12 (1-20) a	-	10 (2-20)	-	-	-	-	10 (2-20)	7 (0-6)	3.5 m
11/14/97	18 (1-22) a	-	-	-	-	-	-	-	-	-	4.0 m
02/09/98	5 (2-15) b	5 (2-15) b	-	10 (2-15)	-	-	-	-	-	-	-
03/03/98	5 (2-20) b	5 (2-20) b	-	5 (2-20)	-	-	-	-	-	-	-
05/12/98	16 (1-22) a	16 (1-22) a	-	-	-	-	-	-	-	-	-
05/20/98	17 (0-22) a	17 (0-22) a	-	-	-	-	-	-	-	-	-
06/16/98	13 (0-22) a	13 (0-22) a	-	-	-	-	-	-	-	10 (0-9)	4.5 m
08/04/98	14 (1-23) a	14 (1-23) a	-	2 (3)	-	-	-	-	-	-	4.0 m
08/15/98	16 (1-24) a	16 (1-24) a	-	-	-	-	-	-	-	10 (0-9)	5.0 m
10/30/98	10 (1-22) a	9 (1-18) a	-	-	-	-	-	-	-	10 (0-9)	5.0 m
03/18/99	17 (0-22) a	-	-	10 (0.5-20)	5 (1.5-20)	10 (0.5-20)	10 (0.5-20)	-	10 (0.5-20)	8 (0-7)	-
04/01/99	20 (0-25) a	-	10 (0.5-20)	10 (0.5-20)	5 (2 & 20)	10 (0.5-20)	10 (0.5-20)	-	10 (0.5-20)	12 (0-10)	-
04/26/99	22 (0-24) a	-	10 (0.5-20)	10 (0.5-20)	2 (2 & 20)	10 (0.5-20)	5 (0.5-20)	5 (0.5-20)	10 (0.5-20)	13 (0-10)	-
05/05/99	17 (0-22) a	17 (0-22) a	10 (2-20)	10 (2-20)	3 (2 & 20)	6 (2-20)	5 (2-20)	5 (2-20)	10 (2-20)	12 (0-10)	3.0 m
05/20/99	20 (0-24) a	19 (0-24) a	10 (2-20)	10 (2-20)	3 (2-20)	5 (2-20)	5 (2-20)	5 (2-20)	10 (2-20)	12 (0-10)	-
06/07/99	20 (0-24) a	19 (0-24) a	10 (2-20)	10 (2-20)	4 (2-20)	5 (2-20)	5 (2-20)	5 (2-20)	10 (2-20)	12 (0-10)	3.75 m
06/27/99	19 (0-24) a	19 (0-24) a	-	-	-	-	-	-	-	12 (0-10)	4.0 m
06/28/99	22 (0-24) a	22 (0-24) a	10 (2-20)	10 (2-20)	3 (2-20)	5 (2-20)	5 (2-20)	5 (2-20)	10 (2-20)	-	-
										12 (0-10)	4.5 m

2.4.1 DIC and pH

All discrete samples were obtained with a vertical Kemmerer water sampler. Replicate samples at depths throughout the water column were obtained from two separate casts. Samples for DIC and pH were transferred to acid-washed 500 mL glass bottles using care to limit gas exchange and were immediately preserved with 100 μL mercury (II) chloride and stored on ice for transport back to the laboratory.

The samples were analyzed for DIC in the laboratory within 24 hr using a DOC/DIC carbon analyzer (Shimadzu, Model TOC5000A). The analyzer was calibrated with three freshly prepared $\text{Na}_2\text{CO}_3/\text{NaHCO}_3$ standards that bracketed the sample concentration. The mean precision for the DIC method, based on three intra-sample measurements, was typically $\pm 0.5\%$ ($\pm 6 \mu\text{M}$ typical) and the average uncertainty between the two separate casts at each depth was $6.6 \pm 9.5 \mu\text{M}$ ($N=101$).

Sample pH was determined within 24 hr using a spectrophotometric method developed for seawater pH (Byrne and Breland 1989). This method was selected over conventional potentiometric (glass pH electrode) methods because of the well-known drift and junction potential error that occurs in low ionic strength samples (Brezinski 1983; Herczeg and Hesslein 1984). In this procedure a 70 μL aliquot of 2.0 mM bromothymol blue solution (BTB) was added to 29 mL of the sample in a thermostated 10-cm pathlength optical cell. The solution absorbances were recorded with a Lambda 11 UV-VIS spectrophotometer (Perkin-Elmer Corp.) at the absorbance maxima of the acid (434 nm, A_1) and base (620 nm, A_2) forms of the indicator and at a reference wavelength (740 nm, A_r). The absorbance ratio (R) was calculated,

$$R = \left(\frac{A_2 - A_r}{A_1 - A_r} \right) \quad (2.4)$$

and used to calculate the solution pH (Byrne and Breland 1989):

$$\text{pH} = \text{p}K_a + \log \left[\frac{R - e_1}{e_2 - R \cdot e_3} \right] \quad (2.5)$$

where $\text{p}K_a$ is the indicator equilibrium constant, and e_1 , e_2 , and e_3 are ratios of the molar absorptivities of the indicator with values of 4.268×10^{-3} , 2.136, and 2.105×10^{-1} , respectively.

The $\text{p}K_a$ for BTB was determined by measuring the indicator absorbances in a low ionic strength (μ) buffer ($\mu=0.0100$ M; $\text{pH} = 7.684$ at 5°C) (Covington et al. 1983). The temperature dependence of the $\text{p}K_a$ was determined from the temperature-pH relationship of the buffer (Covington et al. 1983):

$$\text{p}K_a = \frac{278.0}{T} + 7.424 - 0.4324 \cdot \log(T) \quad (2.6)$$

where T is the temperature in Kelvin.

The accuracy of the freshwater spectrophotometric pH method is dependent upon the accuracy of the $\text{p}K_a$ and the pH perturbation that is caused by adding the weak acid indicator to the water sample (French et al. 2000). Note that the $\text{p}K_a$ represents an apparent dissociation constant, appropriate only for solutions that match the buffer μ . The buffer μ , however, is ~ 5 times greater than Placid Lake (~ 1.8 mM) and thus an error is introduced when using the apparent $\text{p}K_a$ for freshwater measurements. Using the extended Debye-Hückel equation (Stumm and Morgan 1996), relating activity coefficients to ionic strength, the activity coefficient correction is estimated to be $+0.06$ $\text{p}K_a$ unit, but it is highly uncertain because the actual ionic hydrated radii are unknown.

The other source of error, the pH perturbation, was examined by direct addition of the indicator solution to a lake water sample. A 0.016 pH unit decrease was observed by addition of 70 μL of 2.0 mM BTB.

Since preserving samples with HgCl_2 is a common practice in oceanographic studies (e.g., Cai et al. 1999) we chose to adapt this methodology here. Unfortunately, it was not discovered until after our final deployment that the addition of HgCl_2 to our samples adversely affected our pH measurements. The addition of mercury to a freshwater sample likely affects the pH in the following ways:

- 1) Hg^{2+} hydrolyzes water to form the $\text{Hg}(\text{OH})_2$ complex in solution which causes a decrease in sample pH
- 2) Hg^{2+} alters the perturbation of the sulfonephthalein indicator, which is used to determine the spectrophotometric pH of the sample, through complexation of the sulfur groups.

Uncertainty in the $\text{p}K_a$, along with the pH perturbation caused by addition of the indicator and mercuric chloride, resulted in significant uncertainty in the absolute pH.

The precision of the method, however, was excellent and, despite the uncertainty in its accuracy, allowed pH to be used in carbonate system calculations. The intra-sample reproducibility was typically ± 0.005 pH unit and the average inter-cast uncertainty was 0.010 ± 0.011 pH unit ($N=101$). See Chapter 2.5 for a discussion on carbonate system calculations using the DIC and spectrophotometric pH measurements.

It should be noted that an advantage of this pH method over electrochemical methods is that, once the uncertainties in the $\text{p}K_a$ and the effect of mercuric chloride are fully characterized, Equations 2.4 and 2.5 allow the recalculation of past pH

measurements. If, for example, it is determined that a pH electrode was incorrectly calibrated there is no way to go back and correct the data.

2.4.2 DO and temperature

The YSI Model 58, an analog instrument, was used to obtain most of the profile measurements of DO and temperature (Table 2.2; Appendix 2). Prior to each use, the KCl electrode solution was renewed and a new membrane was affixed to the electrode. The instrument was calibrated for DO in water-saturated air before profiling.

2.4.3 Winkler DO titrations

Winkler titration analyses for DO were only performed during the 1999 study. Two 250-mL amber glass bottles were filled with samples collected at each depth in the water column. The bottles were flushed with sufficient sample to fill the bottle three times in a manner that limited gas exchange. The samples were immediately preserved after collection and were analyzed upon return to the laboratory by the method outlined in Wetzel and Likens (1991). The method accuracy, based on the titration error, was estimated to be $\pm 2 \mu\text{mol L}^{-1}$ (0.06 mg L^{-1}). The average reproducibility for two analyses at each depth was $\pm 1 \mu\text{mol L}^{-1}$ (0.03 mg L^{-1}) (N=30).

2.4.4 Total alkalinity (TA)

Samples for TA analysis were taken from the DIC/pH sample bottles in 1999. TA was determined by a potentiometric titration technique with the Gran method for end-point determination (Edmond 1970). Prior to measurement, the electrode (Orion Research Inc., Ross Model 81-02) was allowed to soak in an aliquot of sample for a minimum of 1 hr. This procedure improved electrode stability and thus measurement accuracy and precision. A manual titrator (Denver Instruments, Model 285) was used to

deliver standardized hydrochloric acid to a special vessel designed to limit sample gas exchange with the atmosphere. The accuracy, determined with bicarbonate standards, and the average intra-sample reproducibility of duplicate measurements (N=5) were both $\pm 1 \mu\text{equiv L}^{-1}$.

2.4.5 Chlorophyll-*a*

Samples for chlorophyll-*a* were collected in 1999 in opaque 500 mL Nalgene bottles and filtered onto Whatman (GF/F) filter paper upon return to the laboratory. The filters with filtrate were either analyzed immediately or wrapped individually in aluminum foil and were frozen and analyzed within 2 weeks. The sample filters were macerated with a Teflon pestle/glass tube tissue grinder in a 90% (v/v) solution of acetone and saturated magnesium carbonate. The samples were clarified through centrifugation and analyzed with a benchtop spectrofluorometer (Shimadzu, Model RF-1501) calibrated with fresh spinach-derived chlorophyll-*a* standards. The samples were not corrected for pheophytin (e.g., APHA 1992; Welschmeyer 1994). The molar absorptivity for chlorophyll-*a* is $87.67 \text{ L g}^{-1} \text{ cm}^{-1}$ at 664 nm (Welschmeyer 1994). The average inter-sample precision of the method, based on two sample analyses per depth, was $\pm 4\%$ of the mean.

2.4.6 Nutrients

Samples were collected in 1999 for nutrient analysis and were analyzed for nitrate (cadmium reduction method) and inorganic phosphate (ascorbic acid method) within 48 hr (APHA 1992). Dr. Richard E. Juday, University of Montana Emeritus Professor of Chemistry, performed all nutrient analyses. The reported NO_3^- -N and PO_4^{3-} -P method detection limits are 1 and $0.2 \mu\text{g L}^{-1}$, respectively.

2.4.7 Cations

Samples for cation analysis were acidified with nitric acid and analyzed within two weeks with an atomic absorption spectrophotometer (AAS, Unicam, Model 969). The AAS was calibrated with four acidified standards about the expected concentration range. The intra-sample precision of the methods, based on five measurements per sample, was ± 0.40 and ± 0.16 % of the means for calcium and magnesium, respectively (N=24). Calcite saturation was calculated to determine if the lake was under- or supersaturated with respect to calcite. The temperature-dependent calcite solubility product (K_c) at infinite dilution was calculated with (Jacobson and Langmuir 1974):

$$\log K_c = 13.870 - \frac{3059}{T} - 0.04035 \cdot T \quad (2.7)$$

where T is the temperature in K. Concentrations of CO_3^{2-} were calculated from DIC and TA (see Chapter 2.5). The activity coefficients for Ca^{2+} and CO_3^{2-} were estimated to both be 0.85 at $\mu = 1.8$ mM (Table 3.4 in Stumm and Morgan 1996). The calcite saturation ratio (Ω) was calculated as:

$$\Omega = \frac{\gamma_{\text{Ca}^{2+}} \cdot [\text{Ca}^{2+}] \cdot \gamma_{\text{CO}_3^{2-}} \cdot [\text{CO}_3^{2-}]}{K_c} \quad (2.8)$$

where γ is the activity coefficient for the subscripted ion and a value greater than one indicates supersaturation.

2.4.8 Chromophoric dissolved organic matter (CDOM)

CDOM absorbance was determined with a Lambda 11 UV-VIS spectrophotometer (Perkin-Elmer Corp.). Absorption spectra were obtained from 750 to 250 nm in a 10-cm pathlength cell on aliquots from the DIC/pH sample bottles. Deionized water was used as the blank. The absorbance data were baseline corrected

using the average absorbance from 700 to 750 nm and were then converted to spectral absorption coefficients, $a(\lambda)$ (Green and Blough 1994),

$$a(\lambda) = 2.303 \cdot \frac{A(\lambda)}{l}. \quad (2.9)$$

where $A(\lambda)$ is the absorbance and l is the cell pathlength in meters. A wavelength of 340 nm was chosen to illustrate the variability of the CDOM with time.

2.4.9 Photometry

An analog photometer (Protomatic Inc., Model 1) was used to measure profiles of underwater illumination. The illuminance in foot-candles was converted to units of irradiance by the following conversion: 1 ft-candle = 10.764 lumen m⁻² = 1.610 x 10⁻² W m⁻². These data provided a measure of lake transparency and were used to calculate extinction coefficients via the Lambert-Beer absorption law:

$$I_z = I_o e^{-\eta z} \quad (2.10)$$

where I_z is the irradiance at depth z , I_o is the irradiance at the lake surface, and η is the extinction coefficient.

2.4.10 Optical Transparency

Secchi disk measurements provide a measure of lake transparency and were a good approximation of the depth where 10% of the ambient light intensity remained. Albeit simple, this measurement has been used to classify lakes on their trophic status (e.g., Stefan and Fang 1994). The transparency of the lake is affected by suspended sediment, colored dissolved organic matter (e.g., humic substances), and plankton (as well as detritus). Secchi depths are listed in Table 2.2.

2.5 Carbonate system calculations

Any two of the four carbonate parameters (DIC, pH, TA, and $p\text{CO}_2$) can be calculated from the other two. The DIC and pH combination was used to calculate $p\text{CO}_2$ in this study. An in-house QuickBasic (Microsoft Corp.) program entitled *FreshH₂O CO₂* was written for carbonate system calculations in freshwater (Appendix 3). This simplified program was adapted from an earlier version of a more comprehensive program for carbonate system calculations in seawater (*CO2SYS*, Lewis and Wallace 1998). The *FreshH₂O CO₂* carbonic acid dissociation constants at infinite dilution were obtained from Millero (1979) and the CO_2 solubility-temperature relationship from Weiss (1974). The procedure for calculating $p\text{CO}_2$ from DIC and pH was to first input the measured DIC and pH to calculate TA at the pH measurement temperature (typically 4 °C) and then input the calculated TA with the DIC to calculate the $p\text{CO}_2$ at the *in situ* temperature. These calculations assume TA is 100% carbonate alkalinity and are supported by measurements made in 1999. However, such calculations may be questionable during spring runoff when significant concentrations of organic acids may be present (Juday and Keller 1980).

In the 1999 study the carbonate system was over-determined because three of the four carbonate parameters (DIC, pH, and TA) were measured. This allowed us to check the internal consistency of our measurements and to verify the long-term stability of the *in situ* $p\text{CO}_2$ measurements in this deployment. The $p\text{CO}_2$ was calculated from:

- 1) the TA and DIC at the *in situ* temperature,
- 2) the calculated DIC (from TA and pH at the pH measurement temperature) and pH at the *in situ* temperature, and

- 3) the calculated TA (derived from DIC and pH at the pH measurement temperature) and DIC at the *in situ* temperature.

The results of these calculations are plotted with the surface *in situ* $p\text{CO}_2$ (Figure 2.2). There is good agreement between the DIC/pH and the TA/pH combinations for $p\text{CO}_2$ ($\pm 34 \mu\text{atm}$; $N=7$) and their trend follows the *in situ* $p\text{CO}_2$. An offset exists between the calculated and the *in situ* $p\text{CO}_2$ because of the pH inaccuracy, but the offset is relatively constant ($515 \pm 80 \mu\text{atm}$) because of the excellent reproducibility of the pH measurement (Chapter 2.4.1). There is no evidence of a systematic decrease or increase in the difference between the calculated and *in situ* $p\text{CO}_2$ providing additional evidence that the SAMI- CO_2 was stable. These carbonate calculations also support the assumption that TA is 100% carbonate alkalinity. If organic acids were present in significant concentrations, the alkalinity-derived $p\text{CO}_2$ would differ from the DIC-derived $p\text{CO}_2$ since organic acids affect alkalinity but not DIC. In contrast to the other combinations for $p\text{CO}_2$, TA/DIC gave erratic results because these two carbonate parameters are tightly coupled and small errors in either lead to large errors in $p\text{CO}_2$. Dickson and Riley (1978), in a study of the aquatic CO_2 system in seawater, also showed that $p\text{CO}_2$ cannot be calculated reliably from the TA/DIC combination. The $p\text{CO}_2$ calculations for the measurements made near the lake bottom are not presented because the same conclusions can be drawn.

A constant offset of $-149 \mu\text{atm}$ was applied to the calculated $p\text{CO}_2$ in the 1997 and 1998 winter deployments (Figures 3.1, 3.2). In 1999, offsets of -504 and $-574 \mu\text{atm}$ were applied to the calculated $p\text{CO}_2$ at the surface and bottom, respectively (Figure 4.1).

The analytical precision for $p\text{CO}_2$ calculated from inter-cast averaged DIC and pH was determined to be 3.7% ($N=101$). This precision is limited by the DIC measurement

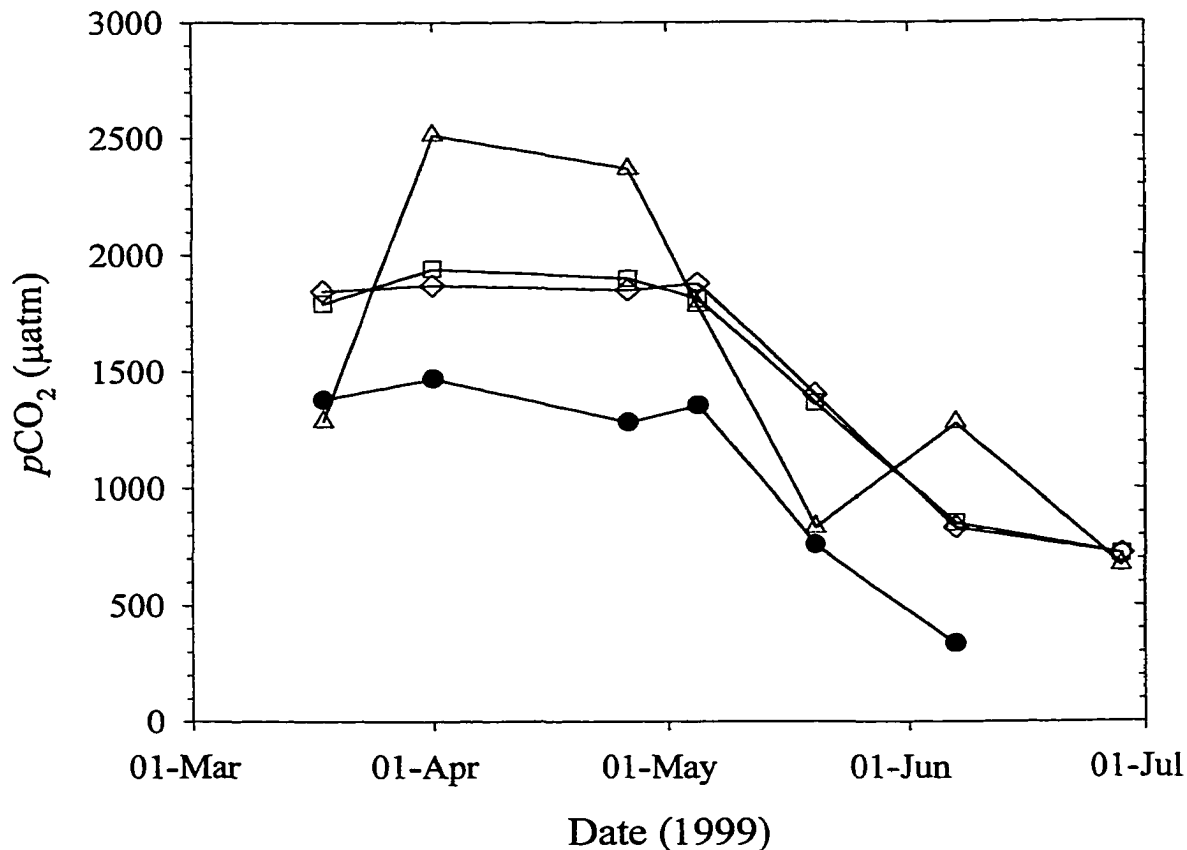


FIGURE 2.2: The measured and calculated $p\text{CO}_2$ at 2 m in Placid Lake. The closed circles represent an average of SAMI- CO_2 measurements taken within 2 hrs of the sample casts. The DIC/TA combination for $p\text{CO}_2$ (triangles) had the most scatter for reasons given within the text. The TA/pH (squares) and DIC/pH (diamonds) combinations for $p\text{CO}_2$ matched well and their relatively constant offset from the *in situ* $p\text{CO}_2$ indicate that there was minimal, if any, drift in the SAMI- CO_2 . The good agreement between the TA/pH and DIC/pH-derived $p\text{CO}_2$ also indicate that organic acids were not present in significant concentrations.

precision and is skewed somewhat higher by the inclusion of samples near the lake bottom that contained a lot of suspended particulates.

Future refinements in the pH method, including better estimates of the pK_a and elimination of mercuric chloride, should improve the pH accuracy and reduce or eliminate the $p\text{CO}_2$ offset found in the present work. Importantly, previous freshwater

$p\text{CO}_2$ equilibria calculations based on pH have been of limited utility because of irreproducibility in electrode-based pH measurements (Herczeg and Hesslein 1984). Although not yet perfected, and perhaps only applicable to buffered waters, the spectrophotometric method is an appealing alternative to glass electrode measurements.

In addition to calculating $p\text{CO}_2$, the periodic DIC and pH measurements were used to calculate TA. TA was needed to convert the continuous $p\text{CO}_2$ records into continuous DIC for estimates of CO_2 accumulation rates, as presented in Chapter 3. To obtain continuous DIC from the $p\text{CO}_2$ records, a mean TA of 1171 and 1051 $\mu\text{eq kg}^{-1}$ was used for the under-ice 1997 and 1998 studies, respectively (Chapter 3).

2.6 Other supporting data

2.6.1 Regional meteorology and river discharge

Daily high and low temperature and total daily precipitation data were obtained from the USDA Forest Service Seeley Lake Ranger District Station, 10 km N of Placid Lake. The time when the daily high and low temperatures occurred was estimated from temperatures recorded at Missoula, Montana. An air temperature time-series was produced from the daily high and low via linear interpolation between these times. Wind speed, barometric pressure, relative humidity, and cloud cover estimates were obtained from a NOAA National Data Center site at Johnson-Bell Field in Missoula, Montana. River discharge data were obtained for the Swan River at Bigfork, Montana (USGS Station 12370000) in the Swan drainage ~32 km N of Placid Lake. These data were used as a proxy for trends in Placid Creek discharge.

Placid Creek and Owl Creek (Figure 1.2) discharge measurements were made with a Marsh-McBirney, Inc. Model 2000 portable flow meter (courtesy of Andrew L. Sheldon, Division of Biological Sciences, The University of Montana) on 4 Aug 1998 and 14 Apr 1999. Owl Creek discharge was also measured on 5 Apr 1997. Past discharge data for Owl Creek were obtained from Vadeboncoeur (1988). These data were used to estimate an average annual discharge of $1.2 \text{ m}^3 \text{ s}^{-1}$ which translates into a hydrologic residence time of ~ 2 yr for Placid Lake. The Owl Creek outflow was slightly less than Placid Creek inflow on the 2 occasions when discharge was measured at both sites (Table 2.3). The differences between the two discharges are in line with estimated evaporation rates (Chapter 2.7.1). Although admittedly limited, these data indicate that groundwater inputs into the lake are minimal. However, it should be noted that discharge measurements are typically in error 5-10%. Consequently, groundwater flux could contribute as much as 10% of the total without being detected.

2.6.2 Local meteorology

Wind speed, wind direction, and atmospheric $p\text{CO}_2$ were measured in 1999 with an autonomous meteorological system stationed in an open meadow near the NW shoreline of Placid Lake (Figures 1.2, 2.3). Ideally this station would have been placed on a platform at the mooring site, but this was not possible due to the problems associated with ice-out and because of its vulnerability to vandalism. The autonomous meteorological system included a Campbell Scientific wind sentry set, consisting of a cup anemometer and wind vane (R.M. Young, Model 03001-5), a non-dispersive infrared instrument (NDIR) for CO_2 (LICOR, Inc., Model LI-6251), and a data logger (Onset Computer Corp., Tattletale Model 4A). A solar panel maintained the charge of two 12-

TABLE 2.3: A summary of the Placid and Owl Creek data.

Location & Date	Discharge (m ³ s ⁻¹)	Temperature (°C)	DO (mmol m ⁻³)	DO %Sat'n	DIC (mmol m ⁻³)	pH	TA (meq m ⁻³)
Placid Creek							
04 Aug 98	0.73	16.5	232.8	89	NA	NA	NA
14 Apr 99	3.17	2.6	368.8	101	NA	7.358	678
26 Apr 99	NA	NA	NA	NA	568	7.512	529
05 May 99	NA	5.2	343.8	100	717	7.427	625
20 May 99	NA	8.9	337.5	108	851	7.518	800
07 Jun 99	NA	9.2	325.0	105	1414	7.821	1292
28 Jun 99	NA	10.1	309.4	102	1794	7.820	1681
Owl Creek							
05 Apr 97	4.22	NA	NA	NA	NA	NA	NA
04 Aug 98	0.72	21.5	191.3	81	NA	NA	NA
14 Apr 99	3.03	5.9	315.6	94	NA	NA	NA

volt batteries used to power the system. The wind sensors were mounted on a cross arm supported at a height of 4.0 m above ground (Figure 2.3) and were interfaced to a circuit board assembly (R.M. Young, P/N 03605BP) that provided calibrated analog DC voltage signals for wind speed and wind direction. The interface board was hardwired to the data logger within the weatherproof atmospheric CO₂ system housing.

Wind speed and wind direction were recorded every half-hr and wind speed (U) was extrapolated to a height of 10 m by the equation (Jensen et al. 1990)

$$U_{10} = U_4 \cdot [10/4]^{0.2}. \quad (2.11)$$

The software used to control the weather station was adapted from the SAMI-CO₂ control software and is presented in Appendix 4.

Ambient air was introduced to the atmospheric system via a pump and valve system controlled by the data logger. The mole fraction of CO₂ (X_{CO_2}) in air was

measured with the NDIR every hr and linear interpolation was used to obtain estimates on the half-hr. The atmospheric $p\text{CO}_2$ was calculated from the X_{CO_2} using the barometric pressure recorded at Missoula, MT offset by the barometric pressure fraction due to differences in altitude (pressure) between Missoula and Placid Lake (~ 0.89 vs. 0.86 atm). Pre- and post-deployment calibrations with a 360 ± 1 ppm NIST-traceable CO_2 gas standard showed a downward drift of 1% in the NDIR CO_2 measurements (negligible for this study).



FIGURE 2.3: Photograph of the meteorological station (looking southeast). The mid-lake mooring is 1.5 km distant at a bearing of 103° from north (Figure 1.2). The NDIR and data logger are housed within the weatherproof gray box on the support platform.

2.7 Physical and biogeochemical models

This section pertains only to the comprehensive 1999 study (Chapter 4), which included physical and biogeochemical modeling for comparison to the *in situ* time-series. These models were required to quantify the contributions of various processes to biogeochemical variability (see Research objectives, Chapter 1.3). The surface energy budget (SEB) for Placid Lake had to be calculated for input into the physical model used to describe the thermal structure of the lake (see Chapter 2.7.2). Descriptions of the SEB calculations of the lake, the physical model, and the biogeochemical models follow.

2.7.1 Air-water fluxes and meteorology

The hydrodynamics and thermodynamics of a water body are dependent on the available energy both at the surface and at depth. Therefore, to model the thermal stratification of a water body, it is necessary to evaluate the SEB and the subsurface absorption of solar radiation. The SEB is based on measured and calculated meteorological parameters and can be expressed as

$$\phi_N = \phi_S - \phi_{Lo} + \phi_{Li} - \phi_{NR} \quad (2.12)$$

where ϕ_N is the net surface energy flux, ϕ_S is the net solar shortwave radiative flux (after reflective losses), ϕ_{Lo} is the outgoing longwave radiative flux, ϕ_{Li} is the net incoming longwave radiative flux (after reflective losses), and ϕ_{NR} is the net non-radiative energy flux. The last term is a sum of the latent (evaporative) energy loss (ϕ_e) and sensible (conduction and convection) heat transfer (ϕ_h). The energy exchanges associated with condensation are much smaller than those associated with evaporation and are ignored.

The net solar shortwave radiative flux (waveband ~0.3 to 4 μm) was estimated as in Stull (1988) with

$$\phi_s = [S \cdot T_k \cdot \sin(Y)] \cdot (1 - A_s) \quad (2.13)$$

where S is the solar constant with a value of 1380 W m^{-2} , T_k is the net transmissivity of the sky, Y is the local solar altitude angle, and A_s is the diel shortwave albedo (reflectivity). The T_k was assigned a value from 0.8 for a cloud free sky to 0.1 for a completely overcast sky. It was assumed that the cloud cover measured at Johnson-Bell Field in Missoula, MT was indicative of the cloud cover at Placid Lake. The local solar angle is given by

$$\sin(Y) = \sin(lat) \cdot \sin(D) - \cos(lat) \cdot \cos(D) \cdot \cos\left[2\pi \cdot \frac{t}{24} - long\right] \quad (2.14)$$

where lat and $long$ are the latitude and longitude in radians, respectively, t is the time in hours UTC, and D is the solar declination angle (radians). The declination angle is given by

$$D = 0.409 \cdot \cos\left[2\pi \cdot \frac{YD - 173}{365.25}\right] \quad (2.15)$$

where YD is the year day. The diel shortwave albedo as a function of time of day was calculated with (Henderson-Sellers 1986)

$$A_s = \frac{a}{a + \sin(Y)} \quad (2.16)$$

where a is the fraction of sky obscured by cloud cover (C) given by

$$a = 0.02 + 0.01 \cdot (0.5 - C) \cdot \left[1 - \sin\left(\pi \cdot \frac{YD - 81}{183}\right)\right]. \quad (2.17)$$

The net incoming atmospheric longwave radiation (waveband ~4 to 50 μm) was calculated with

$$\theta_{Li} = [\varepsilon_a \cdot \sigma \cdot T_a^4] \cdot (1 - A_L) \quad (2.18)$$

where ε_a is the effective atmospheric emissivity, σ is the Stefan-Boltzmann constant ($5.67051 \times 10^{-8} \text{ W m}^{-2} \text{ K}^{-4}$), T_a is the air temperature (K), and A_L is the longwave albedo assumed constant at 0.03 (Henderson-Sellers 1986). The emissivity of the atmosphere, which is defined as the ratio of the energy flux emitted at a given wavelength and temperature to that emitted by a blackbody at the same wavelength and temperature, was calculated by

$$\begin{aligned} \varepsilon_a = & 0.84 - (0.1 - 9.973 \times 10^{-6} \cdot e_a) \cdot (1 - C) \\ & + 3.491 \times 10^{-5} \cdot e_a \quad C \geq 0.4 \end{aligned} \quad (2.19)$$

$$\begin{aligned} \varepsilon_a = & 0.87 - C \cdot (0.175 - 29.92 \times 10^{-6} \cdot e_a) \cdot (1 - C) \\ & + 2.693 \times 10^{-5} \cdot e_a \quad C \leq 0.4 \end{aligned} \quad (2.20)$$

where e_a is the air vapor pressure (kPa) (Hostetler and Bartlein 1990). The air vapor pressure (N m^{-2}) was determined with

$$e_a = e_{sa} \cdot RH \quad (2.21)$$

where RH is the relative humidity fraction and e_{sa} is the saturation vapor pressure of the air determined with (Henderson-Sellers 1984):

$$e_{sa} = 2.1718 \times 10^{10} \cdot \exp\left(\frac{-4157}{T_a - 33.91}\right) \quad (2.22)$$

The outgoing longwave radiative flux was calculated from the surface water temperature (T_w , in K) and the emissivity of the water ($\epsilon_w = 0.97$) using the Stefan-Boltzmann law,

$$\phi_{Lo} = \epsilon_w \cdot \sigma \cdot T_w^4 . \quad (2.23)$$

The flux of evaporative or latent energy was determined with

$$\phi_e = \rho \cdot L_v \cdot E \quad (2.24)$$

where ρ is the surface water density, L_v is the latent heat of vaporization of water, and E is the evaporation rate. The latent heat of vaporization of water was calculated with (Henderson-Sellers 1984):

$$L_v = 1.91846 \times 10^6 \cdot \left(\frac{T_w}{T_w - 33.91} \right)^2 . \quad (2.25)$$

The evaporation rate (m s^{-1}) was determined by the method of Sill (1983),

$$E = 1.15 \times 10^{-8} \cdot C_D \cdot U \cdot (1 + a_l \cdot C_R) (e_{sw} - e_a) \quad (2.26)$$

where C_D is the aerodynamic drag coefficient (see Equation 2.32), U is wind speed, e_{sw} is the saturation vapor pressure at the lake surface (Equation 2.22 with T_w substituted for T_a), C_R is the ratio of the free and forced convection Dalton numbers, and

$$a_l = 0.73 \cdot C_R \quad C_R \leq 1.37 \quad (2.27)$$

$$a_l = 1 \quad C_R \geq 1.37$$

and

$$C_R = \frac{0.0017 \cdot (T_w - T_a)^{1/3}}{C_D \cdot U} \quad (2.28)$$

$$C_R = 0 \quad \text{if } T_w < T_a.$$

The flux of sensible heat was determined with a Bowen ratio approach, which relates the evaporative and sensible energy terms through a Bowen convection ratio (R),

$$\phi_h = R \cdot \phi_e. \quad (2.29)$$

The Bowen convection ratio was determined with (e.g., Hostetler and Bartlein 1990)

$$R = \gamma \cdot \frac{(T_w - T_a)}{(e_{sw} - e_a)} \quad (2.30)$$

where γ is the psychrometric constant, which is a function of L_v and the barometric pressure (see Jensen et al. 1990).

Shortwave solar radiation was absorbed within the water column with double exponential depth dependence (Price et al. 1986),

$$I_z = I_o \cdot [I_1 \cdot \exp(-z/\lambda_1) + I_2 \cdot \exp(-z/\lambda_2)] \quad (2.31)$$

where the subscripts 1 and 2 refer to the surface-absorbed and penetrating components of the shortwave radiation at the lake surface, I_o . The surface-absorbed solar radiation (I_1) was calculated as 60% of the total with an extinction scale (λ_1) of 0.6 m. The remaining 40% was designated as the penetrating solar radiation (I_2) with an extinction scale (λ_2) of 2 m determined from the average of the measured irradiance extinction coefficients ($1/\lambda_2$).

Wind stress (τ) was calculated as

$$\tau = \rho_a \cdot C_D \cdot U^2 \quad (2.32)$$

where $\rho_a = 1.06 \text{ kg m}^{-3}$ is the density of air at 1256 m, C_D (1.2×10^{-3}) is the aerodynamic drag coefficient for neutral conditions (Large and Pond 1981), and U is the wind velocity (m s^{-1}) at 10 m. The physical model (see Chapter 2.7.2) requires the east

and north vector components of the wind stress and these were determined from the wind direction measurements.

When modeling ice-covered conditions, the wind stress and longwave and latent heat fluxes between the air and water were set equal to zero and only the penetrating portion of the shortwave radiation term of the SEB was input into the model (Equation 2.31). The shortwave radiation at the ice-water interface was estimated from the underwater PAR (Chapter 2.3.2), ice thickness, and the extinction coefficients of the water and ice (Chapter 2.4.9).

2.7.2 Physical model

A one-dimensional (vertical) mixed-layer model developed for the upper ocean (PWP model, Price et al. 1986) was adapted for a freshwater lake. The modified PWP model for freshwater was written in Visual FORTRAN V6.0. The PWP model is an integral (or bulk) mixed-layer (ML) stratification model that is an extension of the dynamic instability model (DIM) of Price et al. (1978). Conventional integral ML models assume that there is a sharp discontinuity in density and velocity at the thermocline boundary, which results in unrealistic temperature profiles (Henderson-Sellers and Davies 1989). The PWP model addresses this issue by mixing beneath and across the mixed-layer boundary until a critical value of the gradient Richardson number is met ($R_g \geq 0.25$). This has an effect of smoothing out the sharp jumps at the interface to more realistically simulate observed temperature profiles. For an excellent review of thermal stratification modeling of lakes and oceans see Henderson-Sellers and Davies (1989).

It should be noted that 1-D eddy diffusion models are more commonly used for thermal stratification modeling of lakes because of their relative simplicity. Eddy diffusion models can be used to simulate the behavior and distribution of substances within the water column but are limited to substances that are uniformly distributed with temperature in the water column. Hostetler (1995) points out that many nutrients and chemical species are not uniformly distributed with temperature and are better modeled by ML models because they are able to account for the high-frequency variability of turbulent mixing.

The turbulent kinetic energy (TKE) budgets and momentum parameterizations implemented within the ML model are described in detail in Price et al. (1986). Unlike the marine version of the PWP model, which uses a linear state equation for density, the full nonlinear equation of state for density was used to describe freshwater (Chen and Millero 1986). As with all integral models, the existence of a homogeneous ML is assumed. The ML thickness was defined as the depth above which density is homogeneous to 0.1 g m^{-3} . The model was run with an 1800 s time-step commensurate with the measurement frequency of the *in situ* instrumentation. Temperature and mixed-layer depth (MLD) was output by the physical model with a depth resolution of 0.1 m. The MLD was implemented in the mixing and air-water gas exchange parameterizations within the dissolved gas models.

2.7.3 Biogeochemical models

The mass balance for the dissolved gases at the surface can be expressed as:

$$H \cdot dC/dt = F_{GAS} + F_{BIOL} + F_{ENT} + F_{ADV} \quad (2.33)$$

where H is the MLD and dC/dt is the rate of change of the dissolved gas due to contributing fluxes of air-water gas exchange (F_{GAS}), biology (F_{BIOL}), vertical advection or entrainment (F_{ENT}), and horizontal advection (F_{ADV}). Horizontal advection is assumed to be minor relative to the other terms because the lake has little flow through (Chapter 2.6.1).

The pCO_2 model was initiated by using the initial pCO_2 and DIC to calculate TA with an in-house QuickBasic (Microsoft Corp.) program for carbonate system calculations. At each subsequent time-step the DIC and TA were incremented according to the contributions from air-water gas exchange, production and respiration, and entrainment. The pCO_2 was then solved iteratively from the new DIC, TA, and *in situ* temperature. The effects of heating and cooling on the pCO_2 are intrinsic in the model because the carbonate equilibrium and Henry's law constants are calculated as a function of temperature.

The same processes were considered in the DO model, yet it is comparatively simple because DO exists in only one dissolved form. The different CO_2 and O_2 parameterizations of air-water gas exchange, biology, and entrainment in the dissolved gas models are discussed below.

2.7.3.a Air-water gas exchange

The rate of exchange of CO_2 and O_2 across the air-water interface can be expressed in terms of Fick's law:

$$F_{GAS} = K_T \cdot S \cdot \Delta P \quad (2.34)$$

where K_T is the gas transfer coefficient, S is the solubility of the gas in water (Weiss 1970, 1974) and ΔP is the difference between the partial pressure of the gas in air and

water. Cole and Caraco (1998) developed a relationship between K_T (Schmidt number = 600) and wind speed at 10 m (U_{10}) from data collected at a number of freshwater lakes:

$$K_T = 2.07 + 0.215 U_{10}^{1.7} . \quad (2.35)$$

The relationship between K_T (cm s^{-1}) for different gases can be described with (Jähne et al. 1987):

$$K_{T \text{ gas1}} / K_{T \text{ gas2}} = (\text{Sc}_{\text{gas1}} / \text{Sc}_{\text{gas2}})^n \quad (2.36)$$

where Sc is the temperature-dependent Schmidt number and $n = -\frac{1}{2}$ for intermediate wind speeds (Wanninkhof 1992). Equations 2.35 and 2.36 and the Sc -temperature relationships for gases in freshwater (Wanninkhof 1992) allowed the calculation of K_T for both CO_2 and O_2 as a function of temperature. The measured atmospheric and modeled *in situ* surface $p\text{CO}_2$ were used to determine ΔP . The mole fraction of DO in the atmosphere was assumed constant at 0.20946. The gas fluxes were converted to volumetric rates by dividing by the MLD (H , Equation 2.33).

2.7.3.b Photosynthesis and respiration

The photosynthetic rate as a function of irradiance, chlorophyll, and temperature was calculated with the modified exponential model of Platt et al. (1980):

$$P = [\text{Chl} \cdot (P_s \text{ Chl}^{-1}) \cdot (1 - e^{-a}) \cdot e^{-b}] \cdot \theta_p^{(T-3)} \quad (2.37)$$

where P is the rate of photosynthesis ($\text{mg C m}^{-3} \text{ hr}^{-1}$), Chl is the concentration of chlorophyll- a (mg m^{-3}), $P_s \text{ Chl}^{-1}$ is the assimilation number or chl-specific maximum rate of photosynthesis in the absence of photoinhibition ($\text{mg C mg Chl}^{-1} \text{ hr}^{-1}$), $a = [(\alpha \text{ Chl}^{-1}) \cdot Q_{\text{PAR}} \cdot (P_s \text{ Chl}^{-1})]$, $b = [(\beta \text{ Chl}^{-1}) \cdot Q_{\text{PAR}} \cdot (P_s \text{ Chl}^{-1})]$, $\alpha \text{ Chl}^{-1}$ is the chl-specific rate of light limited photosynthesis ($\text{mg C mg Chl}^{-1} \text{ hr}^{-1} (\mu\text{E m}^{-2} \text{ s}^{-1})^{-1}$), $\beta \text{ Chl}^{-1}$ is

the chl-specific photoinhibition parameter (same units as $\alpha \text{ Chl}^{-1}$), and Q_{PAR} is the downwelling PAR ($2\pi, \mu\text{E m}^{-2} \text{ s}^{-1}$). The Chl and Q_{PAR} parameters were both measured at a depth of 2 m. A value of 1.036 was used for the Arrhenius temperature coefficient (θ_p) to account for the effect of temperature (T) on photosynthesis (Parkhill and Gulliver 1999). Van Duin and Lijklema (1989) report a similar value of 1.03 for θ_p . *Alpha* ($\alpha = 0.2 \text{ mg C m}^{-3} \text{ hr}^{-1} (\mu\text{E m}^{-2} \text{ s}^{-1})^{-1}$), the initial slope of the photosynthesis-irradiance curve, was estimated by averaging the initial slopes of DO, in terms of carbon, in periods when biology was believed to be controlling DO. Note that a constant α was also used in Jewell (1995). The β that provided the best overall fit to the dissolved gases was 0.02 (same units as α).

An assimilation number ($P_s \text{ Chl}^{-1}$) of 2.50 was used in the model except for during turnover and a post-turnover period of episodic mixing to great depth when smaller values, 1.00 and 1.25, respectively, were used. The dates when the assimilation number was changed in the models are summarized in Table 4.1. These assimilation numbers are within the range reported for other studies (e.g., Prézelin et al. 1991; Fee et al. 1992; Carignan et al. 2000).

The rate of heterotrophic respiration (R) as a function of temperature (T) was determined with a modified Arrhenius equation:

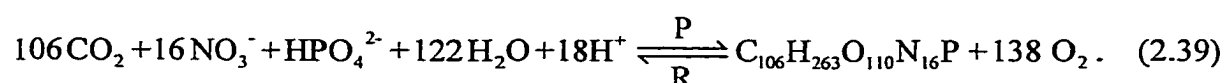
$$R = R_3 \cdot \theta_R^{(T-3)} \quad (2.38)$$

with a value of 1.045 used for the temperature coefficient, θ_R (Parkhill and Gulliver 1999). The respiration rate at 3 °C, R_3 , used for the surface and bottom models was 2.10 and 0.36 $\text{mg C m}^{-3} \text{ hr}^{-1}$, respectively. These respiration rates are within the range of

reported values for other lakes (e.g., del Giorgio and Peters 1993). Respiration rates are typically greater where photosynthesis is occurring in the water column because of phytoplankton photorespiration and dark respiration (Geider 1992).

Note that the difference between the rates of net primary productivity (Equation 2.37) and community respiration (Equation 2.38) is a measure of net community production (Chapter 1.4.1.b).

Conversion between rates of photosynthetic carbon (Equation 2.37) and O_2 was accomplished using Redfield stoichiometry for photosynthesis (P) and respiration (R) (Stumm and Morgan 1996):



Changes in TA that result from biological processes were also estimated using Redfield stoichiometry. For every mole of CO_2 assimilated or respired the model TA was increased or decreased by 18/106 equivalent, respectively.

2.7.3.c Entrainment

Surface ML entrainment (vertical advection) is based on a modified two-box model approach. Out of necessity, the minimum ML is set at 2 m to keep the surface sensors within the top box. Entrainment into the surface 2 m occurs when the ML deepens. There is no change in the modeled surface dissolved gases when the ML shoals. The average concentrations of DO and DIC in the volume of water entrained into the ML (C_E) were estimated by linearly interpolating between the modeled surface (2 m, C_S) and bottom (20 m, C_B) concentrations with:

$$C_E = \frac{1}{2} \cdot \left[\left(\frac{MLD_f - MLD_i}{H_B - MLD_i} \right) \cdot (C_B - C_S) \right] + C_S \quad (2.40)$$

where H_B is the bottom depth and the subscripts i and f refer to the initial and final MLD, respectively. The assumption that DIC and $\dot{D}O$ concentrations vary linearly between the surface and bottom is justified because the linear least squares coefficient of determination (r^2) for the five DO and DIC profiles from 1 Apr to 7 Jun ranged from 0.61 to 0.98 and 0.56 to 0.96, respectively (Figure 2.4). A simple algorithm was used to determine the net contribution of entrainment to the dissolved gas concentrations (C_N) in the ML:

$$C_N = \left(C_E \cdot \left(\frac{ML_{vf} - ML_{vi}}{ML_{vf}} \right) + C_S \cdot \left(\frac{ML_{vi}}{ML_{vf}} \right) \right) - C_S \quad (2.41)$$

where the subscripts Vi and Vf refer to the initial and final ML volumes, respectively. Lake volume as a function of depth was determined using the lake bathymetry (Figure 1.2).

The MLD predicted by the PWP model for the 1999 data (Chapter 4) was at times too dynamic (the model mixed too frequently) when weak thermal stratification existed. This is due to the sensitivity of the model to the diurnal pycnocline, which develops during periods of low wind shear and high buoyancy, and the somewhat arbitrary but constant degree of density homogeneity that defines the ML. For example, on occasion the modeled MLD varied from 10 to 2 m and back again within a 1-hr time period. The interpolation routine assumes that the concentration gradients are reestablished instantaneously, so when the MLD returns to 10 m from 2 m, the ML concentrations are skewed toward bottom water values. The net result is the model predicts DO and pCO_2

that are substantially lower and higher, respectively, than measured. In the PWP model the ML is modeled as a slab with instantaneous mixing when in reality mixing is a slower process. Therefore, to reduce the high frequency MLD variability and to more realistically model entrainment, a 3-hr “reset” or lag time criteria was imposed so that the ML would only shoal if 3 hrs had elapsed from the last change in MLD.

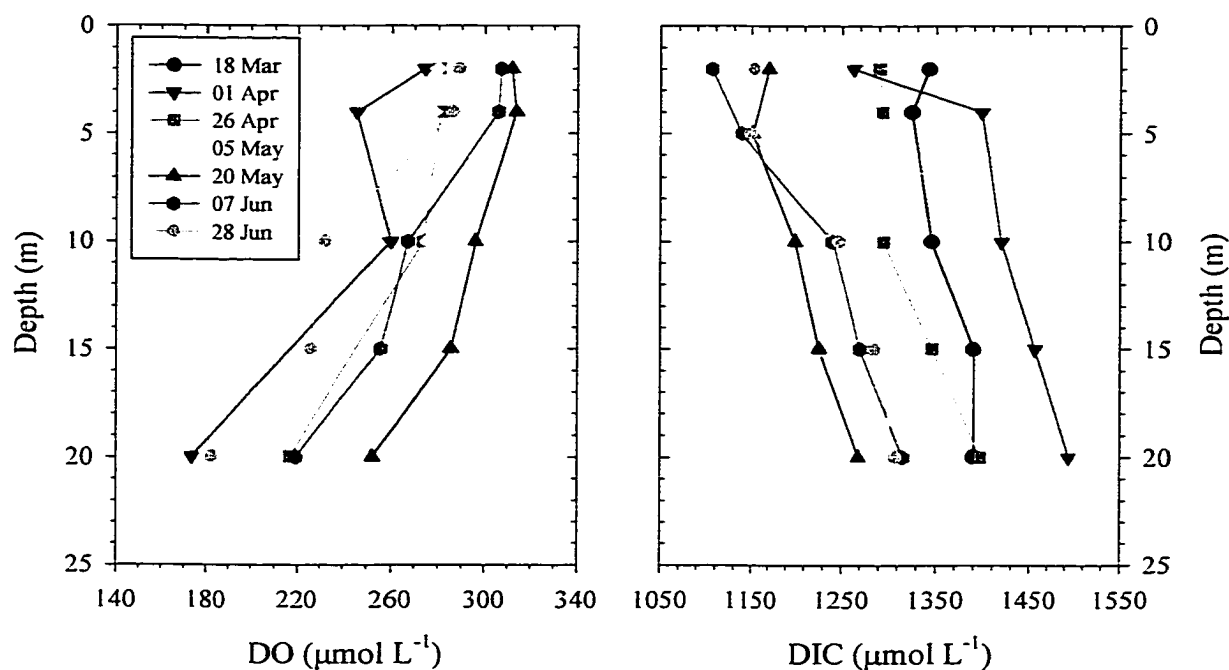


FIGURE 2.4: The profile measurements of DO (left panel) and DIC (right panel) in 1999. The legend in the left panel applies to both panels.

Chapter 3

Under-Ice CO₂ and O₂ Variability in 1997 and 1998

The objective for the studies presented in this chapter was to characterize short-term biogeochemical variability during ice-covered periods, determine its relationship to physical forcings, and evaluate its importance in the observed seasonal trends.

To accomplish this goal, *in situ* sensors for $p\text{CO}_2$, DO, PAR, temperature and depth were deployed on the mid-lake mooring (Table 2.1; Figure 1.2). Samples for DIC and pH were obtained at 2, 5, 10, 15, and 20 m depths on 8 Jan, 3 Feb, 23 Feb, and 17 Mar in 1997 and on 9 Feb and 3 Mar in 1998 (Table 2.2; Appendix 2). Detailed methods are given in Chapter 2.

3.1 Results

3.1.1 Conditions during winter 1997 and 1998

Ice cover records from USDA Forest Service personnel for Seeley Lake 10 km to the north, which often freezes and thaws within a few days of Placid Lake (E. Keller, pers. comm. 1999), were used to estimate Placid Lake ice cover. Based on these observations, ice cover lasted from ~12 Dec 1996 to 19 Apr 1997 for a total of 128 days. Ice cover was 11 days shorter in the second study year, extending from ~19 Dec 1997 to 15 Apr 1998. A summary of the meteorological conditions over these time periods is given in Table 3.1. Total 1997 snowfall was one of the greatest on record, whereas 1998

experienced average snowfall. The 1997 winter was also colder than the same period in 1998 by an average of 2.9 °C (Table 3.1).

TABLE 3.1: Meteorological conditions summary.

Period	Total Snowfall (cm)	Daily Mean Temperature (°C)*
12 Dec 1996 – 30 Apr 1997	470	- 3.62 ±7.20
12 Dec 1997 – 30 Apr 1998	170	- 0.71 ±5.59

*Calculated from the daily high and low temperature for the period.

3.1.2 1997 and 1998 *in situ* time-series

The Year 1 mooring was deployed through the ice on 8 Jan 1997 and was recovered on 29 May 1997 (Table 2.1). The $p\text{CO}_2$, DO, temperature, light, and mooring depth time-series collected during the Year 1 ice-covered period are shown in Figure 3.1. The Year 2 mooring was deployed on 26 Nov 1997, prior to ice-up and recovered on 20 May 1998 (Table 2.1). Due to instrument malfunctions in Year 2, data are reported only during some time periods and there were no time periods when $p\text{CO}_2$ and DO were obtained simultaneously (Figure 3.2).

The surface $p\text{CO}_2$ and DO in Placid Lake were supersaturated and undersaturated, respectively, for the under-ice periods during both years (Figures 3.1a,b and 3.2a). During Year 1, the mean $p\text{CO}_2$ was $1340 \pm 120 \mu\text{atm}$ ($N=4053$) and ranged from ~ 1020 to $1660 \mu\text{atm}$ or ~ 3 to 5 times atmospheric saturation ($\sim 310 \mu\text{atm}$ at the average atmospheric pressure).

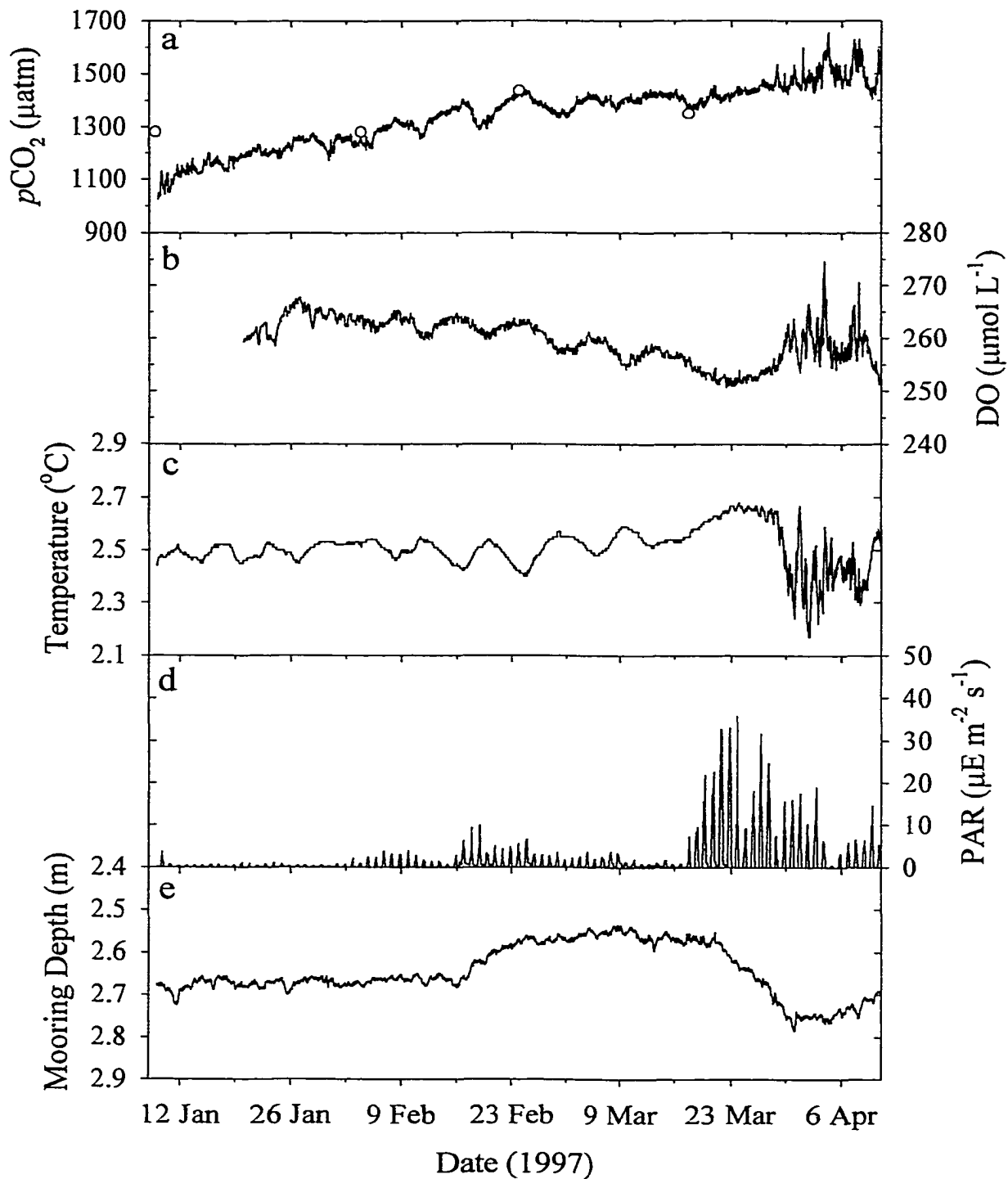


FIGURE 3.1: Under-ice *in situ* time-series collected during Year 1. **a)** *In situ* $p\text{CO}_2$ (line) and $p\text{CO}_2$ calculated from the periodic DIC and pH samples (circles). A constant offset of $-149 \mu\text{atm}$ was applied to the calculated $p\text{CO}_2$ (Chapter 2.5). **b)** Dissolved oxygen. **c)** Water temperature at the instrument depth. **d)** Photosynthetically available radiation. **e)** Depth of the moored instrumentation. All times are UTC.

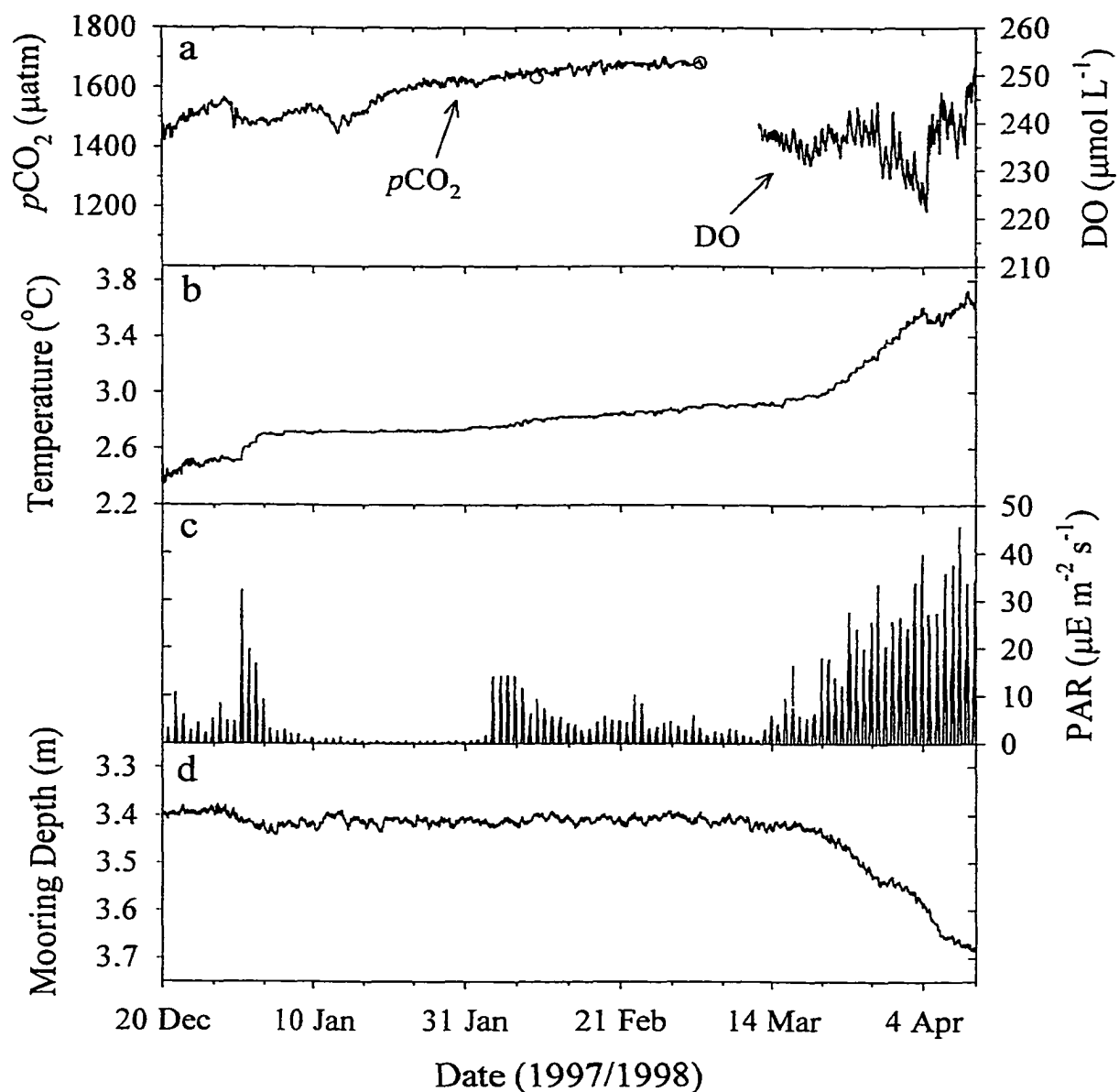


FIGURE 3.2: Under-ice *in situ* time-series collected during Year 2. **a)** The $p\text{CO}_2$ and DO records. The open circles are the $p\text{CO}_2$ calculated from the periodic DIC and pH samples. A constant offset of $-149 \mu\text{atm}$ was applied to the calculated $p\text{CO}_2$ (Chapter 2.5). **b)** Water temperature at the instrument depth. **c)** Photosynthetically active radiation. **d)** Depth of the moored instrumentation.

In Year 2 the mean $p\text{CO}_2$ was $1580 \pm 70 \mu\text{atm}$ ($N=2848$) and ranged from ~ 1420 to $1700 \mu\text{atm}$. The periodic $p\text{CO}_2$ calculated from DIC and pH is also shown in Figures 3.1a and 3.2a. The large offset of the first profile measurement (Figure 3.1a) is believed to be an artifact of the sampling method on that day when deeper samples were obtained first, thereby entraining deeper, higher $p\text{CO}_2$ water to the surface. Omitting the first profile measurement, the agreement in Year 1 was $\pm 19 \mu\text{atm}$ with the $p\text{CO}_2$ offset ($N=3$). The validity of the DIC/pH calculations and use of the constant offset are further supported by Year 2 comparisons. The calculated $p\text{CO}_2$, with the same $p\text{CO}_2$ offset as in Year 1, agreed to within $\pm 29 \mu\text{atm}$ ($N=2$) of the *in situ* $p\text{CO}_2$ (Figure 3.2a). The periodic DIC and pH measurements support that there was minimal drift in the *in situ* $p\text{CO}_2$ measurements, as found in earlier studies (DeGrandpre et al. 1995, 1998). In addition, post-calibration of the SAMI- CO_2 during Year 1 verified that drift was $< 3.5\%$. The drift is an upper bound estimate because the post-calibration was not performed until after the instrument was recovered, nearly 2 months after the data reported in Figure 3.1. No post-calibration was possible for Year 2 due to an instrument malfunction. Both the magnitude and trends in the $p\text{CO}_2$, and its relationship with DO, are consistent with other researcher's observations during ice-cover (e.g., Wetzel 1983; Cole et al. 1994), further supporting the data quality.

During Year 1, mean DO was $259 \pm 3 \mu\text{mol L}^{-1}$ ($N=3648$) and ranged between ~ 275 and $250 \mu\text{mol L}^{-1}$, or 75-69 % saturation, respectively. The mean DO during Year 2 was $238 \pm 6 \mu\text{mol L}^{-1}$ ($N=1441$), and ranged between ~ 250 and $222 \mu\text{mol L}^{-1}$, or 70-63 % saturation, respectively. Comparison of the replicate DO records, obtained at similar depths (Table 2.1), was used to verify the quality of the DO data.

Only one of the two DO sensor records is shown (Figures 3.1b and 3.2a). In Year 1 the DO sensor records initially had large and erratic offsets, however they converged later in the deployment, matching to within $\pm 6 \mu\text{mol L}^{-1}$ (N=1920). The DO data shown are therefore assumed to be accurate to within this amount. In addition, as stated above, the Year 1 DO record is also consistent with trends in the $p\text{CO}_2$ data, further supporting the validity of the DO data. In Year 2, the main mooring DO record agreed with the additional Model 6000 deployed on the thermistor-chain mooring to within $\pm 3 \mu\text{mol L}^{-1}$ (N=1266) later in the field study (Table 2.1). Earlier in the record there were significant erratic offsets. Data are omitted during these time periods. We believe the erratic behavior of the Model 6000's was due to the relatively old electrodes (3 years) that were used in the study.

3.2 Discussion

3.2.1 Temporal scales of variability

Much of the diel and shorter time scale variability was smaller than the resolution of the *in situ* instruments, as noted by the digitized appearance of the DO and temperature data in Figure 3.1. The greatest short-term variability typically occurred during the period prior to ice-out. Clear oscillations and long-term trends are also evident. The large range of temporal scales of variability supports the hypothesis that multiple processes contribute to variability under ice. Our evaluation first focuses on the variability in Year 1 followed by a comparison with the Year 2 time-series data.

3.2.2 Year 1

The low frequency oscillation common in the $p\text{CO}_2$, DO, and water temperature time-series is the most notable variability in Year 1 (Figure 3.1). The oscillations in the three records have the same period, 7.6 ± 1.8 days. The relationships between $p\text{CO}_2$, DO, and temperature can be used to decipher the origin of these oscillations. Oddly, the $p\text{CO}_2$ and DO are positively correlated within the 7.6 day period ($R^2=0.88$), whereas, in most water bodies the biological imprint creates the opposite relationship. Looking closely at Figures 3.1a-c, one can see that the rising $p\text{CO}_2$ and DO levels are associated with slightly colder and less dense water ($T < 4^\circ\text{C}$). While DO is not directly affected by cooling, $p\text{CO}_2$ *decreases* with cooling, ruling out a strictly thermodynamic effect and pointing to some other physical mechanism(s). Water movement can occur under-ice through a number of different physical processes including convective currents generated by light penetration, sediment heating of overlying water, stream flow-through currents, and wind-generated seiche (Matthews and Heaney 1987; Welch and Bergmann 1985; Bengtsson 1996; Malm et al. 1998). The consistent period of the oscillation suggests a seiche. Wind has been found to induce internal seiche in ice-covered lakes through forcing of the ice-cover (Bengtsson 1996; Malm et al. 1998). The oscillations began to develop around 12 Jan 1997 based on the temperature record (Figure 3.1c). A high wind event (Figure 3.3b) also occurred on 12 Jan with peak wind speeds over 11 m s^{-1} and averaging 7.5 m s^{-1} over a 24-hr period. The coincidence of these two events supports that wind initiated a seiche.

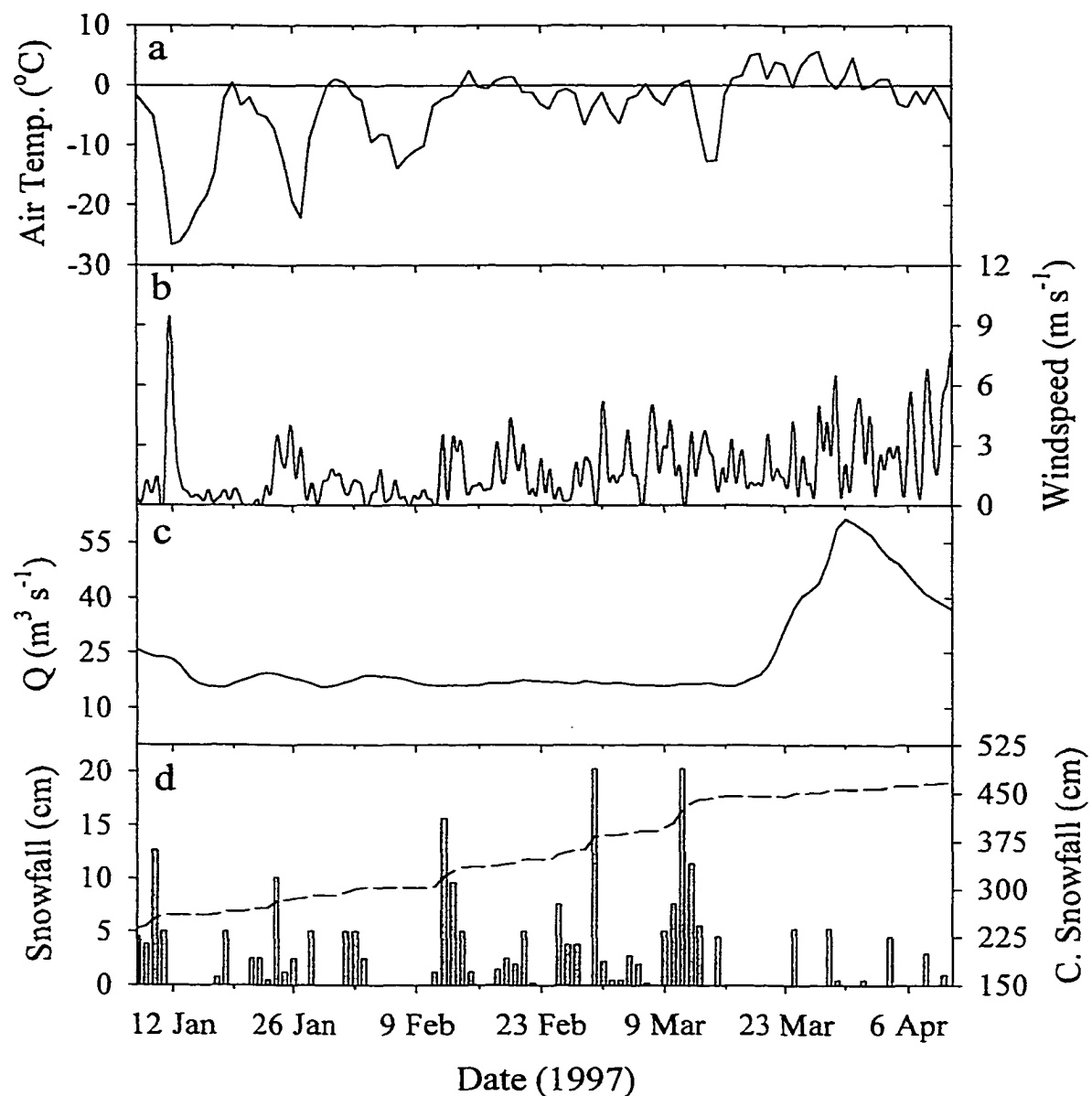


FIGURE 3.3: Year 1 meteorological and discharge data. **a)** Average of daily high and low air temperatures 10 km N of Placid Lake. **b)** Windspeed, measured at the NOAA site in Missoula, Montana, filtered (24-hr low-pass) for clarity. **c)** USGS Swan River discharge record. The discharge pattern for this river is assumed to approximate the discharge pattern of Placid Creek. **d)** Total daily snowfall (bars) and cumulative snowfall from ice-up (dashed line) 10 km N of Placid Lake.

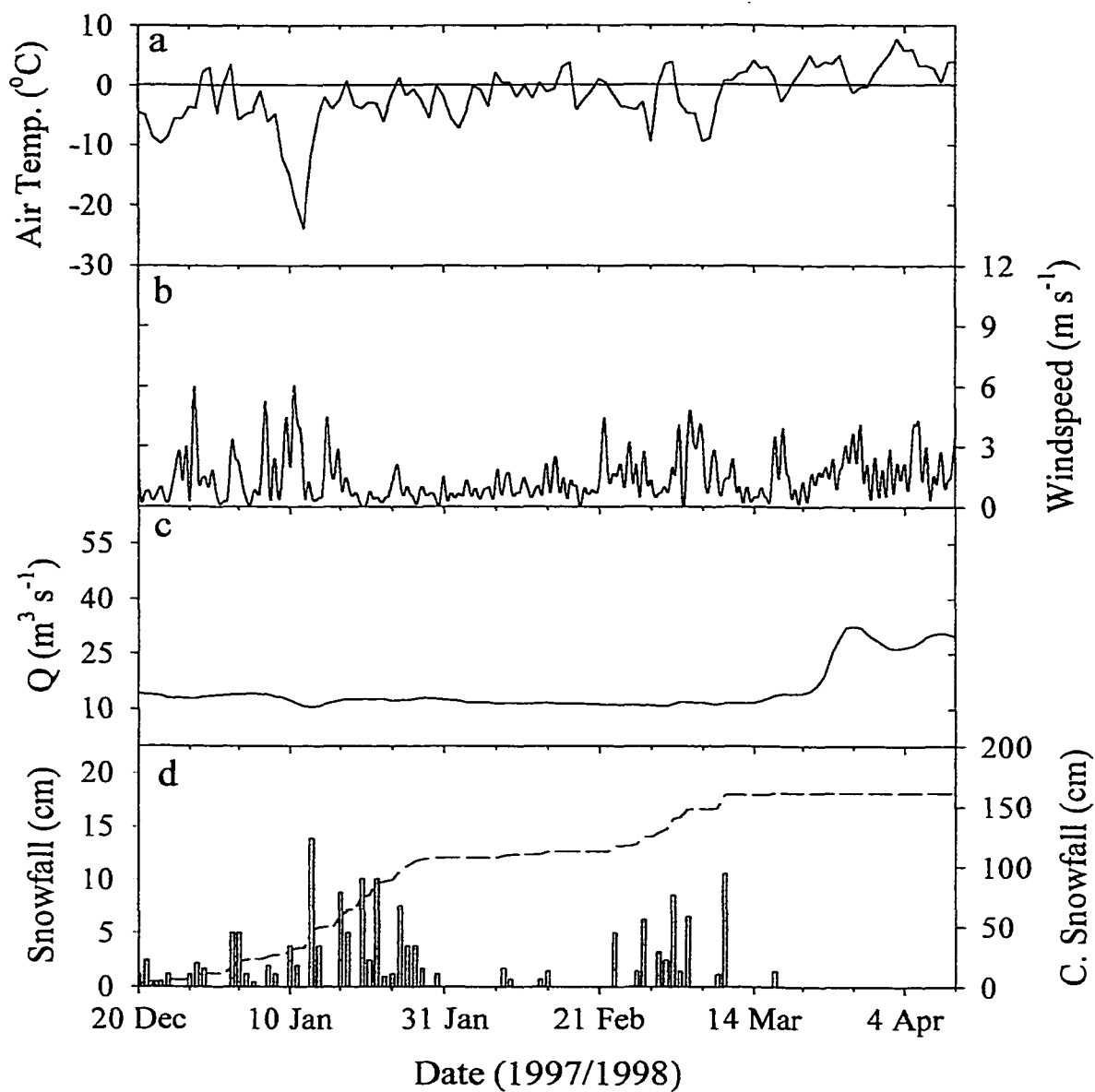


FIGURE 3.4: Year 2 meteorological and discharge data. Detail as in Figure 3.3.

The long period of the oscillations and the presence of slight density stratification (Figure 3.5) suggests a baroclinic seiche (Malm et al. 1998). To verify this connection, the period of a baroclinic seiche mode was estimated using:

$$T_n = \frac{2n\pi L}{NH} \quad (3.1)$$

where n = number of the baroclinic mode, L = maximum length of the lake basin, H = mean depth of the lake minus the ice thickness (~14.5 m), and N = buoyancy frequency, defined by

$$N^2 = -\frac{g}{\rho} \frac{d\rho}{dz} \quad (3.2)$$

where g = gravity acceleration, ρ = average water density (999.957 kg m⁻³), and $d\rho/dz$ is the average vertical density gradient (-0.0010 kg m⁻⁴) (Malm et al. 1998). Both ρ and $d\rho/dz$ were estimated from the temperature profiles shown in Figure 3.5. The period of the first baroclinic mode under these conditions would be 5.5 days which, considering the large uncertainty inherent in this calculation, compares well with the observed 7.6 day period and supports that a baroclinic seiche was responsible for the oscillations. Episodic storms, which pass through the area (see meteorological data in Figure 3.3), could also create a low periodicity variability, however, no correlation was found between these events and the dissolved gas oscillations ($R^2 < 0.2$). In addition, power spectra of barometric pressure, wind, and air temperature did not show a peak at 7.6 days. The high winds on 12 Jan may have initiated the seiche and subsequent prevailing winds or other episodic events (Figure 3.3) presumably acted to sustain the seiche at this resonant oscillation of the lake. A seiche-induced sloshing should also result in an oscillating depth, but this was not observed (Figure 3.1e). However, if the instruments were at the node of the seiche, which would be near the center of the lake where the mooring is located, no depth change would be apparent (Wetzel 1983; Lemmin 1987).

A seiche may be causing the water movement, but what is the origin of the colder, higher $p\text{CO}_2$ and higher DO water associated with the oscillations? Notably, water temperature decreased towards the ice-water interface (Figure 3.5).

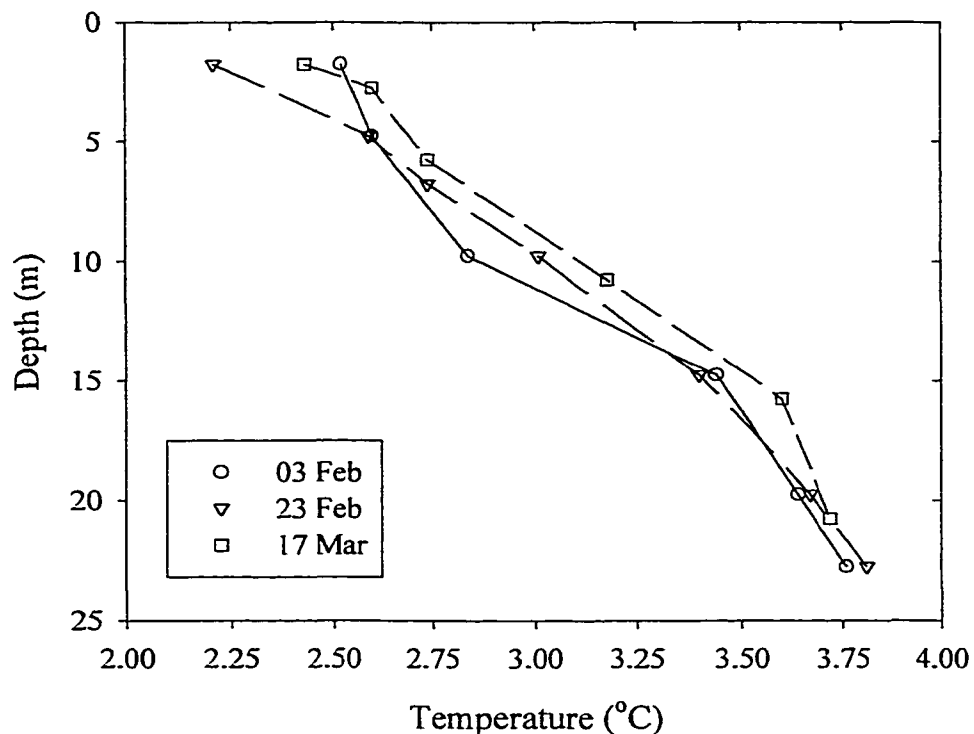


FIGURE 3.5: Under-ice temperature ($^{\circ}\text{C}$) profiles measured during the Year 1 study.

Gases and other solutes are known to partition into the liquid phase when ice forms (Bari and Hallett 1974; Craig et al. 1992). This process would result in an increase in DIC and DO in the colder water above the instrumentation. DIC profile measurements and isopleths (Figures 3.6a and 3.7) reveal that DIC increased near the ice surface with time, presumably due to the above process. Equilibrium calculations using DIC and pH data indicate that a $p\text{CO}_2$ gradient of $\sim 100 \mu\text{atm}$ would be established between 2 and 5 m

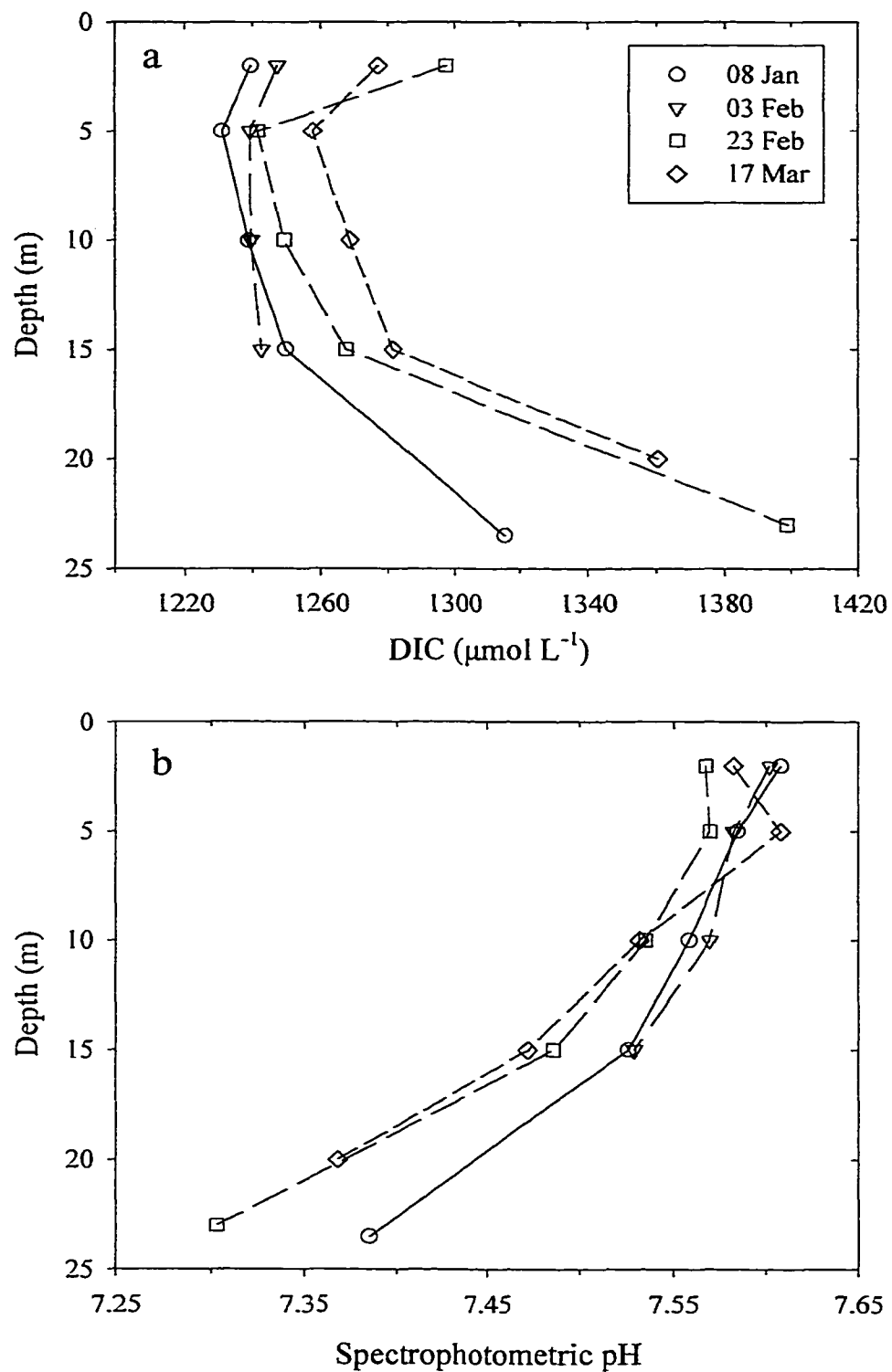


FIGURE 3.6: Chemical profiles obtained during Year 1. **a)** Dissolved inorganic carbon (DIC). **b)** Spectrophotometric pH.

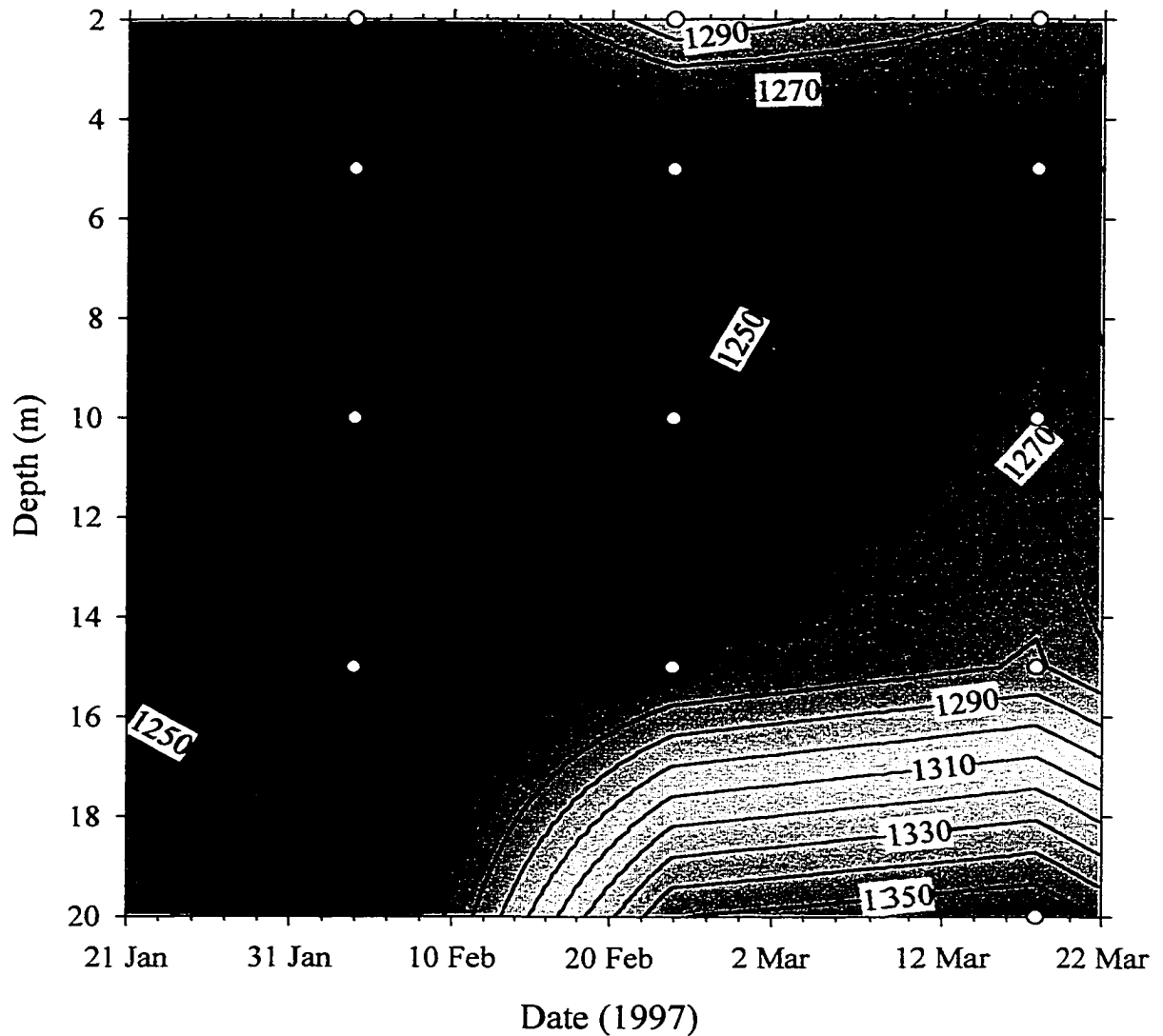


FIGURE 3.7: Year 1 depth-time diagram of DIC isopleths. Contour labels are in $\mu\text{mol L}^{-1}$. Contour interval lines were produced from linear interpolation (both time and depth) of the profiles. The jagged appearance of the contours results from interpolation between large data gaps. The white dots indicate the time and depth of the profile measurements.

later in the ice-covered period.

The vertical profiles and depth record rule out vertical movement of this water, however, a seiche also causes horizontal displacement of surface water with the maximum displacement at the node (Wetzel 1983). To generate the observed

oscillations, surface $p\text{CO}_2$ and O_2 gradients must vary along the surface of the lake perhaps due to variable ice thickness (Stigebrandt 1978).

There are other periods when short-term variability was significant. Just before ice-out $p\text{CO}_2$, DO, and temperature were highly variable relative to earlier in the record. This period, 27 Mar to 11 Apr 1997, is expanded in Figure 3.8. During this period, light penetration increased (Figure 3.8d) and meltwater was present based on the colder temperatures, increased mooring depth, and dramatically increased river discharge (Figures 3.1 and 3.3). The $p\text{CO}_2$ and DO are not significantly correlated ($R^2=0.20$) during this time period which may be in part due to the degradation in $p\text{CO}_2$ resolution at high $p\text{CO}_2$ (Chapter 2.2.1). DO is negatively correlated with temperature, i.e., higher DO in colder water, over the first 7 days of this period ($R^2=0.93$). Their relationship becomes unclear later ($R^2=0.36$ for the entire period in Figure 3.8). After ice-out, a thin layer (~ 1 m) of colored dissolved organic matter (CDOM) was present on the lake surface. The CDOM-rich layer apparently originated from Placid Creek, which was highly colored relative to the lake. Other studies have found that colder, lower density stream water can fan out at the ice-water interface rather than mixing with the whole water column at the stream inlet (Bengtsson 1996). These pieces of evidence suggest that much of the variability during the late-ice period resulted from mixing of runoff and resident waters.

A slow increase and decrease in the $p\text{CO}_2$ and DO levels, respectively, is one of the dominant features of the time-series prior to 23 Mar (Figure 3.1). These trends are commonly observed in ice-covered lakes and are generally attributed to bacterial oxidation of particulate and dissolved organic matter (e.g., Babin and Prepas 1985; Cole et al. 1994). It is possible, nonetheless, that a physical mechanism could generate a

similar trend. Vertical eddy diffusion is one possible mechanism due to existing vertical gradients in lakes, i.e., higher DIC and lower DO with depth. Calculations using expected eddy diffusion coefficients (Quay et al. 1980), however, show that eddy diffusion accounts for less than 1% of the observed changes.

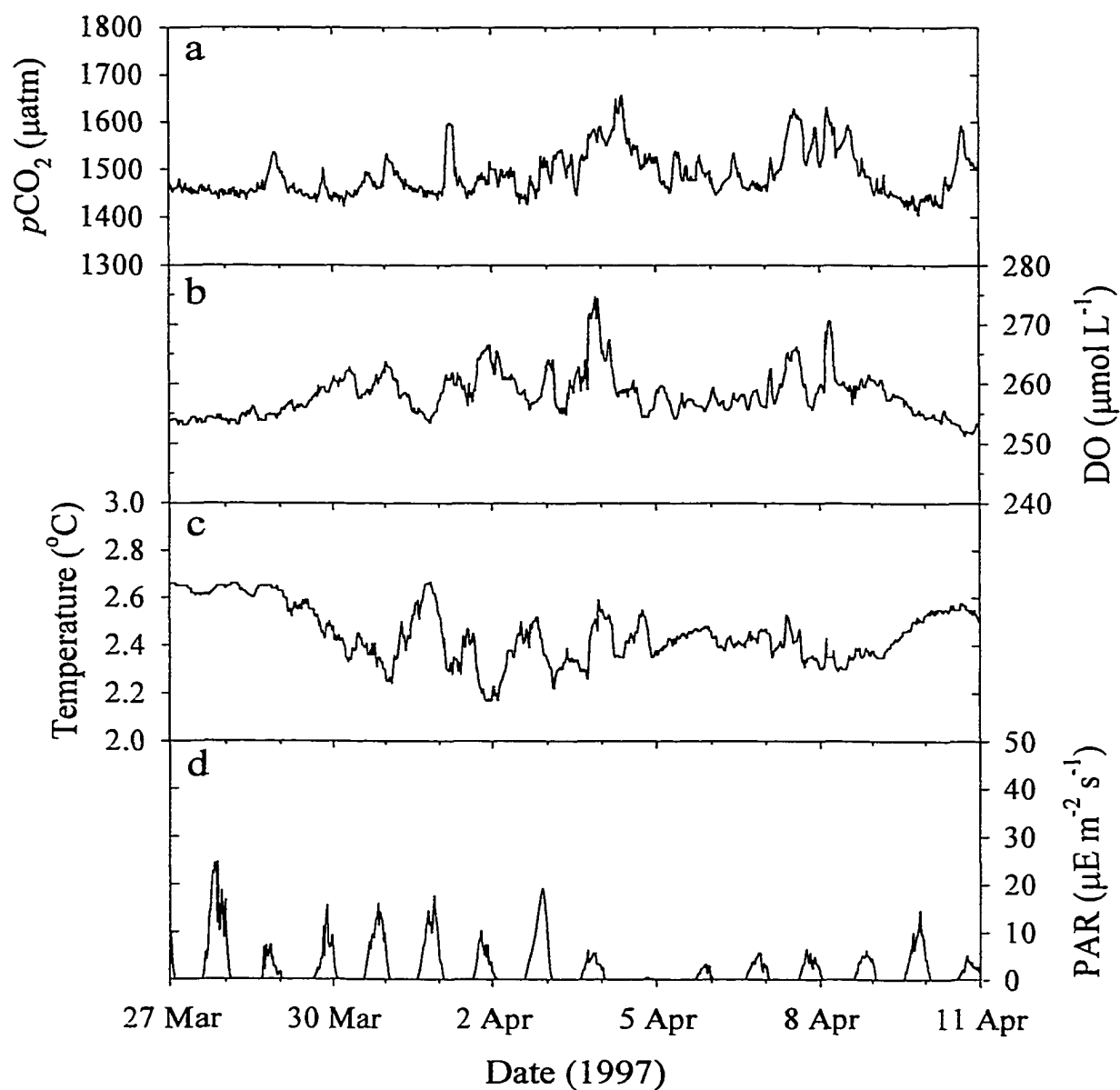


FIGURE 3.8: Expanded time-series for the late-ice period in Figure 3.1. **a)** $p\text{CO}_2$. **b)** DO. **c)** Water temperature. **d)** PAR.

Other possible physical mechanisms for transport of higher $p\text{CO}_2$ and lower DO water include convection from stream flow-through and sediment-heat generated currents (Welch and Bergmann 1985). Surface temperatures and temperature profiles (Figure 3.5) do not support either of these mechanisms. Furthermore, thermodynamic calculations show that the observed temperature changes have no significant effect on the $p\text{CO}_2$ trend. Therefore, the process responsible for the trends is, most plausibly, respiration of organic matter.

Respiration rates were determined by calculating the average rate of change of DIC from the $p\text{CO}_2$ time-series and calculated TA (Chapter 2.5). A 20-day low-pass filter was used to remove short-term variability and obtain a more accurate estimate of the underlying respiration rate. Using the filtered data, the average rate of change for DIC and DO over the period 31 Jan to 17 Mar 1997 was $+0.25 \pm 0.21$ and -0.22 ± 0.14 $\text{mmol m}^{-3} \text{d}^{-1}$, respectively. These rates are consistent with the approximate 1:1 molar ratio of CO_2 release and DO consumption resulting from respiration of organic matter (Wetzel 1983). The rate of DO depletion on an areal basis, calculated from the 3 DIC profiles (Figure 3.6a) by assuming a 1:1 molar ratio was found to be $-16 \text{ mmol O}_2 \text{ m}^{-2} \text{d}^{-1}$ which is within the range of DO depletion rates reported for other lakes during ice-covered periods (Babin and Prepas 1985).

3.2.3 Year 2

The Year 2 time-series are discussed to provide a context for the variability observed in Year 1. This ice-covered period was characterized by greater light penetration and warmer and less variable water temperatures than in Year 1 (Figure 3.2). The overall $p\text{CO}_2$ trend is strikingly similar to Year 1 with increasing $p\text{CO}_2$ through mid-

winter, leveling off later in the ice-covered period. In contrast to Year 1, however, no seiche-like oscillations were observed.

The DO results also show significant diel variability prior to ice-out (Figures 3.2a and 3.9a). Without the complementary $p\text{CO}_2$ record, it is difficult to ascertain whether convection or biology was the source of the diel variability. The peaks in DO are coincident with peaks in PAR, but the lack of a long-term upward trend in DO suggests no significant net primary production (Figure 3.9). Thermistor-chain data (not shown) show that convective mixing may have been important during this period. The temperature record at 1 m increased in ~ 0.3 °C increments during daylight hours followed by a brief cooling period and less variable nighttime temperatures that were slightly higher than the night before. The deeper temperature records (thermistor-chain and Model 6000) showed little temperature variation with depth, indicating that the higher density water at ~ 1 m was rapidly mixing into these waters. It appears that penetrative convection from solar heating (Farmer 1975; Matthews and Heaney 1987) and the retention of the heat at night due to the insulation of the lake from heat loss, resulted in the stepwise appearance of the temperature record (Figure 3.9b). With the progression of winter ice formation, DO accumulates at the ice-water interface, as explained for the Year 1 data. Convective mixing of this surface water downward would therefore lead to diel variability at the depth of the instrumentation. Although this process may have been occurring prior to ice-out during Year 1, the Year 1 variability is more strongly impacted by runoff from the high snowpack (Figure 3.3). Convective mixing was more evident in Year 2, when snowpack and runoff were dramatically reduced (Figure 3.4).

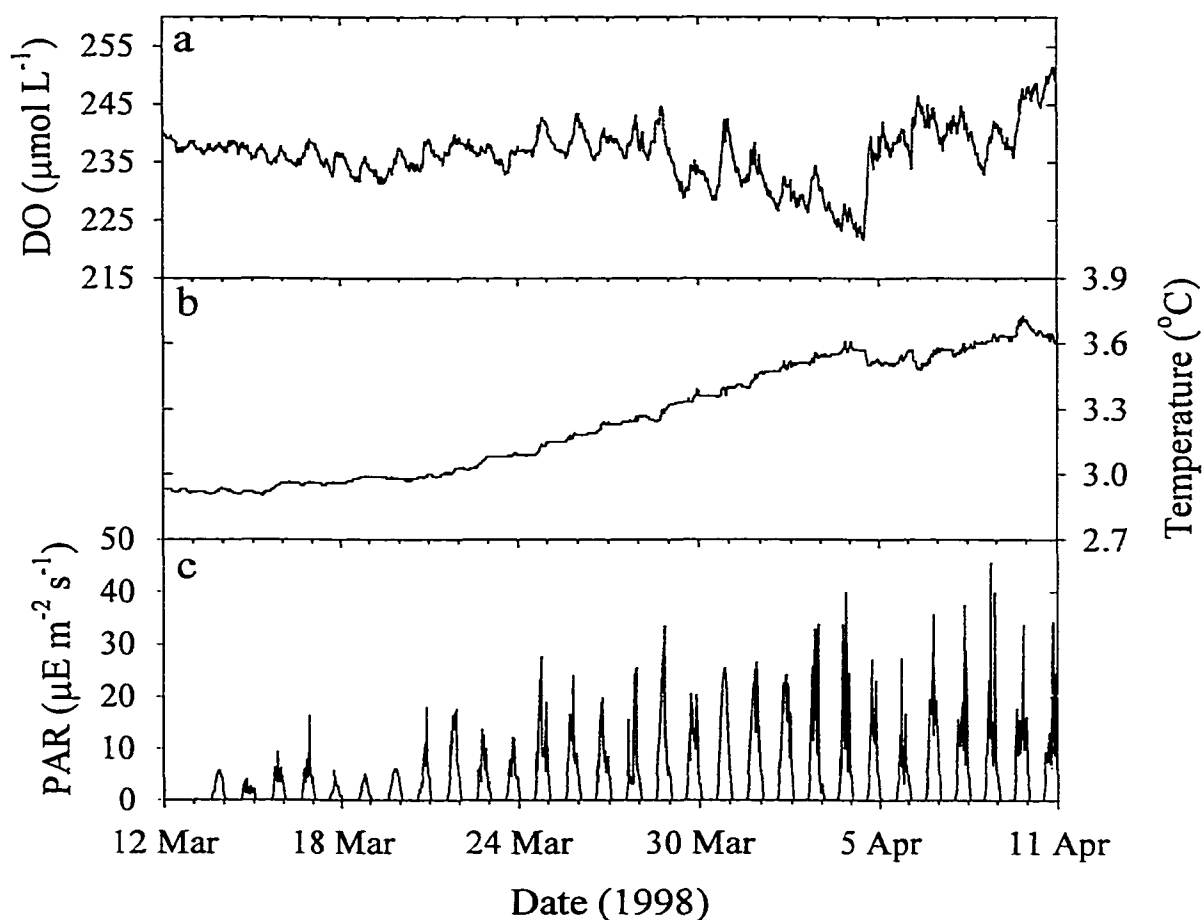


FIGURE 3.9: Expanded time-series for the late-ice period in Figure 3.2. a) DO. The saturation level at 3.3 $^{\circ}\text{C}$ is 359.4 $\mu\text{mol L}^{-1}$. b) Water temperature. c) PAR.

Lastly, as stated above, the overall trend shows that $p\text{CO}_2$ initially increased rapidly and then leveled off. Other studies have shown that DO depletion rates are more rapid early in the under-ice period (e.g., Babin and Prepas 1985; Baird et al. 1987). To obtain respiration rates, the $p\text{CO}_2$ was converted to DIC and then filtered as for Year 1. The average rate of change of DIC from 15 Jan to 1 Mar was $+0.26 \pm 0.28 \text{ mmol m}^{-3} \text{ d}^{-1}$, similar to the Year 1 rate. Over the entire $p\text{CO}_2$ record, the rate is $+0.17 \pm 0.24 \text{ mmol m}^{-3} \text{ d}^{-1}$, reduced by the two large drops in $p\text{CO}_2$ (Figure 3.2a). Comparison of the saturation

levels of $p\text{CO}_2$ and DO during Years 1 and 2 supports that greater respiration of organic material occurred during Year 2. The large snowfall and high runoff in Year 1, as shown in Figure 3.3, resulted in a large input of terrestrial organic matter. Therefore, there was increased oxygen demand in the lake during Year 2, which resulted in higher levels of $p\text{CO}_2$ and lower DO.

3.3 Chapter summary and conclusions

These studies provide a detailed characterization of short-term $p\text{CO}_2$ and DO variability under ice. The high-resolution time-series indicate that respiration of accumulated organic matter dominated the overall trend as expected. Physical mechanisms, which played an important secondary role, included seiche-induced advection, vertical convection from solar heating, and stream flow-through at the surface just prior to ice-out. Ice formation led to an accumulation of dissolved gases just under the ice, which uniquely manifested itself in the seiche oscillations. During some periods, light penetration or dry-fall nutrients may have stimulated biological production but there was no clear evidence of net community production during either year. Although these two studies did not include high resolution spatial time-series (vertical and horizontal), the results suggest that both spatial and temporal variability can be significant over intervals which would not be resolved by traditional sampling-based studies.

Chapter 4

***In situ* Chemical Sensor Measurements in 1999: Comparisons between Observations and Results from Physical and Biogeochemical Modeling**

The objectives of the study presented in this chapter were to characterize the short-term and seasonal biogeochemical variability in a freshwater lake during the transitional period from ice cover to ice out, develop and use coupled physical-biogeochemical models to quantify the relative importance of biology, air-water gas exchange, mixing, and heating and cooling on CO₂ and O₂, and to determine the impact that ice cover, ice out, and turnover have on the dissolved gas budgets.

To accomplish these goals, *in situ* time-series measurements of *p*CO₂, DO, PAR, chlorophyll-*a* fluorescence, temperature, conductivity, and depth were made near the lake surface (1.9 m). Measurements of *p*CO₂, DO, temperature, and conductivity were also made near the lake bottom (19.9 m). In addition, temperature was measured from ~1-10 m depth. The instruments were deployed from 18 Mar to 2 Jul 1999. Their deployment depths are summarized in Table 2.1. Profile measurements of several parameters were made during the study (see Table 2.2 and Appendix 2). Detailed methods are given in Chapter 2. In addition to these measurements, simple two-box biogeochemical models were developed for *p*CO₂ and DO and were coupled to the mixed-layer depth output from the physical model (PWP) to simulate the dissolved gases within the lake. For a detailed explanation of the physical and biogeochemical models see Chapter 2.7.

4.1 Results and discussion

4.1.1 Figure overview

Figures 4.1a-4.3a show the *in situ* and meteorological time-series. Comparisons between the *in situ* and modeled data are shown in Figures 4.3, 4.5, 4.6, and 4.9. The relative contributions of photosynthesis and respiration, air-water gas exchange, entrainment, and temperature to CO₂ and O₂ variability during the ice-covered and ice-free periods are shown in Figures 4.7 and 4.10, respectively.

4.1.2 Time-series overview

The timing of events such as turnover and ice out, which are essential to the interpretation of the *in situ* time-series, is summarized in Table 4.1.

The surface and bottom dissolved gas and temperature records over the entire deployment are shown in Figure 4.1. The ice-covered period is characterized by high $p\text{CO}_2$ and low DO particularly early in the deployment and near the lake bottom. The bottom $p\text{CO}_2$ ranged from >3000 to ~ 1700 μatm and the bottom DO ranged from ~ 110 to 270 $\mu\text{mol L}^{-1}$ (3.5 to 8.6 mg L^{-1}). The average surface $p\text{CO}_2$ under ice was ~ 4.5 times greater than atmospheric saturation (~ 310 μatm at 1256 m) and the average surface DO was undersaturated by $\sim 29\%$. The mean lake temperature under ice rose from ~ 2.6 to 3.8 $^{\circ}\text{C}$. Daytime heat flux at the lake surface was small and positive and the nighttime heat flux was zero as a result of considering only the penetrating shortwave radiation during the ice-covered period (Figure 4.2a). The daytime PAR under ice increased almost 4-fold to ~ 280 $\mu\text{E m}^{-2} \text{ s}^{-1}$ with the waning of the snow and ice cover (Figure 4.2c). Chlorophyll-*a* concentrations also increased with time under ice cover and ranged from ~ 3 to 13 mg m^{-3} (Figure 4.2d).

TABLE 4.1. A summary of important events in the 1999 Placid Lake study.

Event	Date(s)
Mooring deployment	18 Mar – 02 Jul
Turnover (based on temperature)	08 –23 Apr
Ice out	21 – 22 Apr
Post-turnover period of episodic deep mixing	23 Apr – 18 May
Development of strong seasonal stratification	18 May

Ice-out occurred from 21 to 22 Apr. The breakup of the ice cover resulted in sudden surface cooling due to the latent heat of fusion required to melt the broken ice (Figure 4.1c; Farmer 1975). The surface $p\text{CO}_2$ ranged from extreme supersaturation (~450%) immediately following ice out to near saturation levels in early June. Over the same time the surface DO ranged from a saturation deficit of ~25% to a supersaturation of ~120%. The surface temperature ranged from ~3.5 to 19.5 °C. The two dissolved gases at the lake bottom exhibited similar trends. Initially the $p\text{CO}_2$ declined while the DO and temperature rose after ice out. By 18 May the bottom temperature leveled off at ~6 °C and thereafter the $p\text{CO}_2$ rose and the DO decreased, reversing their earlier trends (Figure 4.1). The net heat flux varied considerably after ice out. The net heat flux ranged from daytime highs near +900 to nighttime lows of -500 W m^{-2} (Figure 4.2a). The interplay between net heat input and loss can easily be seen in the thermal profiles of the lake (Figure 4.3a). The PAR after ice out was variable with a maximum daytime high of

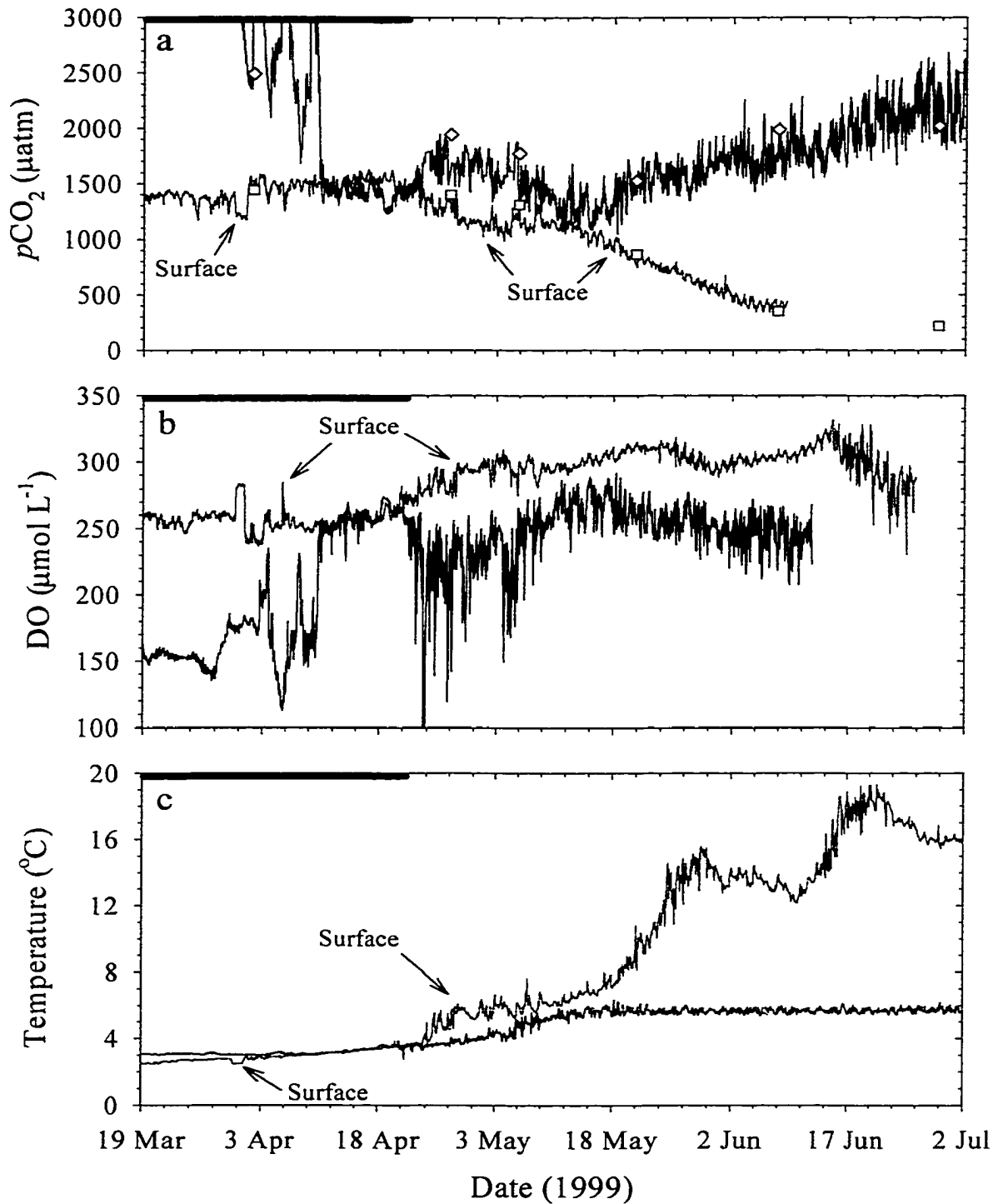


FIGURE 4.1: *In situ* time-series and profile measurements (surface=squares; bottom=diamonds) collected during the study. The black bars at the top of each panel indicate ice cover. **a)** *In situ* $p\text{CO}_2$ measured at the surface (red line) and at the bottom. A constant offset of -504 (surface) and -572 μatm (bottom) was applied to the calculated $p\text{CO}_2$ (Chapter 2.5). **b)** Dissolved oxygen records. **c)** Water temperature records.

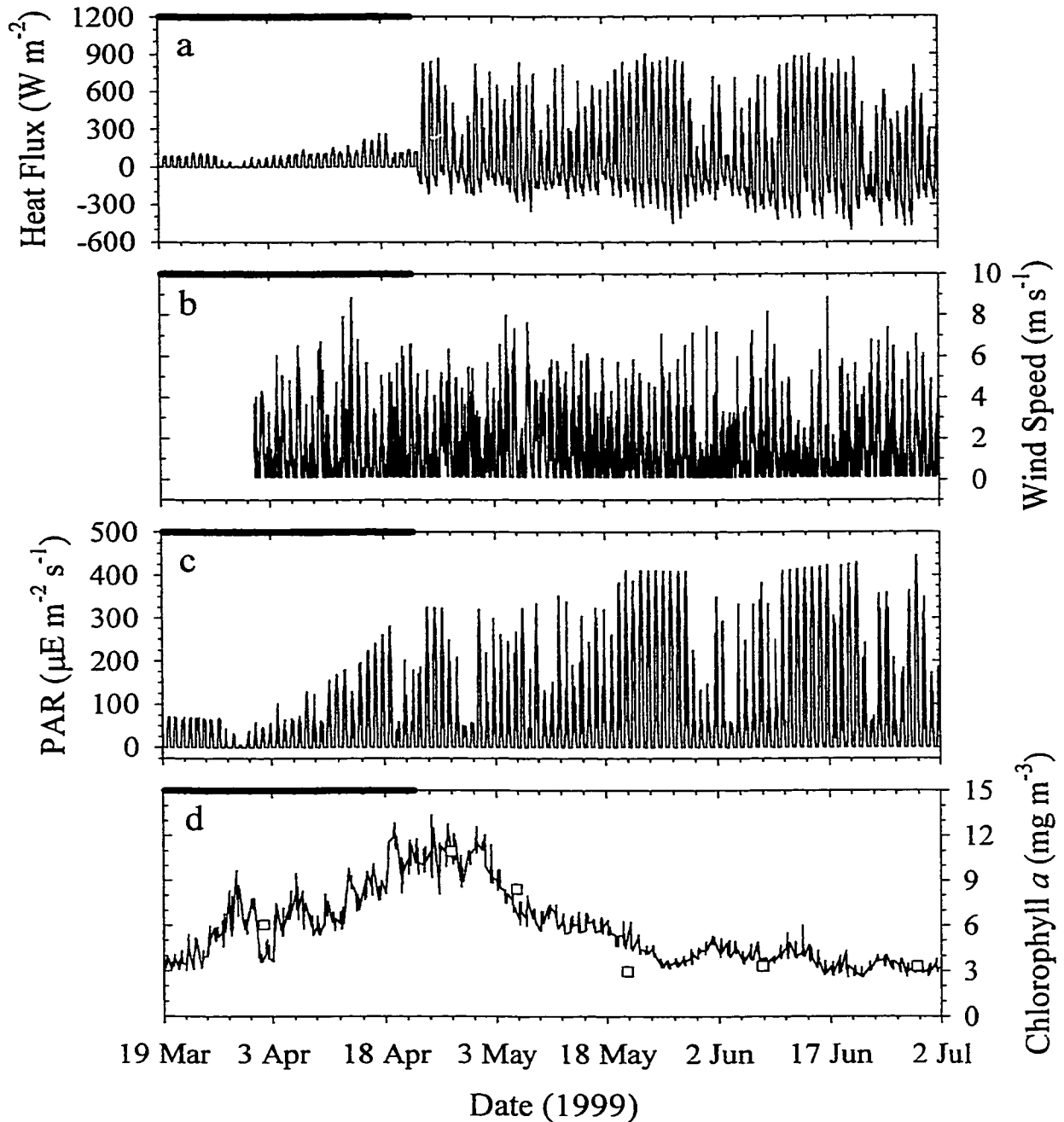


FIGURE 4.2: Meteorological and biomass data. The bold lines at the top of each panel indicate ice cover. **a)** The surface heat flux for the lake. **b)** The wind speed. Note that the east and west vector components of the wind stress are input into the PWP model. **c)** The underwater PAR at 1.9 m estimated from measurements made at 0.7 m. **d)** Chlorophyll- a time-series near the surface (Chapter 2.3.3) and discrete profile measurements (squares, Chapter 2.4.5) measured at 1.9 m.

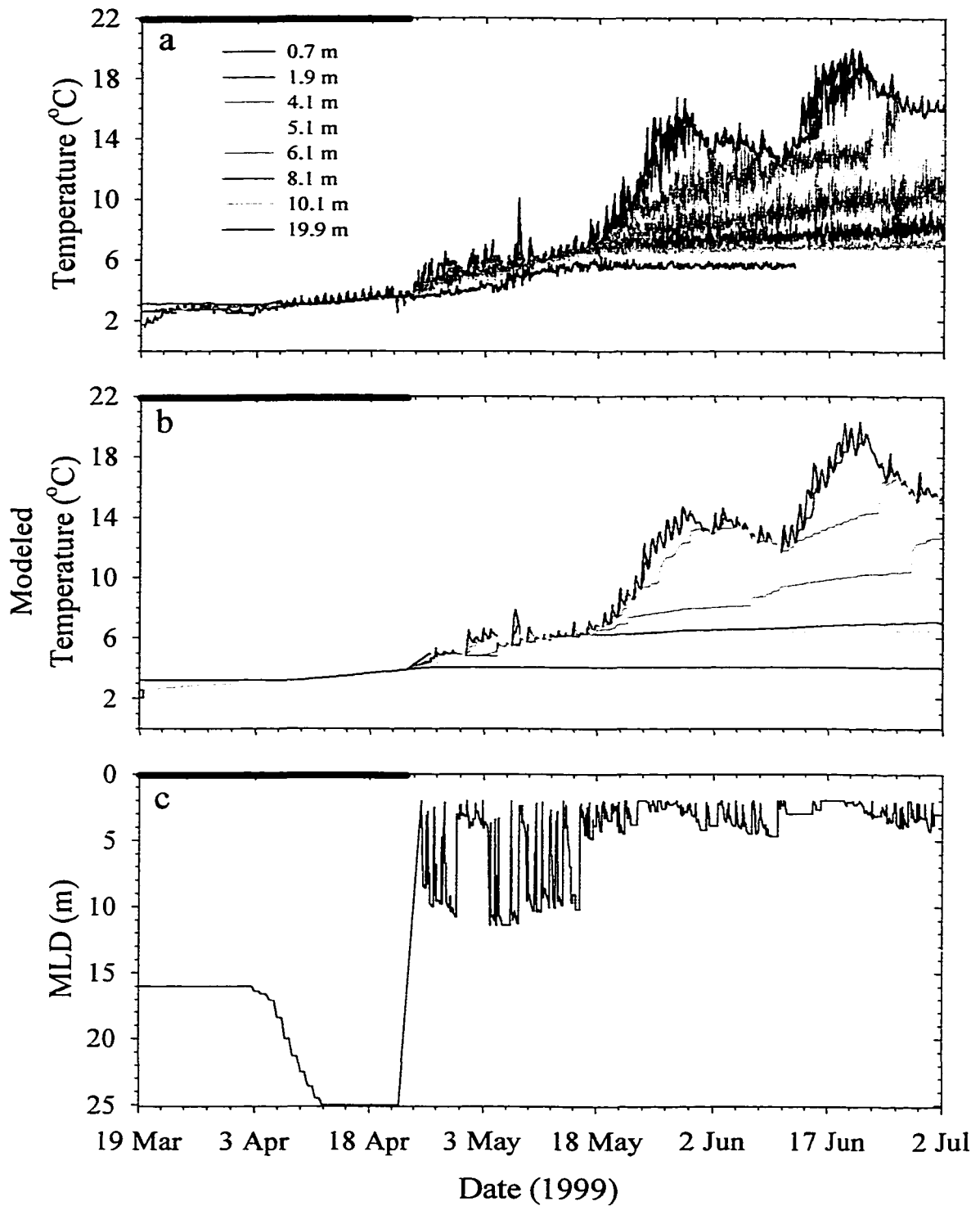


FIGURE 4.3: Water temperatures and MLD. The bold lines indicate ice cover. **a)** The temperature time-series at depths from 0.7 to 19.9 m. **b)** Temperatures predicted by the PWP model. The legend in **a)** also applies here. **c)** The MLD predicted by the PWP model. The minimum MLD was set at 2 m (Chapter 2.7).

$\sim 450 \mu\text{E m}^{-2} \text{ s}^{-1}$ (Figure 4.2c) and chlorophyll-*a* concentrations declined from their highs near ice out to $\sim 3 \text{ mg m}^{-3}$ in early July (Figure 4.2d).

Atmospheric $p\text{CO}_2$ exhibited a diel cycle from a near constant daytime low ($\sim 310 \mu\text{atm}$) to higher nighttime levels (Figure 4.9a). The atmospheric $p\text{CO}_2$ during the day, when differential heating of the atmosphere produced wind, was representative of the regional average whereas at night, when winds were relatively calm, the $p\text{CO}_2$ was locally dominated. The diel swings increased in magnitude over time in response to the growth of local vegetation.

4.1.3 Major features

4.1.3.a Turnover

In temperate lakes, the water at all depths is often near the temperature of maximum density at ice out and it is commonly assumed that wind stress is required to mix the entire water column (e.g., Wetzel 1983). We observed complete water column mixing well before ice out in this study. Initially the water column was inversely stratified but it became isothermal for 15 days from 8 to 23 Apr (Figures 4.1c, 4.3a). Even so, isothermal conditions alone do not guarantee that complete mixing had occurred (e.g., van Senden et al. 1990). Hostetler (1995) points out that many nutrients and chemical species are not uniformly distributed with temperature. The surface and bottom records for both $p\text{CO}_2$ and DO converged on 10 Apr confirming that complete mixing had indeed occurred under ice (Figure 4.1a,b). Turnover may occur under ice in many temperate lakes but because of the general paucity of temperature and biogeochemical data in the late ice period this may often be missed.

There is evidence that penetrative convection led to turnover under ice and that convection sustained the circulation (e.g., Farmer 1975; Matthews and Heaney 1987). The 0.7 m temperature record shows daytime peaks in surface temperature toward the maximum density of water at 4 °C, generating convection currents (Figure 4.3a). At night the surface temperatures dropped to values that were slightly higher than the night before. Convection from solar heating and the retention of the heat at night, due to the ice cover insulating the lake from heat loss, resulted in the stepwise appearance of the temperature record (Figures 4.3a, 4.6c). The temperature records at depths not directly influenced by solar insolation were less variable but also exhibited the stepwise increase as a result of the higher density surface water being mixed downward.

As an alternative estimate of the commencement of turnover, the energy, E , needed to completely mix the water column was calculated from the temperature profile on 6 Apr with (Darbyshire and Edwards 1972):

$$E \text{ (kJ m}^{-3}\text{)} = \frac{1}{h} \int_0^h (\rho_z - \bar{\rho}) g z \, dz \quad (4.1)$$

where ρ_z is the density of water (Mg m⁻³) at depth z (m), $\bar{\rho}$ is the mean density of the water column, g (m s⁻²) is gravitational acceleration, and h (m) is lake depth. Using Equation 4.1 it was determined that the energy associated with the 0.5 °C increase in temperature at 0.7 m on 7 Apr was sufficient to overcome the remaining stratification. These results further support that penetrative convection was the driving force behind turnover under ice.

4.1.3.b Post-turnover episodic deep-mixing events

Turnover ceased soon after ice out on 23 Apr, a day characterized by a high positive heat flux and relatively calm winds (Figure 4.2a,b). The lake surface warmed

above the temperature of maximum density so surface heating no longer resulted in free convection. The slight thermal stratification that developed effectively separated the surface and bottom sensors. At this time the bottom and surface records start to diverge (Figure 4.1). However, this initial stratification was short-lived as periods of low positive or negative heat flux and high wind (e.g., 27-30 Apr and 5-7, 10-15 May) led to water column instability and the turbulent transfer of heat from the surface to greater depth (Figures 4.2a,b and 4.3). These post-turnover periods of forced convection in spring are indicated by the convergence between the temperature-depth records (Figures 4.1c, 4.3a) and observable in the dissolved gas records as a decrease and increase in the $p\text{CO}_2$ and DO, respectively. It was not until 18 May, almost a month after lake turnover, that these deep-mixing events ceased with the onset of seasonal stratification (Table 4.1).

4.1.3.c Seasonal stratification

Prior to turnover, the water column was inversely stratified (Figure 4.1c, 4.3a). As this stratification became eroded by penetrative convection, there were peculiar jumps in the dissolved gases at the bottom with no concomitant change in the surface records. The jumps in $p\text{CO}_2$ and DO occur at the same time and are opposite in direction in accord with the vertical dissolved gas gradients. This is compelling evidence that the large fluctuations in the dissolved gases are from vertical mixing associated with ML deepening near the bottom sensors.

Periods of strong net positive heat flux and low wind stress resulted in intense thermal stratification and surface buoyancy, which began on 18 May. The most intense surface heating occurred around 24 May and 20 Jun and caused significant ML shoaling

(Figure 4.3). Once persistent stratification was established, net community respiration again led to the increase and depletion of $p\text{CO}_2$ and DO, respectively, in the hypolimnion.

4.1.3.d Biomass and nutrients

The chlorophyll-*a* increased under ice to a maximum of $\sim 13 \text{ mg m}^{-3}$ at the end of April (Figure 4.2d). Juday and Keller (1980) have shown that the diatom Bacillariophyceae *Asterionella* dominates spring phytoplankton blooms in Placid Lake. However, this is a rather large, conspicuous, species ($\sim 525 \mu\text{m}^3$) and it is likely that smaller, more efficient (greater surface area to volume ratio), species dominate the nutrient cycles (J.A. Stanford, pers. comm. 2000). High phytoplankton biomass during ice cover has been observed in many lakes and is in response to increasing light with diminishing ice cover, increasing temperature, and the availability of accumulated nutrients from bacterial decomposition processes (e.g., Wright 1964; Wetzel 1983; Nebaeus 1984). Total nutrient inventories, calculated with compensation for volumetric differences with depth, show that the mean nitrate-N and phosphate-P dropped from highs of ~ 3.27 and 0.24 mmol m^{-3} , respectively, on 18 Mar to ~ 0.57 and $0.054 \text{ mmol m}^{-3}$ on 26 Apr. Over the same time, the average chlorophyll-*a* in the lake rose from ~ 1 to 10 mg m^{-3} . Ultimately the bloom subsided by 18 May when the pycnocline developed, which likely limited phytoplankton in the ML to primarily regenerated production (e.g., Platt et al. 1989). Profiles of the nutrients and chlorophyll-*a* are shown in Figure 4.4.

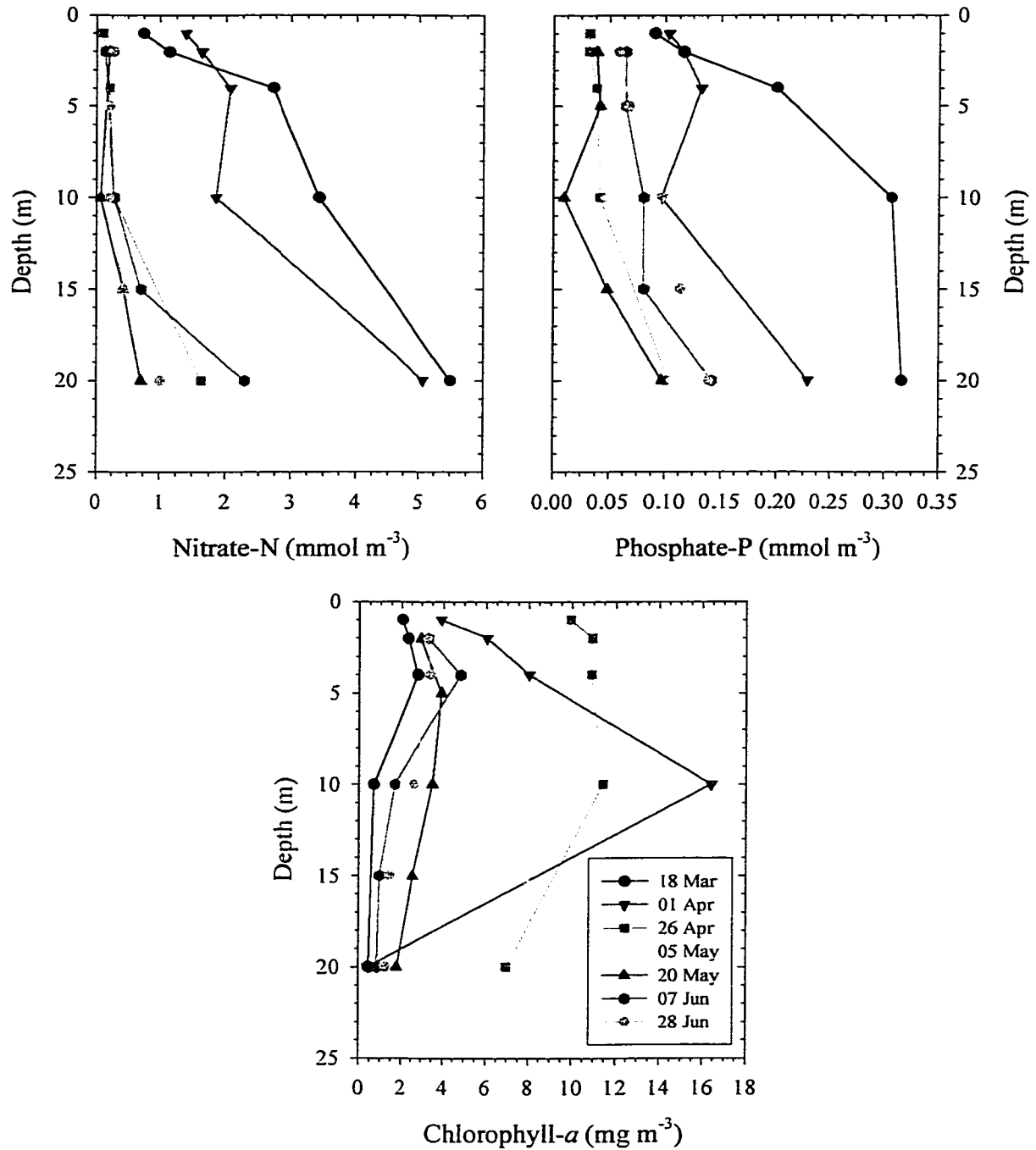


FIGURE 4.4: Profile measurements of nutrients (Chapter 2.4.6) and chlorophyll-*a* (Chapter 2.4.5) in 1999. Notice the drop in nutrient concentrations from 18 Mar to 26 Apr and the associated increase in chlorophyll-*a* concentrations.

4.1.4 Thermal stratification and model comparisons

4.1.4.a Under-ice period

The PWP model does a remarkable job of predicting the under-ice thermal structure and dynamics of the lake (Figure 4.3a,b). The average difference between the measured and modeled temperatures is 0.16 ± 0.11 °C (N=13448). The gradual warming of the mean lake temperature from ~ 2.6 to 3.8 °C and turnover is predicted by the model (Figure 4.3b,c).

The model at each time-step simulated free convection by searching for instability in the water column ($d\rho/dz \leq 0$) and instantaneously mixing the water from the surface downward to achieve static stability (Chapter 2.7). In reality, however, convective mixing is not instantaneous (e.g., Malm et al. 1998) and this simplification in the model resulted in the loss of detail in the surface temperature records. Penetrative convection leading up to turnover was modeled and can be seen as a staircase of steps in the MLD from 16 m on 3 Apr down to the lake bottom on 12 Apr when turnover was predicted to commence (Figure 4.3c).

4.1.4.b Ice-free period

The PWP model also does a good job of predicting the thermal structure of the lake, particularly near the surface, during the ice-free period (Figure 4.3a,b). The average difference between the measured and modeled temperatures after ice out is 0.69 ± 0.64 °C (N=24113). The gross thermal features of the lake were modeled very well including the strong heating periods near 24 May and 20 Jun. These results demonstrate that the PWP model is suitable for describing the TKE and momentum budgets in relatively small lakes like Placid that are morphologically similar to a bowl. Since the model is one-

dimensional in the vertical, the good predictive ability suggests that horizontal advection must have been minimal. The one exception might be near the lake bottom (20 m) where the model predicted the temperature to remain relatively constant at 4 °C. Warming near the lake bottom was observed until 18 May when sufficient density stratification had presumably developed at the surface to stabilize the water column and suppress vertical exchange (Figures 4.3a, 4.5). It is possible that the warming observed near the lake bottom was due to groundwater influx. However, if groundwater influx into the hypolimnion was significant, it is unlikely that the dissolved gases there would agree with the Redfield stoichiometry. The good agreement between the measured and modeled bottom $p\text{CO}_2$ and DO suggests that groundwater influx was minimal (Figure 4.5a,b).

Several model experiments were performed to try to simulate the warming of the bottom water. Varying offsets were applied to the heat and wind stress inputs and the parameterization of mixing including the Coriolis force, which gives inertial motion to the diurnal velocity cycle (see Price et al. 1986). The Coriolis force, a function of latitude and the angular velocity of rotation of the earth, had a profound effect on the resulting profiles. The Coriolis force is usually only considered in large bodies of water, such as the Laurentian Great Lakes, where friction from the sides of the lake can be disregarded (Ivey and Patterson 1984). Decreasing the Coriolis parameter in the model, under the assumption that friction from the sides of the lake might attenuate this effect, resulted in greater vertical heat transfer from the surface to depth but the overall thermal profile was compressed. These model experiments indicated that the distribution of energy in the water column was inadequate but the amount of heat available to the system was reasonable. It should be noted that no parameter adjustments were made in the

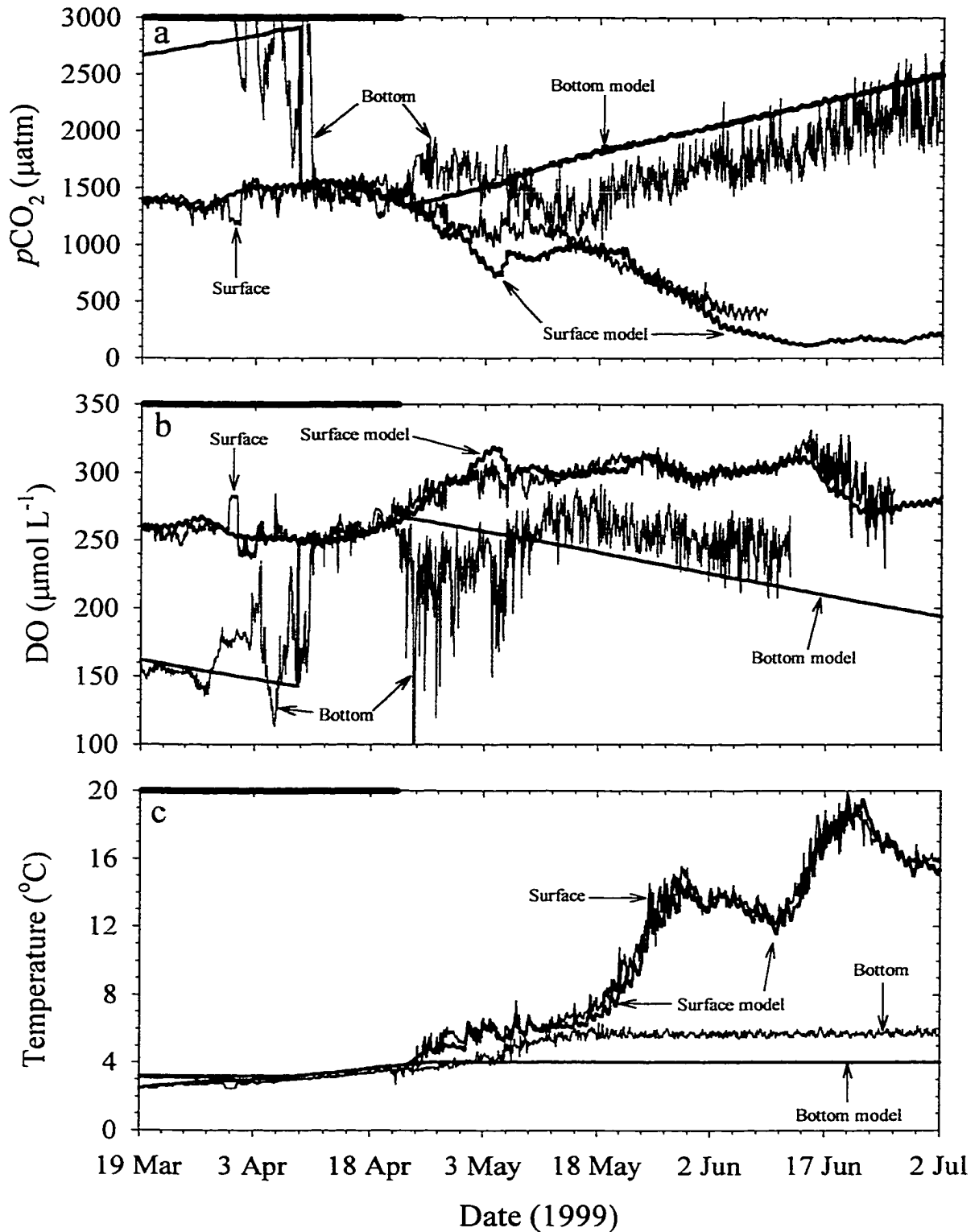


FIGURE 4.5: An overview of the *in situ* surface (black line), *in situ* bottom (green), modeled surface (bold red), and modeled bottom (bold blue) $p\text{CO}_2$ (a), DO (b), and temperature (c) for the deployment.

modeling of the data presented herein. Henderson-Sellers and Davies (1989) state that cross-sectional area variations with depth should be input into lake thermal models and result in heat reaching the bottom of the lake more quickly because of the “funneling effect” of the bathymetry. However in our case, implementation of cross-sectional area variations with depth into the model had little effect on heat distribution. The relationship between the surface and bottom dissolved gases suggests that the ML is deeper than predicted by the PWP model and so it is assumed that the warming of the water at the bottom is a result of episodic surface mixing down to this depth.

4.1.5 Dissolved gas observations and comparisons with model predictions

4.1.5.a Under-ice period

The major features of the dissolved gas time-series were discussed in Chapter 4.1.3. The features discussed in this section are used to illustrate the predictive ability of the coupled physical-biogeochemical models.

The trends in the dissolved gases under ice are modeled well (Figures 4.5, 4.6). The average residual between the measured and simulated surface $p\text{CO}_2$ and DO is $66 \pm 64 \mu\text{atm}$ ($N=1681$) and $6 \pm 5 \mu\text{mol L}^{-1}$ ($0.18 \pm 0.19 \text{ mg L}^{-1}$) ($N=1681$), respectively.

Contributions to the surface dissolved gas variability from net community production (Chapter 2.7.3.b), entrainment (Chapter 2.7.3.c), and temperature were determined from the coupled physical-biogeochemical models (Chapter 2.7) and totaled over 24-hrs to provide daily rates of change (Figure 4.7). These data were used to help determine the process or processes that controlled biogeochemical variability. Note that net community production (Equation 1.2) was determined by subtracting the rate of

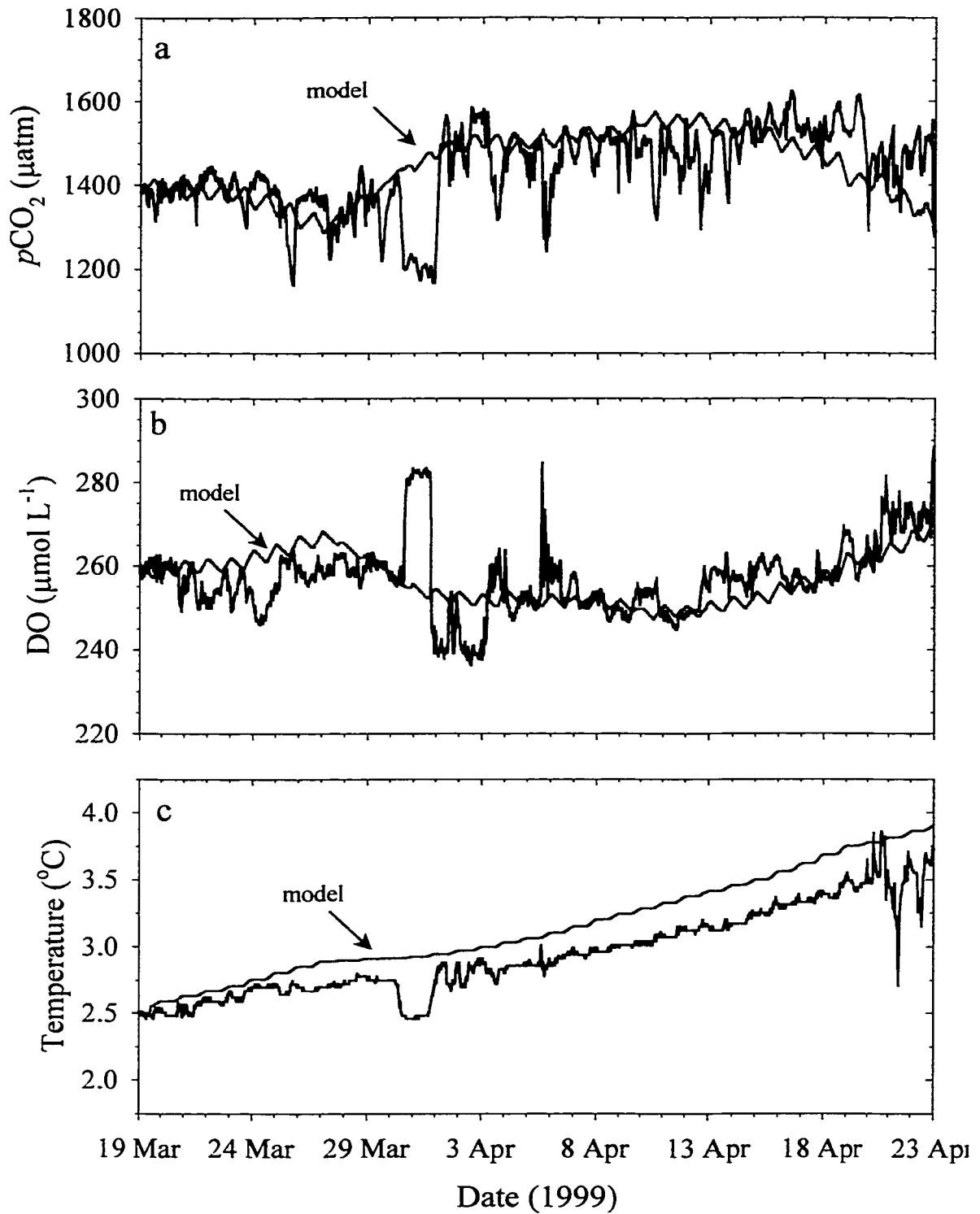


FIGURE 4.6: The under ice dissolved gas time-series (black) and model simulations (red) near the lake surface for **a)** $p\text{CO}_2$, **b)** dissolved O_2 , and **c)** temperature.

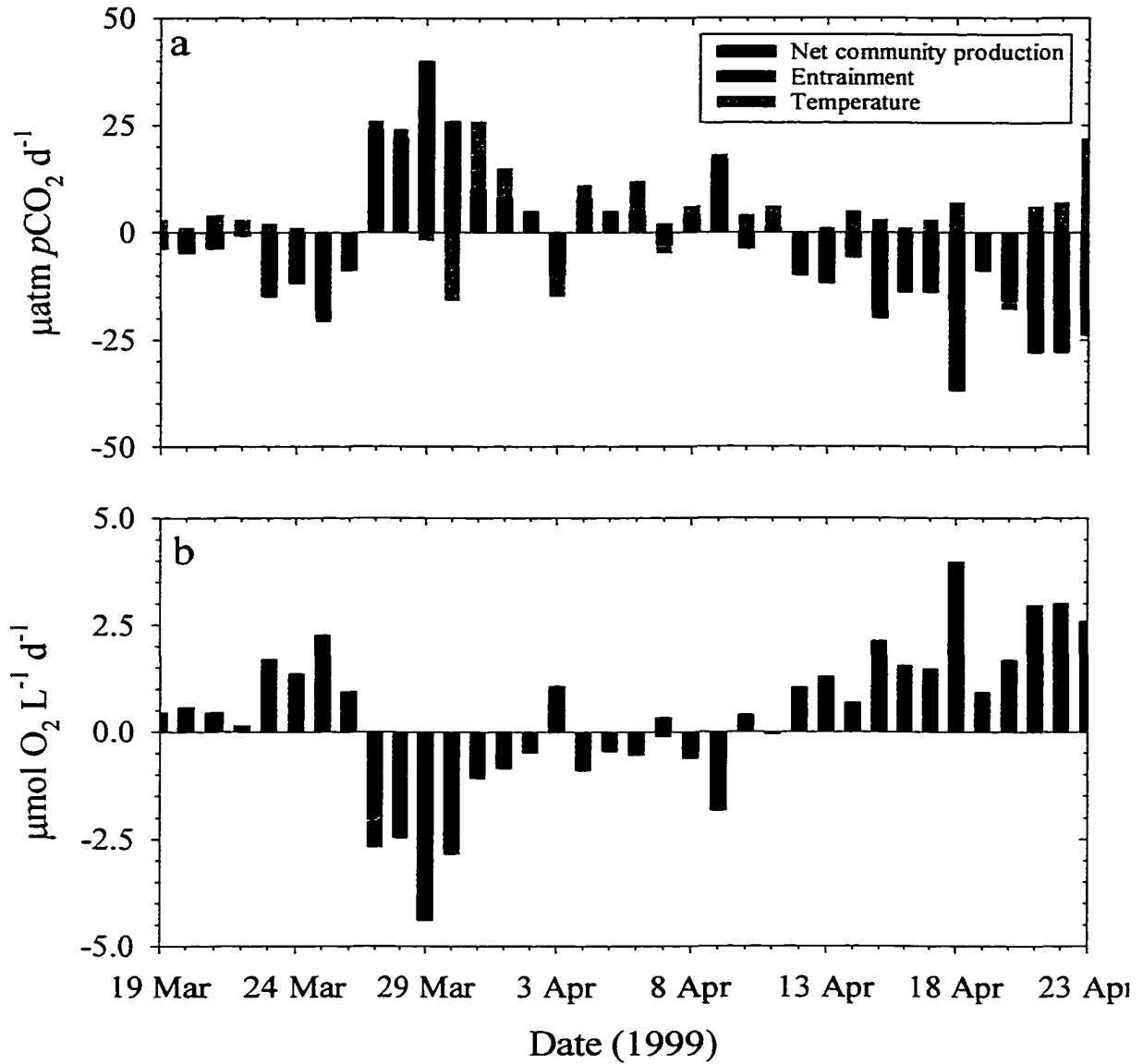


FIGURE 4.7: The contributions of net community productivity and entrainment to the under-ice dissolved gases near the lake surface. **a)** The daily rate of gain (+) or loss (-) of $p\text{CO}_2$. The legend applies to both plots. **b)** The daily rate of gain or loss of DO.

community respiration (Equation 2.38) from the rate of net primary production (Equation 2.37). Entrainment, or vertical advection, was determined from Equations 2.40 and 2.41.

The most prominent feature under ice is the increase and decrease in $p\text{CO}_2$ and DO, respectively, from 27 Mar to 3 Apr (Figure 4.6). The models simulated these trends very well. Community production in this period is low relative to respiration as a result of the low PAR (Figures 4.7, 4.2c) associated with heavy cloud cover and the precipitation of ~5 cm of snow onto the lake surface on 29 Mar. This was the only major precipitation event during the study when the lake was ice-covered

Another trend is the net decrease in $p\text{CO}_2$ and increase in DO over the last 10 days of ice cover (12-22 Apr) which parallels the increase in chlorophyll-*a* under ice. By this time, turnover had commenced, as indicated by the agreement between the surface and bottom sensor measurements (Figure 4.5), and net community production was controlling the dissolved gases (Figure 4.7). The assimilation number ($P_r \text{ Chl}^{-1}$), used in the determination of the photosynthetic rate, was changed from a value of 2.50 to 1.00 on 4 Apr when penetrative convection led to ML deepening (Chapter 2.7.3.b and Figure 4.3c). The smaller assimilation number was used to simulate the decreased photosynthetic rate that likely resulted from ML deepening. Increases in mixing depth tend to reduce total photosynthesis because the average light intensity to which the circulating cells are exposed decreases (Talling 1971; Kirk 1994). Conversely, respiration rates are generally not affected by increases in mixing depth (Kirk 1994). Had the assimilation number been kept constant at 2.50 in the model the photosynthetic rate would have been too high and $p\text{CO}_2$ drawdown and DO production would have been overestimated.

The models predict that the dissolved gas variability at the surface was dominated by net community production and that entrainment was relatively minor because the ML

was near the bottom sensors when the simulation began on 19 Mar (Figures 4.7, 4.3c). The average daily contributions of the modeled parameters to the dissolved gas variability in the surface ML are summarized in Table 4.2.

Short-term fluctuations in the gases that are a result of gradients near the lake surface cannot be modeled. For example, the large two-day swing in dissolved gas levels on 30 Mar (Figure 4.6a,b) is attributed to surface dilution from melt runoff of the recent snowfall. This is supported by the dissolved gases, which exhibited the characteristic signature of a water mass that had been exposed to the atmosphere (low $p\text{CO}_2$ and high DO relative to the average). In addition there was an associated decrease in both water temperature (Figure 4.6c) and specific conductance at 2 m (Figure 4.8), further supporting surface dilution.

The magnitude of short-term variability under ice is much larger than predicted by the model. The diurnal phase of the modeled gases is driven by the light cycle (photosynthesis and respiration), yet the *in situ* data do not consistently show the same relationship. The diel dissolved gas variability is likely associated with gradients above the surface instrumentation, which are convectively mixed downward. The presence of convective currents is illustrated in the stepwise temperature record (Figure 4.6c), as discussed earlier. The surface gradients in biogeochemistry cannot be modeled with the poor spatial resolution of a 2-box model. Furthermore, and most importantly, the ML is modeled as a slab that is completely and instantaneously mixed which precludes the development of gradients at the surface. Therefore, the model is limited in situations as this where there is no well-defined surface ML.

TABLE 4.2. Average daily contributions to dissolved gas variability in the surface ML for different periods.

DO (mol L ⁻¹ d ⁻¹)				
Period	Net Community Production	Air-Water Gas Exchange	Entrainment	Temperature
Ice-covered (19 Mar – 23 Apr)	0.33 ±1.77 (97.9%)	N/A	-0.012 ±0.035 (2.1%)	N/A
Ice-free: Episodic deep mixing (23 Apr – 18 May)	2.25 ±1.92 (31.4%)	2.45 ±1.01 (39.8%)	-2.82 ±3.61 (28.8%)	N/A
Ice-free: Stratified (18 May – 2 Jul)	2.21 ±1.92 (38.4%)	-3.01 ±2.51 (49.0%)	-0.83 ±1.59 (12.6%)	N/A
pCO ₂ (µatm d ⁻¹)				
Period	Net Community Production	Air-Water Gas Exchange	Entrainment	Temperature
Ice-covered (19 Mar – 23 Apr)	-3.1 ±16.2 (78.4%)	N/A	0.1 ±0.4 (0.7%)	2.0 ±4.8 (20.9%)
Ice-free: Episodic deep mixing (23 Apr – 18 May)	-22.1 ±18.5 (27.4%)	-33.3 ±13.1 (41.3%)	10.6 ±18.1 (13.1%)	6.2 ±16.7 (18.1%)
Ice-free: Stratified (18 May – 2 Jul)	-15.2 ±16.7 (38.8%)	2.1 ±10.7 (18.7%)	6.4 ±8.5 (14.6%)	4.1 ±20.4 (27.9%)

As for the bottom dissolved gas models, the large swings in the dissolved gases measured by the bottom sensors (Figure 4.5a,b) are associated with ML deepening and mixing as previously discussed (Figure 4.3c). These large swings could not be modeled with the poor vertical resolution of our model. The modeled dissolved gases at the bottom were subject only to community respiration until the ML reached a depth of 20 m on 8 Apr and the bottom and surface records converged. The *in situ* dissolved gases converged on 10 Apr (Figure 4.5a,b).

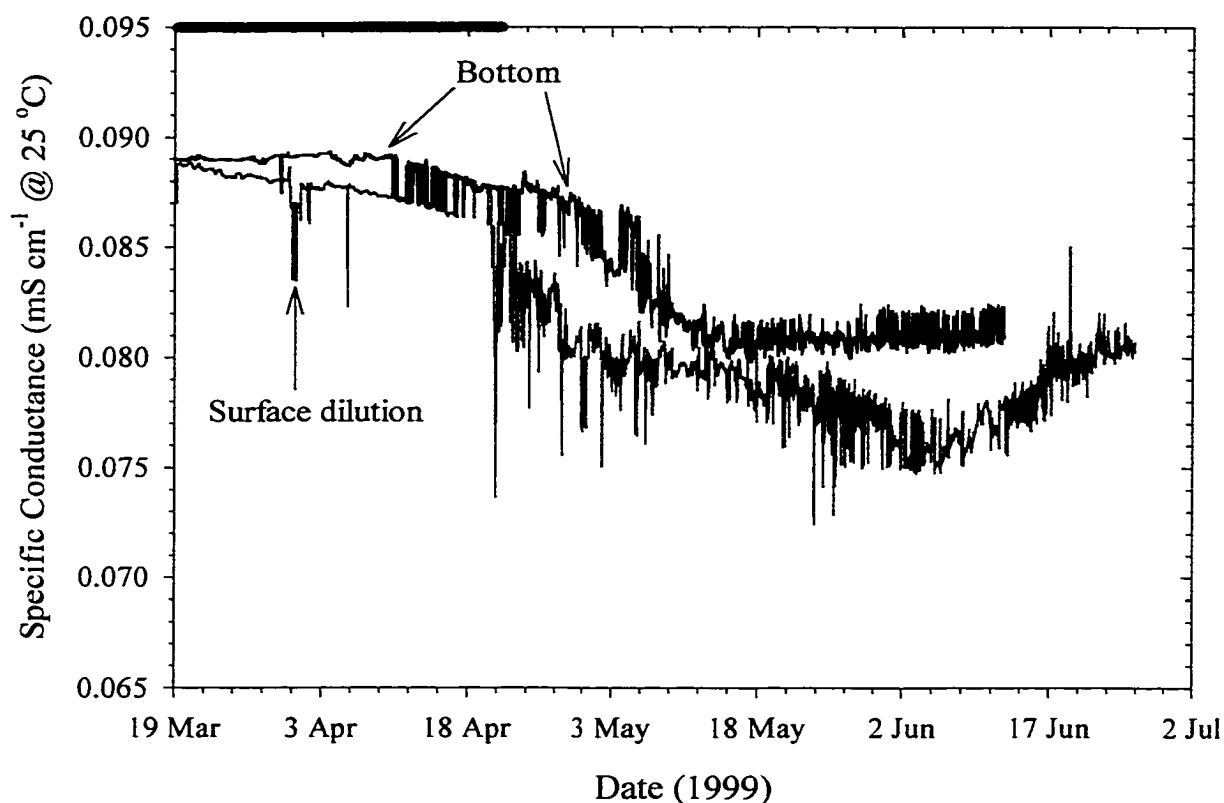


FIGURE 4.8: Specific conductance measured by the YSI 6000s (Chapter 2.3.4). The black bar at the top of the figure indicates ice cover.

4.1.5.b Ice-free period

The dissolved and saturation levels for the dissolved gases at the lake surface are shown for the ice-free period in Figure 4.9. The average residual between the *in situ* and modeled $p\text{CO}_2$ and DO is $137 \pm 101 \mu\text{atm}$ ($N=2113$) and $7 \pm 7 \mu\text{mol L}^{-1}$ ($0.22 \pm 0.22 \text{ mg L}^{-1}$), respectively ($N=2924$).

In addition to the processes of net community production, entrainment, and temperature contributing to biogeochemical variability, the loss of ice cover meant that air-water gas exchange also had to be considered. As with the under-ice data,

contributions from these processes were summed over 24-hrs to provide daily rates of change (Figure 4.10).

The models follow the long-term trends reasonably well during the post-turnover period of episodic deep mixing (Table 4.1). The largest discrepancy between the modeled and measured gases occurred from ~30 Apr to 6 May when the modeled $p\text{CO}_2$ dropped below and the DO rose above the *in situ* measurements. The models predict that entrainment was minimal during this period but air-water gas exchange and biology worked in concert to drive the observed trends (Figures 4.9, 4.10). The modeled MLD in this period shoaled considerably from ~2 to 4 m due to thermal stratification at the surface (Figure 4.3c,b), but thermal stratification was actually weaker than the model predicted (Figure 4.3a). Consequently, there may have been entrainment into the surface ML that was not simulated by the model. This may account for the model discrepancies from ~30 Apr to 6 May.

After seasonal stratification had developed to restrict the ML to depths less than 5 m, the 2-box model adequately described the physical structure of the lake. As a result, the biogeochemical models matched the *in situ* records remarkably well (Figure 4.9). It should be noted that the assimilation number was increased back to 2.50 after seasonal stratification had developed (Table 4.1) because of the relatively shallow ML.

The modeled $p\text{CO}_2$ in the surface ML reached atmospheric equilibrium on 1 Jun, only 4 days earlier than the actual date. The *in situ* surface DO reached atmospheric equilibrium on 21 May and the model predicted 23 May. The saturation level for DO is presented in Figure 4.9b. The DO is supersaturated for the remainder of the deployment,

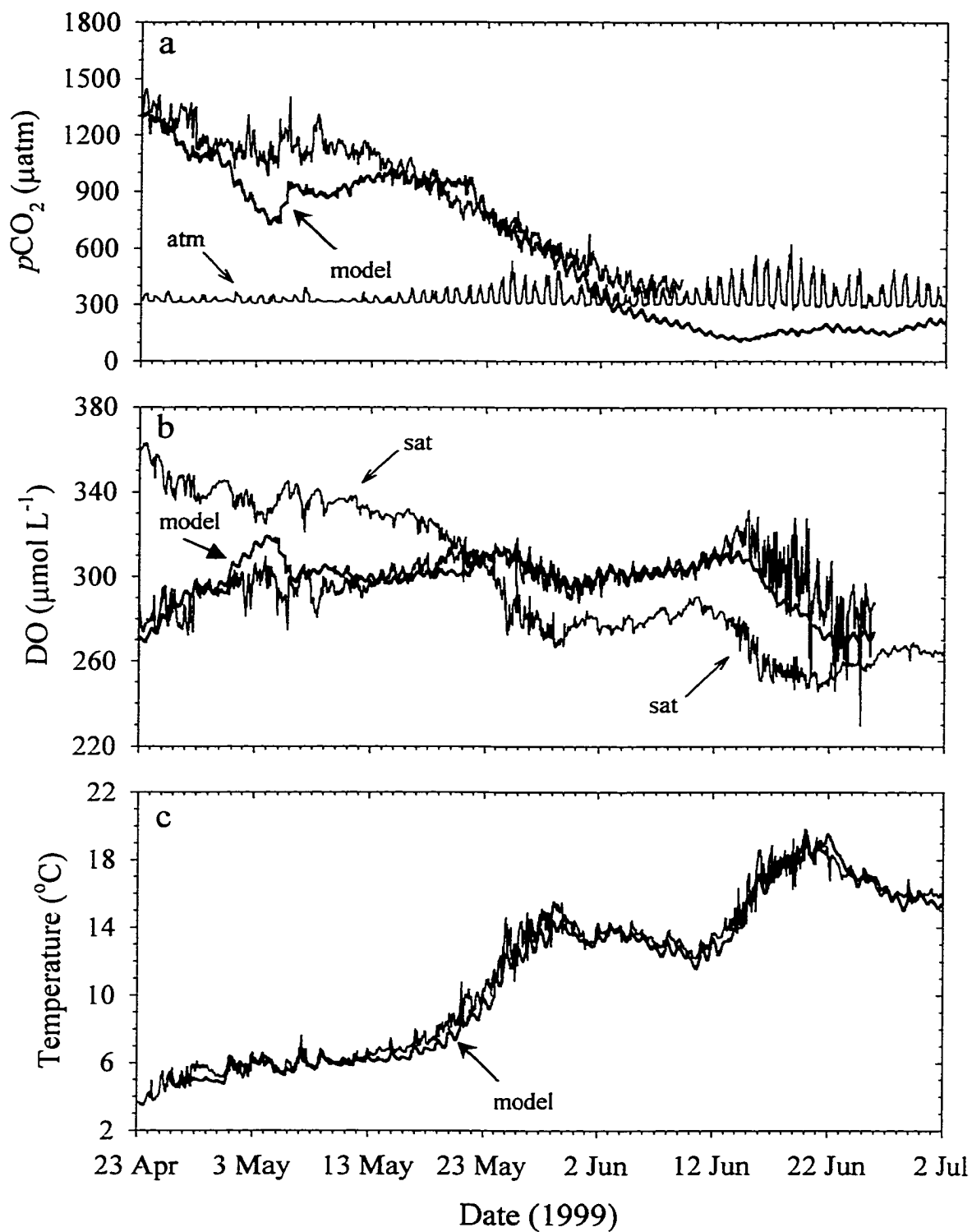


FIGURE 4.9: The dissolved gas *in situ* time-series (black) and model simulations (red) near the lake surface after ice out for **a)** $p\text{CO}_2$ (atm=atmospheric), **b)** dissolved O_2 (sat=atmospheric saturation), and **c)** temperature.

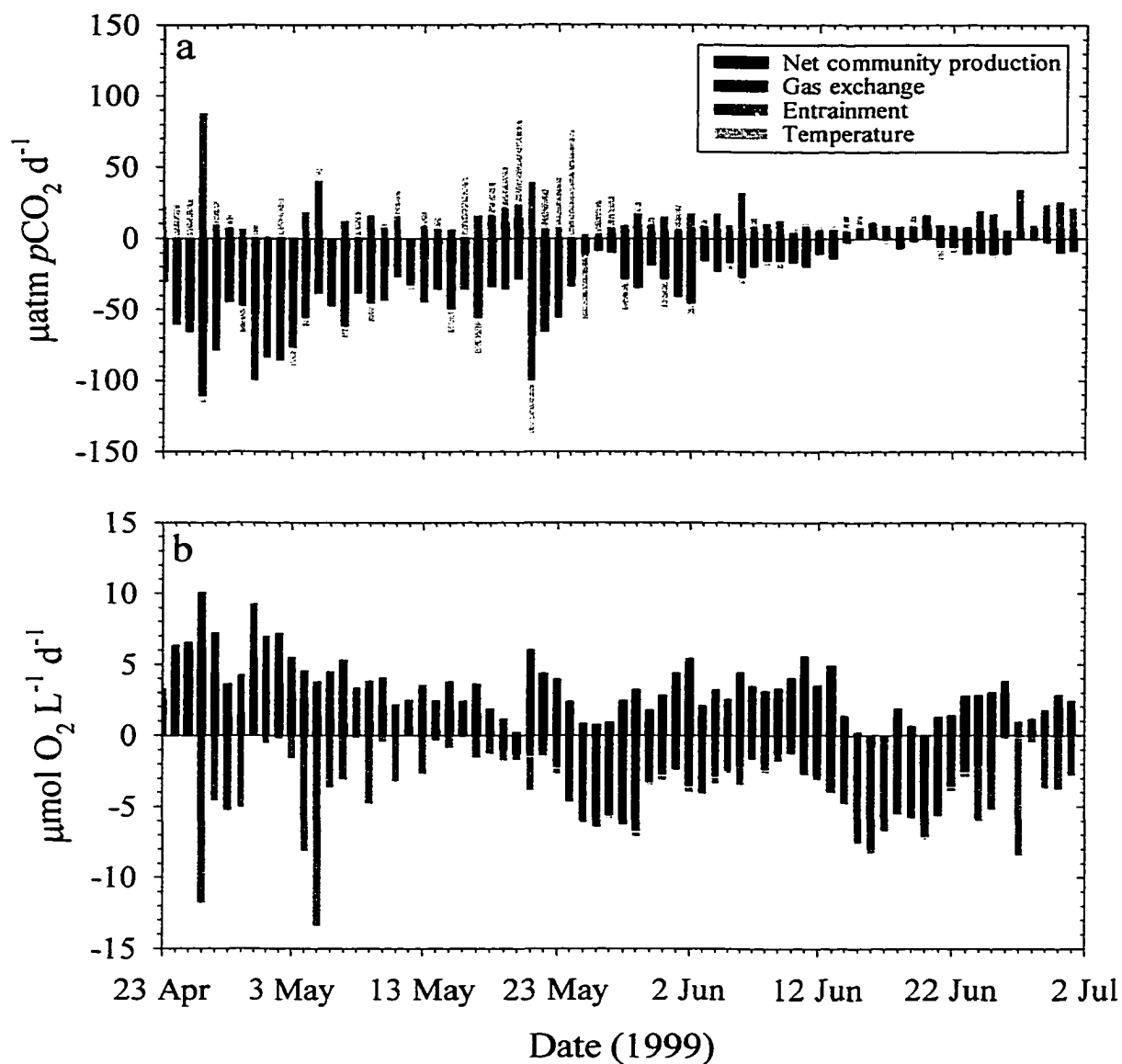


FIGURE 4.10: The contributions of net community productivity, air-water gas exchange, entrainment, and temperature to the dissolved gases after ice out. **a)** The daily rate of gain (+) or loss (-) of $p\text{CO}_2$. The legend applies to both plots. **b)** The daily rate of gain or loss of DO. Note that temperature only affects the $p\text{CO}_2$.

which could only have been a result of net primary production. The model was successful for both $p\text{CO}_2$ and DO supporting the validity of the parameterization of the processes. Had the modeled $p\text{CO}_2$ not fit the data as well as the modeled DO, for

example, then one or more of the model parameterizations might have been questionable or it may have indicated that a process was contributing to $p\text{CO}_2$ variability but not to DO. A process that could potentially contribute to the variability of $p\text{CO}_2$ but not to DO is the formation and dissolution of calcite (Chapter 1.4.1.c). Calcite saturation calculations for the lake surface (2 m) showed that the lake was undersaturated with respect to calcite by an average $90 \pm 7\%$ ($N=5$). The profiles of Ca^{2+} , Mg^{2+} , and TA are shown in Figure 4.11. Calculations of $p\text{CO}_2$ from TA/pH and DIC/pH matched suggesting that no significant concentrations of organic acids, a primary source of DOC, were present (Figure 2.2). These calculations, in addition to the good fit of the $p\text{CO}_2$ and DO models, are evidence that the formation or dissolution of calcite and photooxidative production of DIC were not contributing to the *in situ* $p\text{CO}_2$ variability.

Diel *in situ* gas variability in the post-turnover period of episodic deep mixing was large (Table 4.1; Figure 4.9). As in the under-ice period, the model does not do as well with large short-term variability. The fact that upward (downward) swings in $p\text{CO}_2$ were matched by downward (upward) swings in DO suggests that the same process or processes were controlling the gases. Air-water gas exchange was strong because of the large surface gas gradients but its forcing was only in one direction, toward equilibrium with the atmosphere. The inverse relationship between $p\text{CO}_2$ and DO implicates biological control but the variability was not consistently synchronized with PAR. Much of the large variability was correlated with temperature. For instance, the large increase in $p\text{CO}_2$ and drop in DO on 4 and 5 May were associated with a decrease in temperature. This is consistent with vertical advection because of the gradients within the water column (Figure 2.4). Strong entrainment in this period is also exhibited in the models

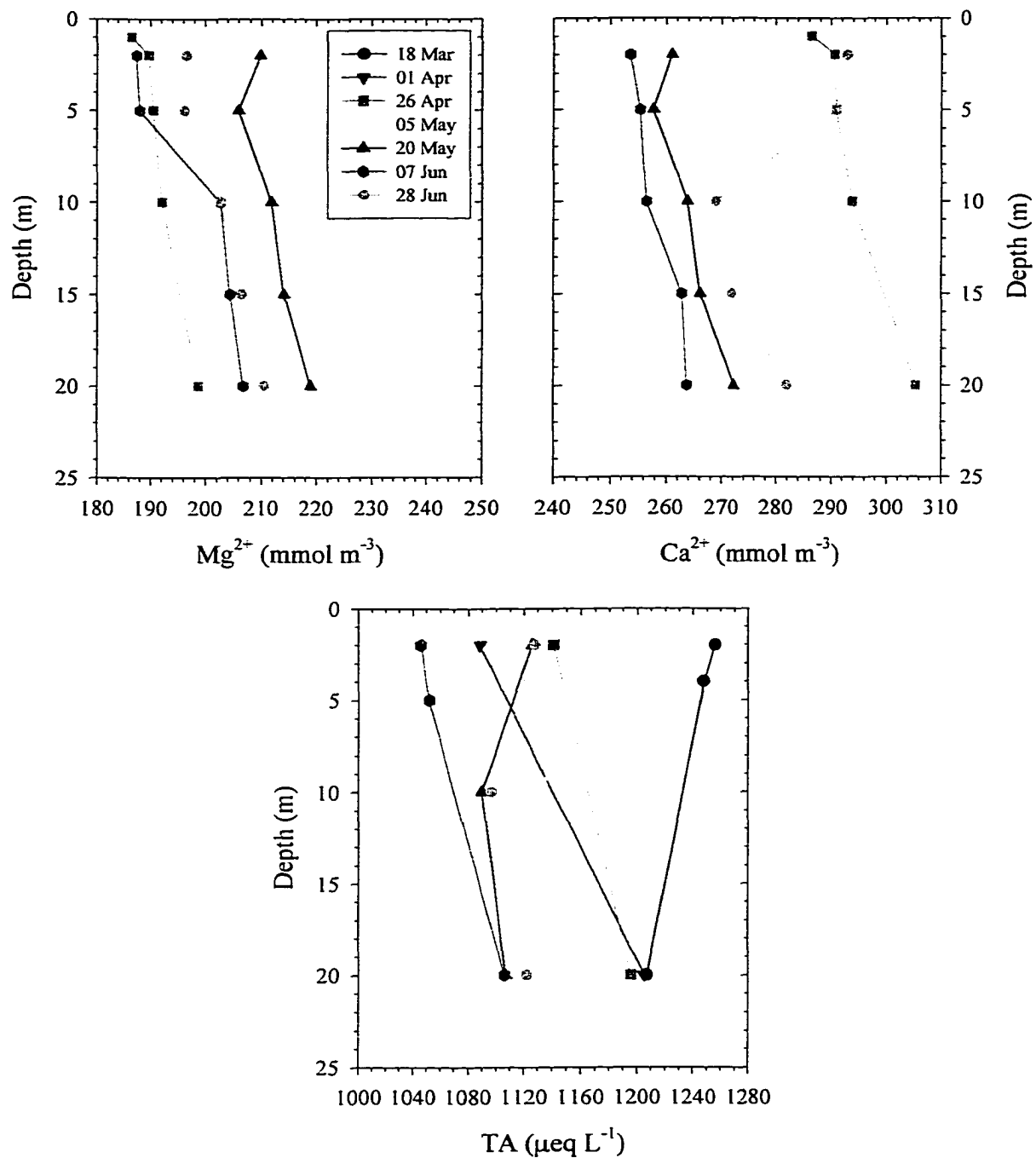


FIGURE 4.11: Profiles of the major cations, Mg^{2+} and Ca^{2+} (Chapter 2.4.7), and TA (Chapter 2.4.4) in 1999.

(Figure 4.9a,b). However, the changes in the dissolved gases at the surface are often greater than entrainment alone can explain. Therefore, it is a combination of all of these processes that makes the gases so dynamic in the post-turnover period of episodic deep-mixing. The models predict that net community production and gas exchange contribute ~30 and 40%, respectively, to the average daily dissolved gas variability in this period from ice out to 18 May. Entrainment contributed ~29 and 13% to the surface DO and $p\text{CO}_2$, respectively, and temperature ~18% to the $p\text{CO}_2$ (Figure 4.10; Table 4.2).

After 18 May, when seasonal stratification developed and the 2-box model was most suitable, short-term dissolved gases dynamics were modeled remarkably well. Daily fluctuations in the *in situ* gases are readily apparent and there is exceptional model agreement for DO from 24 May to 12 Jun (Figure 4.9). The timing of the rise and fall in the dissolved gases coincided with the light-dark cycle illustrating biological control of their variability. Diel variability was typically $\pm 6 \mu\text{mol L}^{-1}$ for DO and $\pm 70 \mu\text{atm}$ for $p\text{CO}_2$. Reaeration and net community production worked in concert to lower the $p\text{CO}_2$ to atmospheric levels whereas DO was supersaturated with respect to the atmosphere for the remainder of the deployment (Figure 4.10). The contributions from each of the modeled processes contributing to dissolved gas variability during the stratified period are given in Table 4.2.

As with the under-ice period, a constant rate of respiration was used to describe the trends in the bottom dissolved gases after ice-out (Figure 4.5). This model was not suitable for describing the convergence of the surface and bottom dissolved gases during the post-turnover mixing events. However, the model was successful at predicting the trends after seasonal stratification on 18 May, which is important for the determination of

seasonal dissolved gas levels in different turnover and stratification scenarios (see Chapter 4.2). Temperature-dependent respiration could not explain the short-term variability at the lake bottom. The *in situ* gases exhibited large variations that were probably associated with steep gradients near the bottom but this cannot be verified. Discrete profile measurements were not made below the bottom instrumentation.

4.2 Chapter summary and conclusions

To our knowledge these are the first long-term *in situ* biogeochemical measurements in a lake during turnover and the onset of stratification. We were able to characterize the biogeochemical variability for over 3 months. Vertically distributed sensors within the water column have shown that convection led to lake turnover and complete mixing under ice. A mixed-layer model (PWP) originally developed for modeling the marine ML predicted the thermal structure of the lake exceptionally well in both ice-covered and ice-free conditions. The biogeochemical models simulated the gross features of the dissolved gases at the lake surface and bottom and were particularly successful at simulating diel variability after seasonal stratification had developed. These models demonstrated their usefulness for estimating the contributions of air-water gas exchange, photosynthesis and respiration, entrainment, and temperature on dissolved gas variability over time.

Turnover and the post-turnover deep-mixing events were important to the seasonal dissolved gas levels in the lake. If seasonal stratification had developed immediately following ice out on 23 Apr (modeled by setting the entrainment to zero) the average surface $p\text{CO}_2$ and DO levels would have changed by $-325 \mu\text{atm}$ and

+16 $\mu\text{mol L}^{-1}$ (+0.5 mg L^{-1}), respectively, over the measurement time periods (Figure 4.5). The surface gases would have reached atmospheric saturation levels sooner (16 May vs. 1 Jun for $p\text{CO}_2$ and 4 vs. 21 May for DO), but the DO at the lake bottom (20 m), assuming the same constant rate of DO consumption, would have dropped from ~215 to 150 $\mu\text{mol L}^{-1}$ (6.9 vs. 4.8 mg L^{-1}) by mid-June (Figure 4.5b). In terms of % saturation, this relates to a drop from 64 down to 42%. The early cessation of whole lake reaeration could lead to hypoxic or even anoxic conditions at the lake bottom and poor water quality later in the year. Simple simulations such as this demonstrate the importance of these major physical events in determining seasonal and annual water quality.

Chapter 5

Placid Lake Data Overview, Summary, and Conclusions

This chapter is intended to provide a brief overview and summary of the Placid Lake data. Detailed analysis of the data germane to the dissertation objectives was covered in Chapters 3 and 4. It is anticipated that those interested in pursuing future limnological studies of Placid Lake will appreciate the long-term trends provided here. Concluding remarks are at the end of the chapter.

5.1 Temperature

A total of 29 profiles of temperature were taken at the mid-lake mooring site from November 1996 to June 1999 (Table 2.2; Appendix 2). These profiles were used to construct a contour plot of temperature (Figure 5.1). Mid-summer surface temperatures reached as high as 23 °C with the lake warming to greater depth during the summer of 1998 than in 1997. It appears that the duration of summer heating was longer in 1998 than in 1997 but this is most likely an artifact of interpolation between intermittent profile measurements in 1998. Interpolation between large data gaps is also responsible for temperatures of up to 8 °C appearing under ice in the spring of 1997 and 1998 (Figure 5.1).

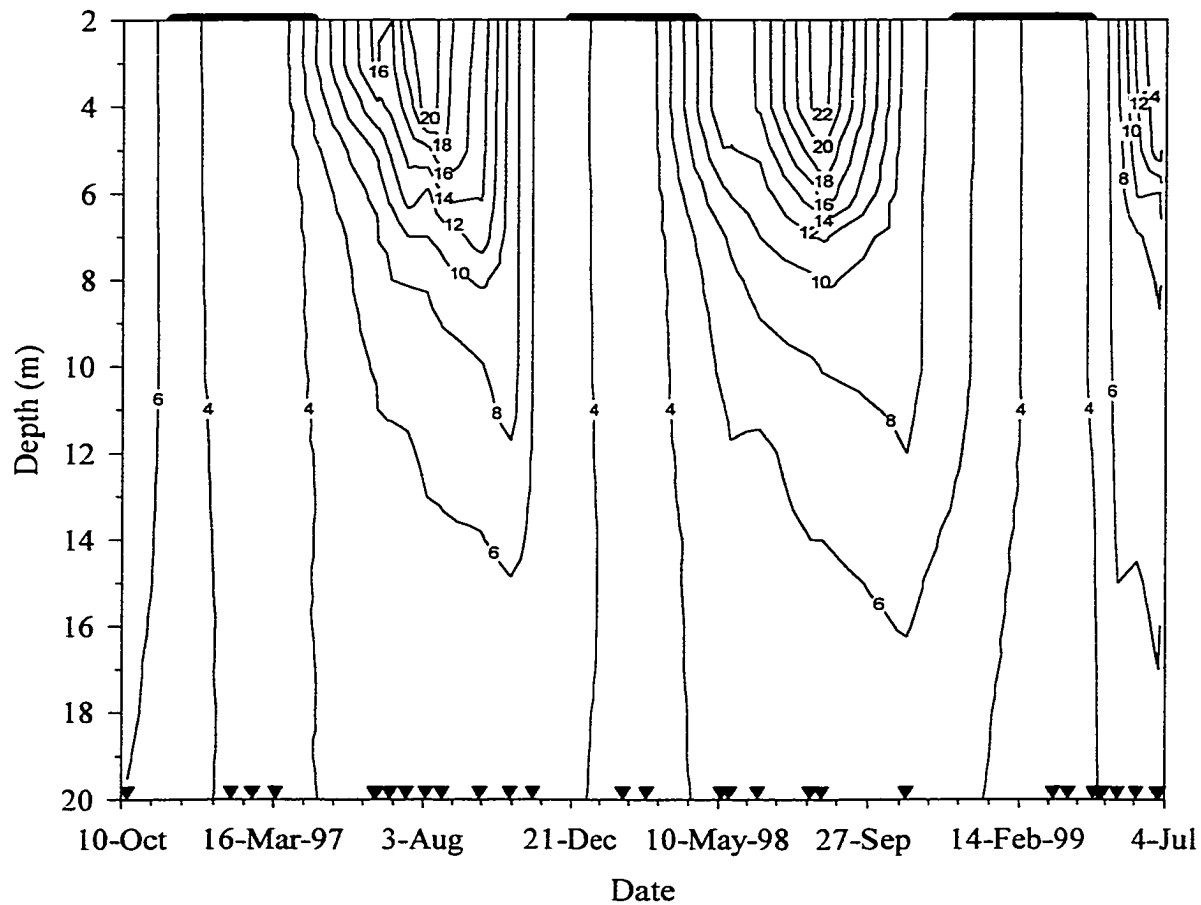


FIGURE 5.1: Temperature ($^{\circ}\text{C}$) contour plot. The black bars at the top of the figure indicate periods of ice cover. The triangles point to dates when profiles were taken. There are 28 days between each minor tick.

5.2 Lake transparency

Irradiance was measured at 1 m depth intervals with an analog photometer (Chapter 2.4.9). The surface extinction coefficients were calculated over a depth range of 1-4 m under ice cover and 1-5 m when ice-free. The topmost 1 m of water was often turbulent and subject to much scattering so was not included in the extinction coefficient determinations. The winter and spring of 1997 were the most turbid with an extinction coefficient ranging from ~0.8 to 1.0 (Figure 5.2). The lake was subject to a significant amount of melt runoff in the spring of 1997 as discussed in Chapter 3 (see also Figure 5.3). There was less snowpack in the winters of 1998 and 1999 and as a result there was likely less allochthonous organic material input into the lake during the spring runoff events in these years to decrease water clarity (Chapter 5.3). Interestingly, each spring when the moorings were recovered, the top of the white mooring float was covered in fine particulate matter. In fact, in the spring of 1998 the float had become so thickly covered that we were unable to locate the mooring by sight. Fortunately, we had stowed a Lotek fish transmitter in the reagent box for just such an emergency. With the help of a Montana Fish, Wildlife, and Parks employee and his acoustic receiver we eventually located the mooring. The particulate matter on the float was probably not associated with terrestrial runoff since runoff was minimal in 1998 and 1999. The particulate matter could have been from dry-fall that had accumulated on the ice surface and was released during ice melt or from the resuspension of fine sediment during turnover.

The Secchi disk depth was a close approximation of where 10% of the ambient visible light remained. The depth of the euphotic zone, in which photosynthesis can occur, is generally considered the level where 1% of the ambient light remains. In this

case, the euphotic zone is approximately twice the Secchi Disk depth. In the spring of 1997 this light level was reached at ~ 4 m whereas in the other two years the spring euphotic zone was nearly twice as deep.

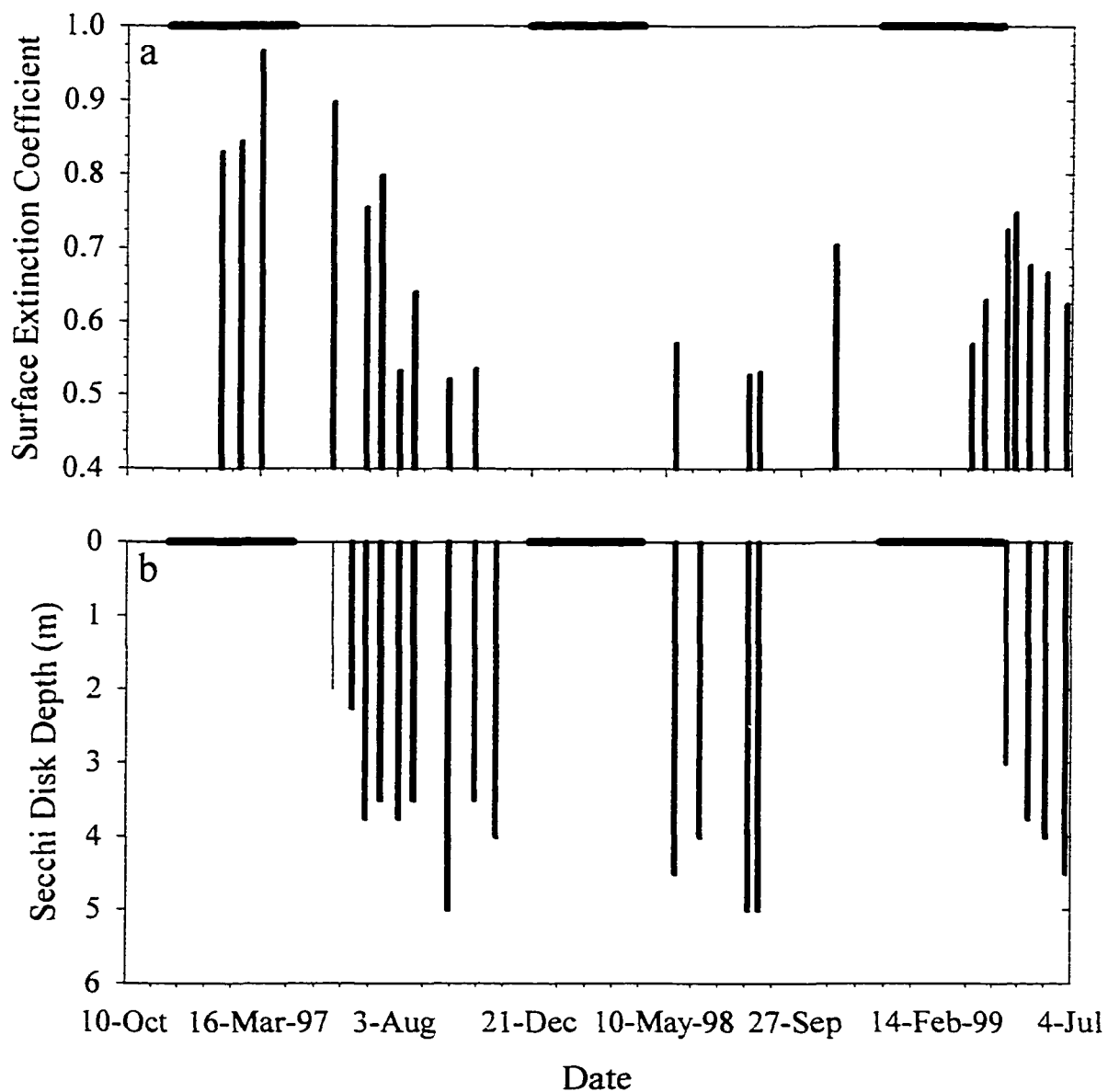


FIGURE 5.2: Extinction coefficient (a) and Secchi Disk measurements (b) made at the mid-lake mooring site (Figure 1.2). The bars at the top of each plot represent ice cover.

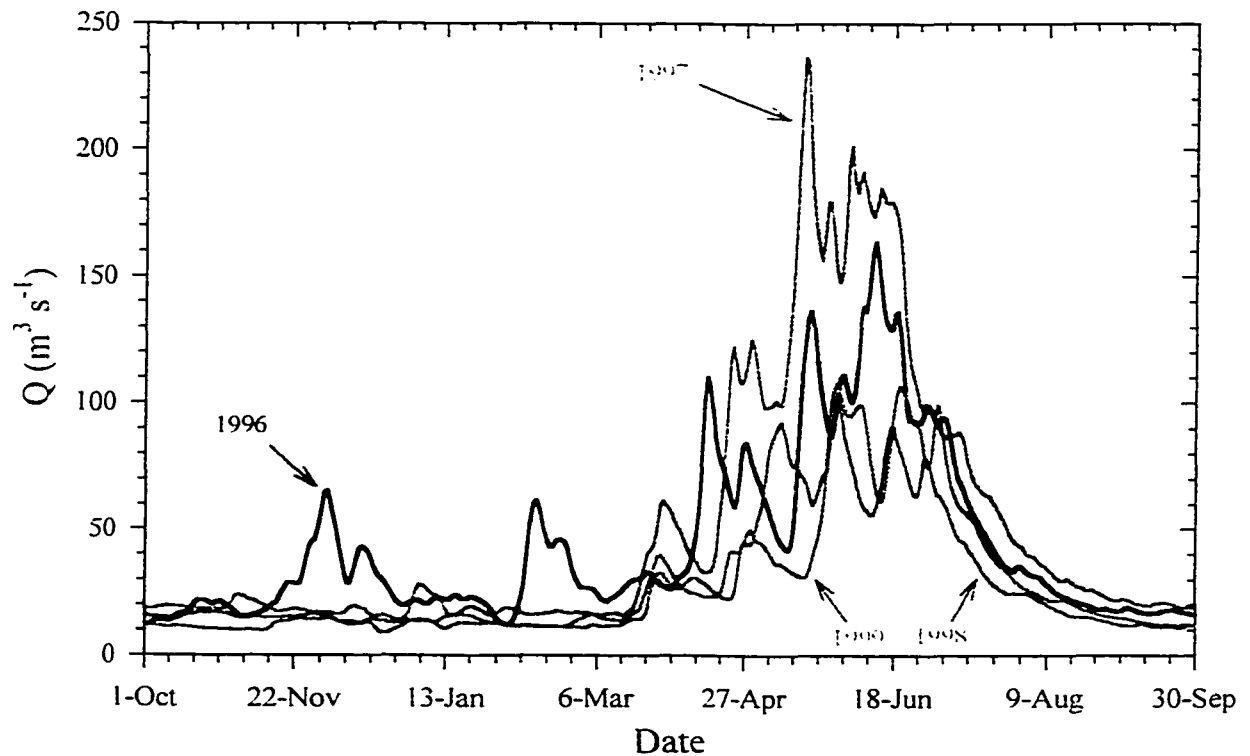


FIGURE 5.3: Swan River discharge (Q) near Bigfork, Montana (U.S.G.S. Station 12370000) for water years 1996 – 1999. The Swan River discharge was used as a proxy for Placid Creek discharge into Placid Lake (Figure 1.2). Snowpacks were above normal in 1996 and 1997 and near average in 1998 and 1999.

5.3 Autonomous *in situ* time-series

The time-series collected from 6 different deployments at the mid-lake mooring site are presented in Figure 5.4. These time-series were collected near the lake surface. See Table 2.1 for the initial deployment depths.

Placid Lake is heterotrophic, meaning that more organic matter is oxidized within the lake than is fixed by photosynthesis. As a result, the lake is supersaturated with respect to CO₂ for most of each calendar year (Figure 5.4a) and is a net source of CO₂ to the atmosphere. Photosynthesis led to surface *p*CO₂ drawdown each summer to lows of near 200 μatm in 1997 and 1998. The surface *p*CO₂ at ice up was significantly higher in the 1997/98 deployment than in the 1996/97 deployment. The 1999 trend also indicates that the *p*CO₂ at ice up was much lower than the previous year. As discussed in Chapters 3 and 5.2 above, it is believed that the high runoff event in spring 1997 resulted in a large input of terrestrial organic matter and greater respiration.

The DO was undersaturated with respect to the atmosphere for much of each year, corroborating that the lake is heterotrophic, with lows of near 185 mmol m⁻³ (~6 mg L⁻¹) (Figure 5.4b). The DO rose rapidly at the surface after ice out and reached or exceeded atmospheric saturation in the spring of 1998 and 1999. In the fall of 1997 there was a significant increase in *p*CO₂ and decrease in DO presumably due to fall turnover, which mixed the epilimnetic and hypolimnetic water (Figure 5.4).

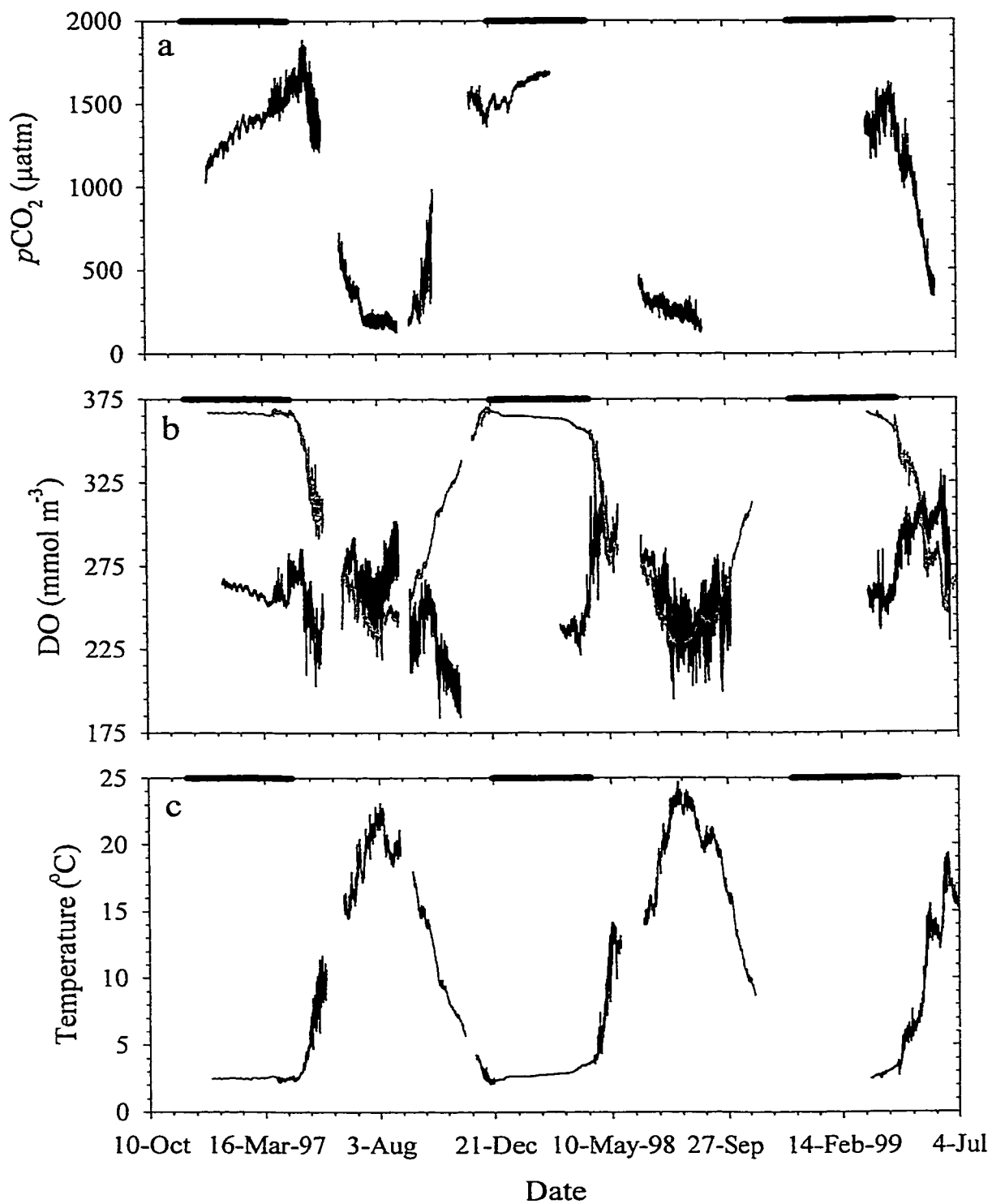


FIGURE 5.4: *In situ* time-series of surface (a) $p\text{CO}_2$, (b) DO measured (black) and saturation (red), and (c) temperature collected for the 6 deployments spanning winter 1997 to summer 1999. The black bars at the top of each plot represent ice cover.

5.4 Profile measurements and total inventories

Total inventory means of DO, DIC, and pH (from $[H^+]$) were determined from discrete profile measurements at depths of 2, 5, 10, 15, and 20 m (Appendix 2). To calculate total inventories, the water column was divided into 5 strata about the measurement depths. It was assumed that the average concentration measured at each depth approximated the concentration for that stratum, permitting the computation of total mass for the lake. The total inventory means were calculated by dividing the total mass by the lake volume (Figure 5.5).

As expected in a mesotrophic lake, clinograde curves were observed for DO, DIC, and pH (Figure 5.5). The DO varied markedly over the year, with minimum concentrations occurring at 20 m in the fall. Lows of ~ 45 and ~ 55 mmol m^{-3} (1.4 and 1.8 mg L^{-1}) were recorded in 1997 and 1998, respectively (Figure 5.5a). Low DO concentrations are typical near the bottom of lakes this time of year due to water column stratification and heterotrophic respiration in the hypolimnion. Fall turnover reaerated the water column as illustrated by the steep increase in bottom DO to near surface concentrations. DIC concentrations varied from a low of ~ 900 to near 1500 mmol m^{-3} . Higher DIC values were typically associated with a decrease in pH. Like the other variables, pH varied markedly with depth and with time. The extremes were recorded in the summer/fall of 1997. Surface pH approached 8.2 pH units as a result of photosynthetic drawdown of CO_2 . More acidic conditions (~ 7 pH units) were found at the bottom where decomposition processes dominated.

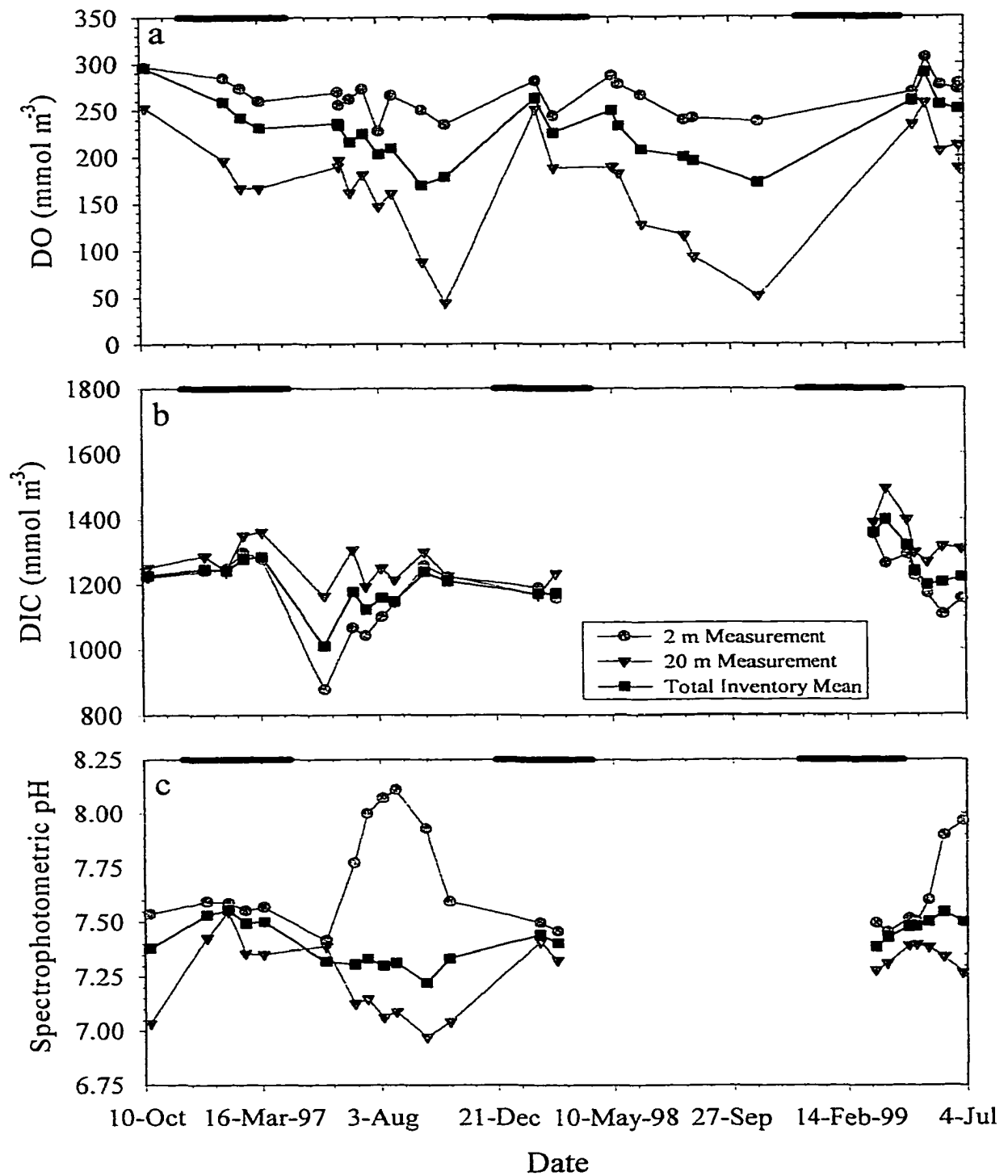


FIGURE 5.5: Selected profile measurements (2 and 20 m) made at the mid-lake mooring site and total inventory means of (a) DO, (b) DIC, and (c) pH. The bars at the top of each plot represent ice cover.

5.5 Conclusions

Autonomous *in situ* biogeochemical sensors were used to obtain high temporal resolution time-series in Placid Lake, a dimictic, freshwater lake. These time-series were collected over six different deployments from winter 1997 to summer 1999. The short-term and seasonal biogeochemical variability in the lake was characterized during ice-covered and ice-free periods, including the important transitional period from ice cover to ice out. A detailed analysis of the under-ice time-series revealed that a wind-induced seiche dominated the short-term variability in 1997. Gas variability on diel or shorter time-scales was typically small or undetectable during most of the ice-covered periods, only becoming significant prior to ice-out when light penetration increased, promoting convective currents and biological production. Vertically distributed sensors within the water column in 1999 showed that convective currents led to lake turnover and complete mixing under ice.

A one-dimensional (vertical) physical mixed-layer model simulated the thermal structure of the lake exceptionally well in both ice-covered and ice-free conditions in 1999. Simple two-box biogeochemical models were developed for $p\text{CO}_2$ and DO and were coupled to the mixed-layer depth output from the physical model. The biogeochemical models simulated the gross features of the dissolved gases at the lake surface and bottom and were particularly successful at simulating diel variability in the surface mixed-layer after seasonal stratification had developed. The models demonstrated their usefulness for quantifying the relative importance of biology, air-water gas exchange, mixing, and heating and cooling on $p\text{CO}_2$ and DO. Net community production dominated the average daily variability of $p\text{CO}_2$ (78%) and DO (98%) under

ice. After ice out, net community production, gas exchange, mixing, and heating and cooling each contributed 33, 30, 14, and 23%, respectively, to $p\text{CO}_2$ variability in the surface mixed-layer. These same processes contributed 36, 45, 19 and 0% to the DO.

The results from this research show that both spatial and temporal variability can be significant over intervals that would not be resolved by traditional sampling-based studies. Further refinement of studies that utilize autonomous biogeochemical sensors and modeling will undoubtedly continue to advance our understanding of biogeochemical cycling in aquatic ecosystems.

Appendix 1

***** SAMI-CO2 Data Manipulation Program *****

Version 3.6

Matthew M. Baehr

NOTE: This program written for the "new" SAMI data output format.

Version 3.3 to 3.4 - Changed program to use the second order log pCO2 fit instead of a normal second order polynomial fit through the calibration data.

Version 3.4 to 3.5 - Was not reading the file correctly to obtain AD1 (light channel) so corrected this. Also incorporated the AD2 (fluorometer channel) in the program.

Version 3.5 to 3.6 - Will now output the 740 nm Intensity when there is an error.

```
DECLARE SUB AnError (QProDat, JulianDay, dat$, tim$, temp, AD1, AD2, AveAbs740, Check, notneeded$)
```

```
DECLARE SUB CalibFactors (DataSearch$(), AveCalFact434, StdCalFact434, AveCalFact620, StdCalFact620, BatteryA, BatteryB)
```

```
DECLARE SUB Equations (DataSearch$(), QProDat, JulianDay, dat$, tim$, temp, AD1, AD2, Check, filetype$, AveA, StdA, AveB, StdB, AveAbs740, AveRatio, StdRatio, pCO2, AveCalFact434, StdCalFact434, AveCalFact620, StdCalFact620, caltemp, power2, power1, power0)
```

```
DECLARE SUB FindBeginning (find$)
```

```
DECLARE SUB FindFirstBlank (DataSearch$())
```

```
DECLARE SUB GitTemp (temp, AD1, AD2)
```

```
DECLARE SUB GitTimNDat (QProDat, JulianDay, dat$, tim$)
```

```
DECLARE SUB GitUserInput (filename$, filetype$, output$, caltemp, power2, power1, power0)
```

```
DECLARE SUB Main (find$, QProDat, JulianDay, dat$, tim$, temp, AD1, AD2)
```

```
DECLARE SUB WriteBlank (QProDat, JulianDay, dat$, tim$, temp, AD1, AD2, AveAbs740, AveCalFact434, StdCalFact434, AveCalFact620, StdCalFact620)
```

```
DECLARE SUB WriteOutput (QProDat, JulianDay, dat$, tim$, temp, AD1, AD2, filetype$, AveA, StdA, AveB, StdB, AveRatio, StdRatio, pCO2, AveCalFact434, StdCalFact434, AveCalFact620, StdCalFact620, AveAbs740)
```

```
DIM DataSearch$(12)
```

```

CLS

CALL GitUserInput(filename$, filetype$, output$, caltemp, power2, power1, power0)

OPEN filename$ FOR INPUT AS #1
OPEN output$ FOR OUTPUT AS #1

CALL FindBeginning(find$)
CALL FindFirstBlank(DataSearch$())
CALL CalibFactors(DataSearch$(), AveCalFact434, StdCalFact434, AveCalFact620,
  StdCalFact620, BatteryA, BatteryB)
CLOSE #1

OPEN filename$ FOR INPUT AS #1

WRITE #2, "QProDate", "JulianDay", "Date", "Time", "Temp.", "Light", "Fluor.",
  "Abs.A Avg.", "Std.A", "Abs.B Avg.", "Std.B", "740 Int.", "RatioAvg.",
  "Std.Ratio", "pCO2", "CalFactAAvg.", "StdCalA", "CalFactBAvg.", "StdCalB"

*****MAIN PROGRAM LOOP*****

DO UNTIL EOF(1)

CALL Main(find$, QProDat, JulianDay, dat$, tim$, temp, AD1, AD2)
CALL Equations(DataSearch$(), QProDat, JulianDay, dat$, tim$, temp, AD1, AD2,
  Check, filetype$, AveA, StdA, AveB, StdB, AveAbs740, AveRatio, StdRatio,
  pCO2, AveCalFact434, StdCalFact434, AveCalFact620, StdCalFact620, caltemp,
  power2, power1, power0)

LOOP

*****
END

SUB AnError (QProDat, JulianDay, dat$, tim$, temp, AD1, AD2, AveAbs740, Check,
  notneeded$)

' The following IF statement makes sure that only one error message prints for each data
' set. (i.e. if more than one error in a data set it will only be printed once in the output
' file.)

IF JulianDay = Check THEN
  GOTO 200
ELSE

```



```
WRITE #2, QProDat, JulianDay, dat$, tim$, temp, AD1, AD2, "**ERROR*",
      "NA", "NA", "NA", AveAbs740, "NA", "NA", "NA", "NA", "NA",
      "NA", "**ERROR**"
```

```
END IF
```

```
Check = JulianDay
```

```
200 END SUB
```

```
SUB CalibFactors (DataSearch$, AveCalFact434, StdCalFact434, AveCalFact620,
      StdCalFact620, BatteryA, BatteryB)
```

```
' This subroutine calculates K for use in subroutine "Equations" where the indicator
' absorbances are calculated. NOTE: K = Io/Iref.
```

```
AveCalAbs740 = VAL(RIGHT$(DataSearch$(1), 5))
AveCal434n620$ = LEFT$(DataSearch$(1), 25)
AveCalAbs620 = VAL(RIGHT$(AveCal434n620$, 5))
AveCal434$ = LEFT$(AveCal434n620$, 11)
AveCalAbs434 = VAL(RIGHT$(AveCal434$, 5))
```

```
StdCalAbs740 = VAL(RIGHT$(DataSearch$(2), 4))
StdCal434n620$ = LEFT$(DataSearch$(2), 25)
StdCalAbs620 = VAL(RIGHT$(StdCal434n620$, 5))
StdCal434$ = LEFT$(StdCal434n620$, 11)
StdCalAbs434 = VAL(RIGHT$(StdCal434$, 5))
```

```
Batteries$ = LEFT$(DataSearch$(3), 37)
BatteryB = VAL(RIGHT$(Batteries$, 5))
BattA$ = LEFT$(Batteries$, 17)
BatteryA = VAL(RIGHT$(BattA$, 5))
```

```
AveCalFact434 = AveCalAbs434 / AveCalAbs740
AveCalFact620 = AveCalAbs620 / AveCalAbs740
```

```
***The following uses propagation of errors to figure out the absolute
***standard deviation for the two previous equations.
```

```
StdCalFact434 = AveCalFact434 * (SQR((StdCalAbs434 / AveCalAbs434) ^ 2 +
      (StdCalAbs740 / AveCalAbs740) ^ 2))
StdCalFact620 = AveCalFact620 * (SQR((StdCalAbs620 / AveCalAbs620) ^ 2 +
      (StdCalAbs740 / AveCalAbs740) ^ 2))
```

```
END SUB
```

SUB Equations (DataSearch\$(), QProDat, JulianDay, dat\$, tim\$, temp, AD1, AD2, Check, filetype\$, AveA, StdA, AveB, StdB, AveAbs740, AveRatio, StdRatio, pCO2, AveCalFact434, StdCalFact434, AveCalFact620, StdCalFact620, caltemp, power2, power1, power0)

' This subroutine calculates the indicator absorbances using the equation

' $A = -\log \{I/(I_{ref} * K)\}$ where I_{ref} = transmitted light @ nonabsorbing wavelength (720 nm) and $K = I_0/I_{ref}$ where I_0 = transmitted intensity with no indicator present (a blank solution)

FOR D = 1 TO 3

INPUT #1, DataSearch\$(D)

AveAbs740 = VAL(RIGHT\$(DataSearch\$(1), 5))
 AveAbs434n620\$ = LEFT\$(DataSearch\$(1), 25)
 AveAbs620 = VAL(RIGHT\$(AveAbs434n620\$, 5))
 Locate434Ave\$ = LEFT\$(AveAbs434n620\$, 11)
 AveAbs434 = VAL(RIGHT\$(Locate434Ave\$, 5))

StdAbs740 = VAL(RIGHT\$(DataSearch\$(2), 5))
 StdAbs434n620\$ = LEFT\$(DataSearch\$(2), 25)
 StdAbs620 = VAL(RIGHT\$(StdAbs434n620\$, 5))
 Locate434Std\$ = LEFT\$(StdAbs434n620\$, 11)
 StdAbs434 = VAL(RIGHT\$(Locate434Std\$, 5))

BlankSearch = VAL(RIGHT\$(DataSearch\$(3), 4))

NEXT D

IF BlankSearch = 2222 THEN

CALL CalibFactors(DataSearch\$(), AveCalFact434, StdCalFact434,
 AveCalFact620, StdCalFact620, BatteryA, BatteryB)

CALL WriteBlank(QProDat, JulianDay, dat\$, tim\$, temp, AD1, AD2,
 AveAbs740, AveCalFact434, StdCalFact434, AveCalFact620,
 StdCalFact620)

GOTO 100

END IF

AveA = -1 * (LOG(AveAbs434 / (AveCalFact434 * AveAbs740)) / LOG(10))

AveB = -1 * (LOG(AveAbs620 / (AveCalFact620 * AveAbs740)) / LOG(10))

IF AveA < 0 OR AveB < 0 THEN

CALL AnError(QProDat, JulianDay, dat\$, tim\$, temp, AD1, AD2, AveAbs740,
 Check, notneeded\$)

```

    GOTO 100
  END IF

  IF AveB / AveA * .2105 > 2.1362 OR AveB / AveA < .0043 THEN
    CALL AnError(QProDat, JulianDay, dat$, tim$, temp, AD1, AD2, AveAbs740,
      Check, notneeded$)
    GOTO 100
  END IF

  AVE740 = AveAbs740

  AvgRatio = -1 * (LOG((AveB / AveA - .0043) / (2.136 - .2105 * AveB / AveA)) /
    LOG(10))

  IF filetype$ = "F" THEN    'If FIELD data then do the following:

    AveRatio = (temp - caltemp) * .0072 + AvgRatio    'Temp. corrected Ratio

    pCO2 = 10 ^ (((-1 * power1) + (SQR(ABS((power1 ^ 2) - (4 * power2 * (power0
      - AveRatio)))))) / (2 * power2))

  ELSE    'If CALIBRATION data then do not want the ratio corrected for temp.
    AveRatio = AvgRatio

  END IF

  ***The following uses propagation of errors to figure out the absolute standard deviation
  ***for the three previous equations.
  ***See "Instrumental Analysis" by Skoog/Leary Appendix a1B

  x = AveA * (SQR((StdAbs434 / AveAbs434) ^ 2 + (StdCalFact434 / AveCalFact434) ^ 2
    + (StdAbs740 / AveAbs740) ^ 2))
  StdA = .434 * x / AveA
  y = AveB * (SQR((StdAbs620 / AveAbs620) ^ 2 + (StdCalFact620 / AveCalFact620) ^ 2
    + (StdAbs740 / AveAbs740) ^ 2))
  StdB = .434 * y / AveB
  Z = AveRatio * SQR((StdB / AveB) ^ 2 + (StdA / AveA) ^ 2)
  StdRatio = .434 * Z / AveRatio

  CALL WriteOutput(QProDat, JulianDay, dat$, tim$, temp, AD1, AD2, filetype$, AveA,
    StdA, AveB, StdB, AveAbs740, AveRatio, StdRatio, pCO2, AveCalFact434,
    StdCalFact434, AveCalFact620, StdCalFact620)

  100 END SUB

```

```
SUB FindBeginning (find$)
```

```
Counter = 0
```

```
DO
```

```
    Counter = Counter + 1
```

```
    IF Counter > 75 THEN
```

```
        PRINT ""
```

```
        PRINT ""
```

```
        PRINT ""
```

```
        PRINT ""
```

```
        PRINT "End of file has been reached!"
```

```
    END
```

```
    END IF
```

```
    find$ = INPUT$(1, #1)
```

```
    IF find$ = "@" THEN
```

```
        EXIT DO
```

```
    END IF
```

```
LOOP
```

```
END SUB
```

```
SUB FindFirstBlank (DataSearch$())
```

```
DO
```

```
    FOR x = 1 TO 2
```

```
        LINE INPUT #1, scrap$
```

```
    NEXT x
```

```
    FOR y = 1 TO 3
```

```
        INPUT #1, DataSearch$(y)
```

```
    NEXT y
```

```
Identify$ = RIGHT$(DataSearch$(3), 4)
```

```
LINE INPUT #1, scrap$
```

```
LINE INPUT #1, scrap$
```

```
LOOP WHILE Identify$ <> "2222"
```

```
END SUB
```

```
SUB GitTemp (temp, AD1, AD2)
```

```
LINE INPUT #1, FullLine$
```

```
templines$ = LEFT$(FullLine$, 27)
```

```
AD1 = VAL(RIGHT$(templines$, 6))           'Gets LiCor underwater light sensor data
```

```
AD2 = VAL(RIGHT$(FullLine$, 5))
```

```
TempPortion$ = LEFT$(templines$, 12)
```

```
temp = (VAL(RIGHT$(TempPortion$, 5))) / 100
```

```
END SUB
```

```
SUB GitTimNDat (QProDat, JulianDay, dat$, tim$)
```

```
INPUT #1, TimNDat$
```

```
tim$ = LEFT$(TimNDat$, 8)
```

```
dat$ = RIGHT$(TimNDat$, 8)
```

```
hrmin$ = LEFT$(tim$, 5)
```

```
hr$ = LEFT$(hrmin$, 2)
```

```
min$ = RIGHT$(hrmin$, 2)
```

```
hr = VAL(hr$)
```

```
min = VAL(min$)
```

```
year$ = RIGHT$(dat$, 2)
```

```
year = VAL(year$)
```

```
daymonth$ = LEFT$(dat$, 5)
```

```
day$ = RIGHT$(daymonth$, 2)
```

```
month$ = LEFT$(daymonth$, 2)
```

```
day = VAL(day$)
```

```
month = VAL(month$)
```

```
*****Changing Date and Time into QPro compatible number*****
```

```
SumDays = 0
```

```
FOR Z = 0 TO (month - 1)
```

```
SELECT CASE Z
```

```
  CASE 0
```

```
    m = 0
```

```
  CASE 2
```

```
    m = 0
```

CASE 1, 3, 5, 7, 8, 10, 12
 m = 31

CASE 4, 6, 9, 11
 m = 30

END SELECT

SumDays = SumDays + m

NEXT Z

NOTE: 1996 and 2000 are Leap Years so Feb has 29 days

feb = 0

IF year = 95 AND month >= 3 THEN
 feb = 28
 ELSEIF year = 96 AND month >= 3 THEN
 feb = 29
 ELSEIF year = 97 AND month >= 3 THEN
 feb = 28
 ELSEIF year = 98 AND month >= 3 THEN
 feb = 28
 ELSEIF year = 99 AND month >= 3 THEN
 feb = 28
 ELSEIF year = 0 AND month >= 3 THEN
 feb = 29
 ELSEIF year = 1 AND month >= 3 THEN
 feb = 28

END IF

TotalDays = SumDays + feb

NOTES: Need to subtract 1 from "day" so that the current day in question is not included in the calculation. 34700 corresponds to Jan-1-1995 in Quattro Pro. Program automatically compensates for year of data.

```

ELSEIF year = 98 THEN
    Number = 35796
ELSEIF year = 99 THEN
    Number = 36161
ELSEIF year = 0 THEN
    Number = 36526
ELSEIF year = 1 THEN
    Number = 36892

```

```

END IF

```

```

QProDat = TotalDays + (day - 1) + (hr / 24) + (min / 1440) + Number
JulianDay = TotalDays + (day - 1) + (hr / 24) + (min / 1440)

```

```

END SUB

```

```

SUB GitUserInput (filename$, filetype$, output$, caltemp, power2, power1, power0)

```

```

PRINT "***** WELCOME TO MATT'S SAMI-CO2 DATA MANIPULATION
PROGRAM! *****"

```

```

PRINT ""

```

```

PRINT ""

```

```

PRINT "NOTE: Data must be from Years 1995 to 2001. If not see Matt."

```

```

PRINT ""

```

```

INPUT "Please provide full syntax of data file to be manipulated: ", filename$

```

```

PRINT ""

```

```

300 INPUT "Is this data file from FIELD(F) or CALIBRATION(C) measurements";
filetypes$

```

```

PRINT ""

```

```

filetype$ = UCASE$(filetypes$)

```

```

IF filetype$ <> "F" AND filetype$ <> "C" THEN

```

```

    GOTO 300

```

```

END IF

```

```

IF filetype$ = "F" THEN

```

```

    PRINT "What are the calibration coefficients for this SAMI instrument?"

```

```

    PRINT "(2nd order polynomial) - Separate the coefficients with a comma"

```

```

    INPUT "starting with the log pCO2 squared term. ", power2, power1, power0

```

```

    PRINT ""

```

```

    INPUT "What was the average SAMI calibration temperature (C)"; caltemp

```

```

    PRINT ""

```

```

END IF

```

```

INPUT "Where (full syntax) do you want the output to be filed"; output$
PRINT ""
INPUT "Press ENTER if everything entered is CORRECT; if not enter any letter. ",
      correct$

  IF correct$ <> "" THEN
    BEEP
    CLS
    CALL GitUserInput(filename$, filetype$, output$, caltemp, power2, power1,
                      power0)
  ELSE
    PRINT ""
    PRINT ""
    PRINT "Make yourself at home while I work!"
  END IF

END SUB

SUB Main (find$, QProDat, JulianDay, dat$, tim$, temp, AD1, AD2)

CALL FindBeginning(find$)
CALL GitTimNDat(QProDat, JulianDay, dat$, tim$)
CALL GitTemp(temp, AD1, AD2)

END SUB

SUB WriteBlank (QProDat, JulianDay, dat$, tim$, temp, AD1, AD2, AveAbs740,
               AveCalFact434, StdCalFact434, AveCalFact620, StdCalFact620)

WRITE #2, QProDat, JulianDay, dat$, tim$, temp, AD1, AD2, "*BLANK*", "NA",
      "NA", "NA", AveAbs740, "NA", "NA", "NA", AveCalFact434, StdCalFact434,
      AveCalFact620, StdCalFact620

END SUB

```



```
SUB WriteOutput (QProDat, JulianDay, dat$, tim$, temp, AD1, AD2, filetype$, AveA,
  StdA, AveB, StdB, AveAbs740, AveRatio, StdRatio, pCO2, AveCalFact434,
  StdCalFact434, AveCalFact620, StdCalFact620)

IF filetype$ = "F" THEN
  WRITE #2, QProDat, JulianDay, dat$, tim$, temp, AD1, AD2, AveA, StdA,
    AveB, StdB, AveAbs740, AveRatio, StdRatio, pCO2, AveCalFact434,
    StdCalFact434, AveCalFact620, StdCalFact620
ELSE
  WRITE #2, QProDat, JulianDay, dat$, tim$, temp, AD1, AD2, AveA, StdA,
    AveB, StdB, AveAbs740, AveRatio, StdRatio, "NA", AveCalFact434,
    StdCalFact434, AveCalFact620, StdCalFact620

END IF

END SUB
```

Appendix 2

The tables in this appendix are a listing of the results of the discrete profile measurements made at the mid-lake station in Placid Lake (Figure 1.2). All samples that were transported back to the laboratory were collected with a vertical PVC Kemmerer water sampler. Detailed methods for the analysis of these parameters are given in Chapter 2. Only the mean values, where applicable, are provided. The format for the tables is as follows:

- 1st row: Date
- 2nd row: Year Day
- 3rd row: Microsoft Excel or Corel Quattro Pro Date Number
- 1st column: Sample Depth (m)

Temperature (°C)
YSI Model 58 and 6000*

1 of 3

	11/01/96	02/03/97*	02/23/97*	03/17/97*	06/18/97	06/19/97	07/02/97	07/17/97	08/05/97	08/20/97	09/25/97	10/23/97
	305.75	33.91	53.89	75.82	168.75	169.90	182.72	197.90	216.73	231.88	267.80	295.88
<u>Depth (m)</u>	<u>35370.75</u>	<u>35464.91</u>	<u>35484.89</u>	<u>35506.82</u>	<u>35599.75</u>	<u>35600.90</u>	<u>35613.72</u>	<u>35628.90</u>	<u>35647.73</u>	<u>35662.88</u>	<u>35698.80</u>	<u>35726.88</u>
1	7.3	-	-	-	-	16.4	-	-	-	-	15.7	8.7
2	7.3	2.52	2.21	2.43	16.9	16.1	16.0	20.2	22.0	18.9	15.2	8.9
3	-	-	-	2.60	16.7	15.9	15.8	19.0	21.9	18.6	14.9	8.9
4	-	-	-	-	13.6	13.5	14.6	17.0	21.8	18.5	14.6	8.9
5	7.3	2.60	2.59	-	10.3	10.5	12.5	14.7	15.5	18.1	14.6	8.9
6	-	-	-	2.74	8.6	9.1	10.7	13.0	11.6	14.6	14.2	8.9
7	-	-	2.74	-	7.4	-	8.4	10.0	10.0	10.7	13.0	8.9
8	-	-	-	-	-	7.0	8.0	8.1	8.2	9.3	10.3	8.9
9	-	-	-	-	-	-	-	-	7.5	8.1	8.7	8.9
10	7.3	2.84	3.01	-	6.2	6.3	6.4	6.6	-	7.2	7.9	8.9
11	-	-	-	3.18	-	-	-	-	6.6	-	-	8.7
12	-	-	-	-	5.2	-	-	-	-	-	-	7.7
13	-	-	-	-	-	5.5	5.4	5.4	-	-	-	6.9
14	-	-	-	-	5.0	-	-	-	-	-	-	6.6
15	6.8	3.44	3.40	-	-	-	-	-	-	5.4	5.4	5.9
16	-	-	-	3.60	4.7	5.0	4.8	5.1	5.0	-	-	-
17	-	-	-	-	-	-	-	-	-	-	-	-
18	-	-	-	-	-	-	-	-	-	-	-	-
19	-	-	-	-	-	-	-	-	-	-	-	-
20	5.9	3.64	3.67	-	4.4	4.5	4.4	4.7	-	4.6	4.7	4.8
21	-	-	-	3.72	-	-	-	-	4.5	-	-	-
22	-	-	-	-	-	4.3	4.4	4.5	-	4.6	-	-
23	-	3.76	3.81	-	-	-	-	-	-	-	-	-
24	-	-	-	-	-	-	-	-	-	-	-	-
25	5.6	-	-	-	-	-	-	-	-	-	-	-

Temperature (°C)
YSI Model 58 and 6000*

2 of 3

	11/14/97	02/09/98*	03/03/98*	05/12/98	05/20/98	06/16/98	08/04/98	08/15/98	10/30/98	03/18/99	04/01/99	04/26/99
	317.88	39.77	61.77	131.92	139.79	166.77	215.81	226.90	302.88	76.60	90.80	115.90
Depth (m)	35748.88	35835.77	35857.77	35927.92	35935.79	35962.77	36011.81	36022.90	36098.88	36237.60	36251.80	36276.90
1	5.8	-	-	13.9	13.0	-	23.3	23.1	9.0	1.6	2.6	5.0
2	5.7	2.87	2.96	13.9	12.8	14.4	22.5	23.1	8.8	2.5	2.8	4.7
3	5.7	2.83	-	13.8	12.6	-	22.4	23.0	-	2.5	2.8	4.5
4	5.7	-	-	13.8	12.6	14.3	22.2	22.6	8.7	2.6	2.9	4.4
5	5.7	2.82	2.90	11.9	11.9	12.4	18.9	19.9	-	2.6	2.9	4.4
6	5.7	-	-	9.6	10.1	11.0	15.0	17.4	8.6	2.6	2.9	4.4
7	5.7	-	-	7.8	8.4	10.0	11.9	12.2	-	2.6	2.9	4.4
8	5.7	-	-	7.1	7.5	8.7	9.6	10.3	8.6	2.6	2.9	4.4
9	5.7	-	-	6.6	6.8	7.9	8.7	8.9	-	2.6	2.9	4.4
10	5.7	3.00	3.14	6.3	6.4	7.3	7.8	8.1	8.6	2.6	2.9	4.4
11	-	-	-	-	-	-	-	-	-	-	-	4.3
12	5.7	-	-	5.4	5.9	5.5	6.9	6.7	8.0	-	2.8	4.1
13	-	-	-	-	-	-	-	-	-	-	-	4.0
14	-	-	-	4.8	5.2	5.1	-	-	-	2.8	-	3.8
15	5.6	3.32	3.36	-	-	-	5.6	5.6	6.4	-	2.9	3.8
16	-	-	-	4.6	4.8	-	-	-	-	-	-	3.7
17	5.5	-	-	-	-	-	-	-	-	-	-	-
18	5.2	-	-	4.5	4.5	4.7	-	5.1	5.4	3.0	3.0	-
19	5.1	-	-	-	-	-	-	-	-	-	-	-
20	5.0	-	3.41	4.4	4.4	-	4.8	4.9	-	3.0	3.0	3.6
21	4.9	-	-	-	-	-	-	-	-	-	-	-
22	4.8	-	-	4.3	4.3	4.4	-	4.7	4.8	3.2	3.1	3.5
23	-	-	-	-	-	-	4.6	-	-	-	3.3	3.5
24	-	-	-	-	-	-	-	4.6	-	-	-	-
25	-	-	-	-	-	-	-	-	-	-	3.4	3.5

Temperature (°C)
 YSI Model 58 and 6000*
 3 of 3

	05/05/99	05/20/99	06/07/99	06/27/99	06/28/99
	124.80	139.77	157.83	177.96	178.65
<u>Depth (m)</u>	<u>36285.80</u>	<u>36300.77</u>	<u>36318.83</u>	<u>36338.96</u>	<u>36339.65</u>
1	5.3	8.8	14.0	15.9	15.8
2	5.3	8.2	13.1	15.9	15.7
3	5.2	8.1	12.6	15.9	15.6
4	5.2	7.9	12.0	15.8	15.6
5	5.2	7.3	11.4	15.4	14.0
6	5.2	7.1	10.2	9.9	11.3
7	5.2	6.9	7.8	8.7	9.1
8	5.2	6.8	7.3	8.2	8.1
9	5.2	6.8	7.1	7.9	7.4
10	5.2	6.6	6.8	7.6	6.9
11	5.2	-	-	-	-
12	5.1	6.4	6.3	6.7	6.5
13	-	-	-	-	-
14	-	6.2	6.1	6.4	6.1
15	4.8	6.0	5.9	6.2	6.1
16	-	5.9	5.8	6.1	6.0
17	4.5	-	-	-	-
18	-	5.8	5.6	5.9	5.8
19	-	-	-	-	5.7
20	4.3	5.7	5.4	5.7	5.5
21	-	-	-	-	5.5
22	4.0	5.5	5.3	5.4	5.5
23	-	-	-	-	-
24	-	5.4	5.3	5.4	5.4
25	-	-	5.3	5.4	-

Dissolved Oxygen (mg L⁻¹)
YSI Model 58 and 6000*

1 of 3

	11/01/96	02/03/97*	02/23/97*	03/17/97*	06/18/97	06/19/97	07/02/97	07/17/97	08/05/97	08/20/97	09/25/97	10/23/97
	305.75	33.91	53.89	75.82	168.75	169.90	182.72	197.90	216.73	231.88	267.80	295.88
<u>Depth (m)</u>	<u>35370.75</u>	<u>35464.91</u>	<u>35484.89</u>	<u>35506.82</u>	<u>35599.75</u>	<u>35600.90</u>	<u>35613.72</u>	<u>35628.90</u>	<u>35647.73</u>	<u>35662.88</u>	<u>35698.80</u>	<u>35726.88</u>
1	-	-	-	-	-	8.30	-	-	-	-	8.09	7.70
2	-	9.11	8.75	8.32	8.62	8.17	8.39	8.73	7.27	8.50	8.00	7.50
3	-	-	-	8.28	8.60	8.25	8.57	9.08	7.32	8.38	8.02	7.45
4	-	-	-	-	8.76	8.50	8.22	8.84	7.46	8.19	8.00	7.40
5	9.50	8.96	8.57	-	8.40	8.20	7.73	8.20	8.73	8.19	7.63	7.30
6	-	-	-	8.18	7.85	7.88	7.33	7.68	6.55	7.21	7.35	7.30
7	-	-	8.41	-	7.63	-	7.14	7.05	5.99	5.64	5.30	7.25
8	-	-	-	-	-	7.72	6.83	6.78	5.82	5.36	3.60	7.55
9	-	-	-	-	-	-	-	-	5.74	5.24	3.51	7.50
10	10.70	8.78	8.08	-	7.34	7.38	6.45	6.54	-	5.22	3.60	7.15
11	-	-	-	7.60	-	-	-	-	5.98	-	-	-
12	-	-	-	-	7.10	-	-	-	-	-	-	4.90
13	-	-	-	-	-	7.26	6.53	6.45	-	-	-	-
14	-	-	-	-	6.82	-	-	-	-	-	-	-
15	9.00	7.56	7.24	-	-	-	-	-	-	5.84	4.10	3.43
16	-	-	-	6.46	6.72	6.80	6.04	6.00	5.01	-	-	-
17	-	-	-	-	-	-	-	-	-	-	-	-
18	-	-	-	-	-	-	-	-	-	-	-	-
19	-	-	-	-	-	-	-	-	-	-	-	-
20	8.10	6.28	5.32	-	6.07	6.30	5.17	5.80	-	5.14	2.80	1.40
21	-	-	-	5.04	-	-	-	-	4.61	-	-	-
22	-	-	-	-	-	4.30	3.93	4.76	-	3.14	-	-
23	-	4.37	4.97	-	-	-	-	-	-	-	-	-
24	-	-	-	-	-	-	-	-	-	-	-	-
25	6.90	-	-	-	-	-	-	-	-	-	-	-

Dissolved Oxygen (mg L⁻¹)
YSI Model 58 and 6000*
 2 of 3

	02/09/98*	03/03/98*	05/12/98	05/20/98	06/16/98	08/04/98	08/15/98	10/30/98	05/05/99	05/20/99	06/07/99	06/27/99
	39.77	61.77	131.92	139.79	166.77	215.81	226.90	302.88	124.80	139.77	157.83	177.96
Depth (m)	35835.77	35857.77	35927.92	35935.79	35962.77	36011.81	36022.90	36098.88	36285.80	36300.77	36318.83	36338.96
1	-	-	9.13	9.30	-	7.43	7.72	7.87	8.70	9.81	9.10	8.86
2	9.01	7.80	9.18	8.89	8.51	7.66	7.72	7.60	8.61	9.80	8.85	8.70
3	8.60	-	9.25	8.91	-	7.66	7.74	-	8.57	9.69	9.25	8.75
4	-	-	9.26	8.89	8.45	7.66	7.81	7.40	8.62	9.82	9.10	8.80
5	8.54	7.68	9.24	8.49	8.13	9.87	9.86	-	8.66	9.66	8.95	8.90
6	-	-	9.03	8.11	7.64	11.15	11.02	7.35	8.60	9.33	9.05	8.53
7	-	-	8.54	7.68	7.17	7.80	8.35	-	8.62	9.46	8.75	8.05
8	-	-	8.25	7.41	6.66	5.73	6.08	7.28	8.58	9.55	8.75	7.90
9	-	-	8.10	7.12	6.36	5.20	5.00	-	8.57	9.62	8.60	7.88
10	8.28	7.28	8.00	6.96	6.20	4.94	4.78	7.22	8.52	9.37	8.15	7.87
11	-	-	-	-	-	-	-	-	8.57	-	-	-
12	-	-	7.40	6.83	6.00	4.95	4.83	4.00	8.60	9.30	8.10	7.52
13	-	-	-	-	-	-	-	-	-	-	-	-
14	-	-	6.96	6.65	5.64	-	-	-	-	9.20	8.05	7.52
15	8.04	6.92	-	-	-	4.75	4.73	1.77	8.00	9.00	7.85	7.40
16	-	-	6.35	6.25	-	-	-	-	-	8.90	7.60	7.28
17	-	-	-	-	-	-	-	-	7.70	-	-	-
18	-	-	6.33	5.92	4.30	-	4.57	1.65	-	8.70	7.40	7.35
19	-	-	-	-	-	-	-	-	-	-	-	-
20	-	6.02	6.06	5.84	-	3.70	2.97	-	7.50	8.25	6.60	6.78
21	-	-	-	-	-	-	-	-	-	-	-	-
22	-	-	5.62	5.05	3.84	-	2.56	-	6.50	8.10	6.00	5.61
23	-	-	-	-	-	1.40	-	-	-	-	-	-
24	-	-	-	-	-	-	0.96	-	-	-	6.00	5.18
25	-	-	-	-	-	-	-	-	-	-	-	5.00

Dissolved Oxygen (mg L⁻¹)
 YSI Model 58 and 6000*
 3 of 3

	06/28/99
	178.65
<u>Depth (m)</u>	<u>36339.65</u>
1	9.00
2	8.91
3	8.85
4	8.95
5	9.25
6	9.13
7	8.31
8	8.15
9	8.04
10	7.85
11	-
12	7.85
13	-
14	7.48
15	7.45
16	7.55
17	-
18	7.10
19	7.00
20	6.00
21	5.80
22	5.60
23	-
24	3.10
25	-

Dissolved Oxygen (% saturation)
YSI Models 58 and 6000*

1 of 3

	11/01/96	02/03/97*	02/23/97*	03/17/97*	06/18/97	06/19/97	07/02/97	07/17/97	08/05/97	08/20/97	09/25/97	10/23/97
	305.75	33.91	53.89	75.82	168.75	169.90	182.72	197.90	216.73	231.88	267.80	295.88
Depth	<u>35370.75</u>	<u>35464.91</u>	<u>35484.89</u>	<u>35506.82</u>	<u>35599.75</u>	<u>35600.90</u>	<u>35613.72</u>	<u>35628.90</u>	<u>35647.73</u>	<u>35662.88</u>	<u>35698.80</u>	<u>35726.88</u>
1	-	-	-	-	-	98.9	-	-	-	-	95.0	76.7
2	-	77.7	74.0	70.8	103.8	96.7	99.1	112.4	96.8	106.7	92.9	75.1
3	-	-	-	70.7	103.2	97.3	100.8	114.2	97.2	104.6	92.5	74.6
4	-	-	-	-	98.1	95.0	94.2	106.7	98.9	102.0	91.6	74.1
5	91.4	76.5	73.2	-	87.0	85.4	84.4	94.1	102.0	101.2	87.4	73.1
6	-	-	-	70.1	78.0	79.3	76.7	84.8	70.0	82.6	83.4	73.1
7	-	-	72.1	-	73.6	-	70.6	72.5	61.6	59.0	58.5	72.6
8	-	-	-	-	-	73.7	66.9	66.6	57.3	54.2	37.3	75.6
9	-	-	-	-	-	-	-	-	55.5	51.4	35.0	75.1
10	103.0	75.5	69.8	-	68.7	69.3	60.7	61.8	-	50.1	35.2	71.6
11	-	-	-	65.9	-	-	-	-	56.5	-	-	-
12	-	-	-	-	64.8	-	-	-	-	-	-	47.6
13	-	-	-	-	-	66.8	59.9	59.2	-	-	-	-
14	-	-	-	-	61.9	-	-	-	-	-	-	-
15	85.5	66.0	63.1	-	-	-	-	-	-	53.6	37.6	31.9
16	-	-	-	56.6	60.6	61.8	54.6	54.6	45.5	-	-	-
17	-	-	-	-	-	-	-	-	-	-	-	-
18	-	-	-	-	-	-	-	-	-	-	-	-
19	-	-	-	-	-	-	-	-	-	-	-	-
20	75.3	55.1	46.7	-	54.3	56.5	46.2	52.3	-	46.2	25.2	12.6
21	-	-	-	44.3	-	-	-	-	41.3	-	-	-
22	-	-	-	-	-	38.4	35.2	42.7	-	28.2	-	-
23	-	-	43.8	-	-	-	-	-	-	-	-	-
24	-	-	-	-	-	-	-	-	-	-	-	-
25	63.6	-	-	-	-	-	-	-	-	-	-	-

Dissolved Oxygen (% saturation)
YSI Models 58 and 6000*
 2 of 3

	02/09/98*	03/03/98*	05/12/98	05/20/98	06/16/98	08/04/98	08/15/98	10/30/98	05/05/99	05/20/99	06/07/99	06/27/99
	39.77	61.77	131.92	139.79	166.77	215.81	226.90	302.88	124.80	139.77	157.83	177.96
Depth	35835.77	35857.77	35927.92	35935.79	35962.77	36011.81	36022.90	36098.88	36285.80	36300.77	36318.83	36338.96
1	-	-	102.9	102.7	-	101.1	104.7	79.0	79.6	98.0	102.8	104.5
2	77.5	67.2	103.5	97.7	97.0	102.8	104.7	75.9	78.8	96.4	98.0	102.6
3	73.9	-	104.1	97.5	-	102.7	104.8	-	78.2	95.1	101.2	103.2
4	-	-	104.2	97.3	96.1	102.3	105.0	73.7	78.7	95.9	98.2	103.5
5	73.4	66.1	99.4	91.4	88.5	123.9	126.2	-	79.0	93.0	95.2	103.8
6	-	-	92.0	83.6	80.5	128.9	134.2	73.0	78.5	89.3	93.5	87.5
7	-	-	83.2	75.9	73.7	84.0	90.5	-	78.7	90.1	85.3	80.2
8	-	-	79.0	71.7	66.3	58.4	63.0	72.3	78.3	90.8	84.2	77.7
9	-	-	76.6	67.7	62.1	51.8	50.1	-	78.2	91.4	82.3	77.0
10	71.5	63.1	75.1	65.5	59.7	48.1	46.9	71.8	77.8	88.6	77.4	76.3
11	-	-	-	-	-	-	-	-	78.2	-	-	-
12	-	-	67.9	63.5	55.2	47.2	45.8	39.2	78.3	87.5	76.0	71.3
13	-	-	-	-	-	-	-	-	-	-	-	-
14	-	-	62.9	60.7	51.3	-	-	-	-	86.1	75.2	70.7
15	70.0	60.3	-	-	-	43.8	43.6	16.7	72.3	83.8	72.9	69.3
16	-	-	57.1	56.5	-	-	-	-	-	82.7	70.4	68.0
17	-	-	-	-	-	-	-	-	69.0	-	-	-
18	-	-	56.8	53.1	38.8	-	41.6	15.1	-	80.6	68.2	68.3
19	-	-	-	-	-	-	-	-	-	-	-	-
20	-	52.5	54.2	52.2	-	33.4	26.9	-	66.9	76.3	60.5	62.7
21	-	-	-	-	-	-	-	-	-	-	-	-
22	-	-	50.1	45.1	34.3	-	23.1	-	57.5	74.5	54.9	51.5
23	-	-	-	-	-	12.6	-	-	-	-	-	-
24	-	-	-	-	-	-	8.6	-	-	-	54.9	47.5
25	-	-	-	-	-	-	-	-	-	-	-	45.9

Dissolved Oxygen (% saturation)
YSI Models 58 and 6000*

3 of 3

	06/28/99
	178.65
Depth	36339.65
1	105.9
2	104.6
3	103.7
4	104.8
5	104.5
6	96.9
7	83.6
8	80.0
9	77.6
10	74.8
11	-
12	74.0
13	-
14	69.8
15	69.6
16	70.3
17	-
18	65.8
19	64.7
20	55.2
21	53.3
22	51.5
23	-
24	28.4
25	-

Dissolved Oxygen
Winkler Titration

DO (mg L⁻¹)									
	04/01/99	04/26/99	05/05/99	05/20/99	06/07/99	06/28/99			
	90.73	115.90	124.80	139.77	157.90	178.65			
Depth (m)	36251.73	36276.90	36285.80	36300.77	36318.90	36339.65			
1	9.45	9.02	-	-	-	-			
2	8.78	8.98	8.95	9.98	9.83	9.25			
4	7.87	8.99	8.88	10.04	9.79	9.16			
10	8.32	8.76	8.83	9.48	8.55	7.43			
15	-	-	8.80	9.14	8.19	7.23			
20	5.56	6.94	7.24	8.08	7.02	5.84			
DO (% saturation)									
	04/01/99	04/26/99	05/05/99	05/20/99	06/07/99	06/28/99			
	90.80	115.90	124.80	139.77	157.83	178.65			
Depth (m)	36251.80	36276.90	36285.80	36300.77	36318.83	36339.65			
1	81.0	81.9	-	-	-	-			
2	76.4	80.9	81.9	98.2	108.8	108.6			
4	67.7	80.4	81.1	98.1	105.6	107.3			
10	71.6	78.4	80.6	89.6	81.3	70.8			
15	-	-	79.5	85.1	76.1	67.5			
20	48.0	60.8	64.6	74.7	64.4	53.7			

Total Dissolved Inorganic Carbon ($\mu\text{mol L}^{-1}$)

	11/01/96	01/08/97	02/03/97	02/23/97	03/17/97	05/29/97	07/02/97	07/17/97	08/05/97	08/20/97	09/25/97
	305.75	7.91	33.91	53.89	75.82	148.88	182.72	197.90	216.73	231.88	267.80
<u>Depth (m)</u>	<u>35370.75</u>	<u>35438.91</u>	<u>35464.91</u>	<u>35484.89</u>	<u>35506.82</u>	<u>35579.88</u>	<u>35613.72</u>	<u>35628.90</u>	<u>35647.73</u>	<u>35662.88</u>	<u>35698.80</u>
2	-	1239.4	1247.2	1297.4	1277.0	876.3	1063.0	1041.3	1097.8	1141.3	1256.5
5	1219.8	1230.9	1239.2	1241.4	1257.6	945.6	1213.1	1198.0	1213.5	1150.0	1243.1
10	1220.9	1238.8	1239.5	1249.1	1268.7	1014.9	1128.9	1065.5	1095.4	1117.2	1196.0
15	1230.3	1249.6	1242.5	1267.5	1281.5	1115.5	1215.3	1136.3	1161.8	1129.3	1205.6
20	1251.4	-	-	-	1360.3	1163.7	1305.6	1192.6	1249.1	1213.0	1298.3
23	-	-	1236.9	1398.8	-	-	-	-	-	-	-
24	-	1315.4	-	-	-	-	-	-	-	-	-
25	1218.8	-	-	-	-	-	-	-	-	-	-
	10/23/97	02/09/98	03/03/98	08/04/98	03/18/99	04/01/99	04/26/99	05/05/99	05/20/99	06/07/99	06/28/99
	295.88	39.77	61.77	215.81	76.60	90.80	115.90	124.80	139.77	157.83	178.65
<u>Depth (m)</u>	<u>35726.88</u>	<u>35835.77</u>	<u>35857.77</u>	<u>36011.81</u>	<u>36237.60</u>	<u>36251.80</u>	<u>36276.90</u>	<u>36285.80</u>	<u>36300.77</u>	<u>36318.83</u>	<u>36339.65</u>
1	-	-	-	-	1366.9	1184.0	1288.9	-	-	-	-
2	1221.5	1189.3	1155.2	-	1342.8	1262.8	1290.2	1224.6	1170.2	1106.0	1153.0
3	-	1153.3	-	1086.3	-	-	-	-	-	-	-
4	-	-	-	-	1324.6	1398.4	1293.7	-	-	-	-
5	1232.2	1160.5	1171.6	-	-	-	-	1231.0	1151.3	1138.9	1149.4
10	1208.4	1164.8	1156.8	-	1345.6	1419.6	1295.0	1235.7	1200.1	1240.7	1247.0
15	1150.3	1166.1	1161.7	-	1390.4	1456.9	1346.1	1226.5	1225.8	1269.7	1284.8
20	1225.1	-	1232.5	-	1390.4	1494.3	1397.3	1297.2	1268.3	1315.5	1308.3

Spectrophotometric pH

	11/01/96	01/08/97	02/03/97	02/23/97	03/17/97	05/29/97	07/02/97	07/17/97	08/05/97	08/20/97	09/25/97
	305.75	7.91	33.91	53.89	75.82	148.88	182.72	197.90	216.73	231.88	267.80
Depth (m)	35370.75	35438.91	35464.91	35484.89	35506.82	35579.88	35613.72	35628.90	35647.73	35662.88	35698.80
2	-	7.592	7.586	7.551	7.566	7.413	7.772	7.998	8.071	8.108	7.926
5	7.535	7.568	7.566	7.553	7.592	7.368	7.540	7.706	7.949	8.051	7.901
10	7.524	7.542	7.553	7.519	7.516	7.240	7.165	7.159	7.094	7.074	7.020
15	7.362	7.510	7.513	7.470	7.456	7.219	7.160	7.130	7.097	7.129	7.033
20	7.033	-	-	-	7.352	7.387	7.125	7.146	7.062	7.088	6.970
23	-	-	7.567	7.287	-	-	-	-	-	-	-
24	-	7.369	-	-	-	-	-	-	-	-	-
25	7.527	-	-	-	-	-	-	-	-	-	-
	10/23/97	02/09/98	03/03/98	08/04/98	03/18/99	04/01/99	04/26/99	05/05/99	05/20/99	06/07/99	06/28/99
	295.88	39.77	61.77	215.81	76.60	90.80	115.90	124.80	139.77	157.83	178.65
Depth (m)	35726.88	35835.77	35857.77	36011.81	36237.60	36251.80	36276.90	36285.80	36300.77	36318.83	36339.65
1	-	-	-	-	7.513	7.417	7.514	-	-	-	-
2	7.593	7.496	7.457	-	7.493	7.448	7.515	7.499	7.598	7.896	7.964
3	-	7.448	-	8.210	-	-	-	-	-	-	-
4	-	-	-	-	7.414	7.476	7.502	-	-	-	-
5	7.581	7.450	7.422	-	-	-	-	7.505	7.572	7.728	8.003
10	7.572	7.429	7.407	-	7.392	7.486	7.507	7.488	7.492	7.464	7.359
15	7.074	7.409	7.385	-	7.336	7.399	7.448	7.492	7.444	7.420	7.302
20	7.042	-	7.325	-	7.279	7.312	7.390	7.395	7.382	7.340	7.268

Total Alkalinity ($\mu\text{equiv L}^{-1}$)
Gran Titration

	03/18/99	04/01/99	04/26/99	05/05/99	05/20/99	06/07/99	06/28/99
	76.60	90.80	115.90	124.80	139.77	157.83	178.65
<u>Depth (m)</u>	<u>36237.60</u>	<u>36251.80</u>	<u>36276.90</u>	<u>36285.80</u>	<u>36300.77</u>	<u>36318.83</u>	<u>36339.65</u>
2	1256.0	1088.5	1141.0	1113.5	1126.0	1046.0	1128.0
4	1248.0	-	-	-	-	-	-
5	-	-	-	-	-	1052.0	-
10	-	-	-	-	1090.0	-	1097.0
20	1207.0	1205.3	1196.0	1169.0	1107.0	1106.5	1122.0

Chlorophyll-*a* ($\mu\text{g L}^{-1}$)

	03/18/99	04/01/99	04/26/99	05/05/99	05/20/99	06/07/99	06/28/99
	76.60	90.80	115.90	124.80	139.77	157.83	178.65
Depth (m)	36237.60	36251.80	36276.90	36285.80	36300.77	36318.83	36339.65
1	2.03	3.92	9.96	-	-	-	-
2	2.34	6.06	10.94	8.45	2.97	3.31	3.28
4	2.81	8.03	10.92	-	-	4.82	3.41
5	-	-	-	8.39	3.93	-	-
10	0.70	16.42	11.44	7.96	3.52	1.68	2.60
15	-	-	-	7.93	2.56	0.96	1.44
20	0.47	0.42	6.97	6.43	1.79	0.87	1.24

Nutrients ($\mu\text{g L}^{-1}$)

Phosphate-P		03/18/99	04/01/99	04/26/99	05/05/99	05/20/99	06/07/99	06/28/99
		76.60	90.80	115.90	124.80	139.77	157.83	178.65
<u>Depth (m)</u>	<u>36237.60</u>	<u>36251.80</u>	<u>36276.90</u>	<u>36285.80</u>	<u>36300.77</u>	<u>36318.83</u>	<u>36339.65</u>	
1	2.8	3.2	1.0	-	-	-	-	-
2	3.6	3.6	1.0	1.3	1.2	2.0	1.8	
4	6.2	4.1	1.2	-	-	-	-	-
5	-	-	-	1.0	1.3	2.0	2.1	
10	9.5	3.0	1.3	1.5	0.3	2.5	3.0	
15	-	-	-	2.8	1.5	2.5	3.5	
20	9.8	7.1	3.2	3.3	3.0	4.4	4.3	
Nitrate-N		03/18/99	04/01/99	04/26/99	05/05/99	05/20/99	06/07/99	06/28/99
		76.60	90.80	115.90	124.80	139.77	157.83	178.65
<u>Depth (m)</u>	<u>36237.60</u>	<u>36251.80</u>	<u>36276.90</u>	<u>36285.80</u>	<u>36300.77</u>	<u>36318.83</u>	<u>36339.65</u>	
1	11	20	2	-	-	-	-	-
2	16	23	2	9	3	2	4	
4	38	29	3	-	-	-	-	-
5	-	-	-	3	<1	<1	3	
10	48	26	4	3	1	4	3	
15	-	-	-	2	6	10	6	
20	77	71	23	14	10	32	14	

Cations (mg L⁻¹)

Ca²⁺								
	04/26/99	05/05/99	05/20/99	06/07/99	06/28/99			
	115.90	124.80	139.77	157.83	178.65			
<u>Depth (m)</u>	<u>36276.90</u>	<u>36285.80</u>	<u>36300.77</u>	<u>36318.83</u>	<u>36339.65</u>			
1	11.5	-	-	-	-			
2	11.6	10.8	10.5	10.2	11.7			
4	-	10.9	-	-	-			
5	11.7	-	10.3	10.2	11.7			
10	11.8	10.9	10.6	10.3	10.8			
15	-	-	10.7	10.5	10.9			
20	12.2	11.2	10.9	10.6	11.3			
Mg²⁺								
	04/26/99	05/05/99	05/20/99	06/07/99	06/28/99			
	115.90	124.80	139.77	157.83	178.65			
<u>Depth (m)</u>	<u>36276.90</u>	<u>36285.80</u>	<u>36300.77</u>	<u>36318.83</u>	<u>36339.65</u>			
1	4.5	-	-	-	-			
2	4.6	5.3	5.1	4.6	4.8			
4	-	5.2	-	-	-			
5	4.6	-	5.0	4.6	4.8			
10	4.7	5.2	5.1	4.9	4.9			
15	-	-	5.2	5.0	5.0			
20	4.8	5.5	5.3	5.0	5.1			

Appendix 3

```
' ***** PROGRAM FRESHH2O.BAS *****
'
'   MATT BAEHR (Adapted from CO2SYSTEM.BAS by LEWIS and WALLACE
' 1998)
'
' THIS IS A QBASIC PROGRAM TO FIND ANY TWO FROM THE OTHER TWO
' OF: pH, pCO2, TA, AND TC
' ALL CALCULATIONS ARE DONE IN mol/kg-soln AND ON THE TOTAL pH
' SCALE
' ALL RESULTS ARE GIVEN IN umol/kg-soln AND u-atm AND ON THE TOTAL
' pH SCALE
'
'   LAST REVISION 07/28/97
'
' *****
DeclareStuff:
  DECLARE SUB ChooseWhich (ICASE%)
  DECLARE SUB Constants (TempC, D, K0, K(), NERNST, FugFac)
  DECLARE SUB FindH2 (TA, fCO2, K0, K(), pH)
  DECLARE SUB FindH3 (TC, fCO2, K0, K1, K2, pH)
  DECLARE SUB FindfCO2 (TC, pH, K0, K1, K2, fCO2)
  DECLARE SUB FindH1 (TA, TC, K(), pH)
  DECLARE SUB FindTA (TC, pH, K(), TA)
  DECLARE SUB FindTC (TA, pH, K(), TC)
  DECLARE SUB InputStuff (TempC)
  DECLARE SUB PrintHeader ()
'
' *****
DimensionStuff:
  DIM K(3):          ' THESE ARE THE EQUILIBRIUM CONSTANTS
'
' *****
  CALL PrintHeader
  ON ERROR GOTO ErrorHandler:
Start:
  CALL ChooseWhich(ICASE%)
  CLS
  PRINT "NOTE: TA, TC in umol/kg-soln, pCO2 in u-atm, pH on the total scale "
  CALL InputStuff(TempC)
  CALL Constants(TempC, D, K0, K(), NERNST, FugFac)
  K1 = K(1): K2 = K(2)
```

```

SELECT CASE ICASE%
*****
CASE 1
  LOCATE 7, 1: INPUT "ENTER TA: ", TA$: IF LEN(TA$) < 0 THEN TA =
    VAL(TA$) * 10 ^ (-6)
  LOCATE 7, 1: PRINT USING "TA = ####.# "; TA * 10 ^ 6
  INPUT "ENTER TC: ", TC$: IF LEN(TC$) < 0 THEN TC = VAL(TC$) * 10
    ^ (-6)
  LOCATE 8, 1: PRINT USING "TC = ####.# "; TC * 10 ^ 6

  DO AT GIVEN TA AND TC
    CALL FindH1(TA, TC, K(), pH): pH0 = pH
    CALL FindfCO2(TC, pH, K0, K1, K2, fCO2)
    pCO2 = fCO2 / FugFac: pCO20 = pCO2

  LOCATE 10, 1
  PRINT USING "pH = #.#### "; pH0
  PRINT USING "pCO2 = ####.# "; pCO20 * 10 ^ 6
  pH = pH0: pCO2 = pCO20
*****
CASE 2
  LOCATE 7, 1: INPUT "ENTER TA: ", TA$: IF LEN(TA$) < 0 THEN TA =
    VAL(TA$) * 10 ^ (-6)
  LOCATE 7, 1: PRINT USING "TA = ####.# "; TA * 10 ^ 6
  INPUT "ENTER pH: ", pH$: IF LEN(pH$) < 0 THEN pH = VAL(pH$)
  LOCATE 8, 1: PRINT USING "pH = #.#### "; pH

  DO AT GIVEN TA, pH
    CALL FindTC(TA, pH, K(), TC): TC0 = TC
    CALL FindfCO2(TC, pH, K0, K1, K2, fCO2)
    pCO2 = fCO2 / FugFac: pCO20 = pCO2

  LOCATE 10, 1
  PRINT USING "TC = ####.# "; TC0 * 10 ^ 6
  PRINT USING "pCO2 = ####.# "; pCO20 * 10 ^ 6
  TC = TC0: pCO2 = pCO20
*****
CASE 3
  LOCATE 7, 1: INPUT "ENTER TA: ", TA$: IF LEN(TA$) < 0 THEN TA =
    VAL(TA$) * 10 ^ (-6)
  LOCATE 7, 1: PRINT USING "TA = ####.# "; TA * 10 ^ 6
  INPUT "ENTER pCO2: ", pCO2$: IF LEN(pCO2$) < 0 THEN pCO2 =
    VAL(pCO2$) * 10 ^ (-6)

```

```
LOCATE 8, 1: PRINT USING "pCO2 = #####.# "; pCO2 * 10 ^ 6
fCO2 = pCO2 * FugFac
```

```
DO AT GIVEN TA,pCO2
  CALL FindH2(TA, fCO2, K0, K0), pH): pH0 = pH
  CALL FindTC(TA, pH, K(), TC): TC0 = TC
```

```
LOCATE 10, 1
PRINT USING "TC = #####.# "; TC0 * 10 ^ 6
PRINT USING "pH = #.##### "; pH0
TC = TC0: pH = pH0
```

```
*****
```

CASE 4

```
LOCATE 7, 1: INPUT "ENTER TC: ", TC$: IF LEN(TC$) <> 0 THEN TC =
  VAL(TC$) * 10 ^ (-6)
LOCATE 7, 1: PRINT USING "TC = #####.# "; TC * 10 ^ 6
INPUT "ENTER pH: ", pH$: IF LEN(pH$) <> 0 THEN pH = VAL(pH$)
LOCATE 8, 1: PRINT USING "pH = #.##### "; pH
```

```
DO AT GIVEN TC,pH
  CALL FindTA(TC, pH, K(), TA): TA0 = TA
  CALL FindfCO2(TC, pH, K0, K1, K2, fCO2)
  pCO2 = fCO2 / FugFac: pCO20 = pCO2
```

```
LOCATE 10, 1
PRINT USING "TA = #####.# "; TA0 * 10 ^ 6
PRINT USING "pCO2 = #####.# "; pCO20 * 10 ^ 6
TA = TA0: pCO2 = pCO20
```

```
*****
```

CASE 5

```
LOCATE 7, 1: INPUT "ENTER TC: ", TC$: IF LEN(TC$) <> 0 THEN TC =
  VAL(TC$) * 10 ^ (-6)
LOCATE 7, 1: PRINT USING "TC = #####.# "; TC * 10 ^ 6
INPUT "ENTER pCO2: ", pCO2$: IF LEN(pCO2$) <> 0 THEN pCO2 =
  VAL(pCO2$) * 10 ^ (-6)
LOCATE 8, 1: PRINT USING "pCO2 = #####.# "; pCO2 * 10 ^ 6
fCO2 = pCO2 * FugFac
```

```
DO AT GIVEN TC,pCO2
  CALL FindH3(TC, fCO2, K0, K1, K2, pH): pH0 = pH
  CALL FindTA(TC, pH, K(), TA): TA0 = TA
```

```
LOCATE 10, 1
PRINT USING "TA = #####.# "; TA0 * 10 ^ 6
```

```

PRINT USING "pH = #.#### "; pH0
TA = TA0: pH = pH0
,
*****
CASE 6
LOCATE 7, 1: INPUT "ENTER pH: ", pH$: IF LEN(pH$) < 0 THEN pH =
VAL(pH$)
LOCATE 7, 1: PRINT USING "pH = #.#### "; pH
INPUT "ENTER pCO2: ", pCO2$: IF LEN(pCO2$) < 0 THEN pCO2 =
VAL(pCO2$) * 10 ^ (-6)
LOCATE 8, 1: PRINT USING "pCO2 = #####.# "; pCO2 * 10 ^ 6
fCO2 = pCO2 * FugFac
,
DO AT GIVEN pH,pCO2
H = 10 ^ (-pH)
TC = K0 * fCO2 * (1! + (K1 / H) * (1! + K2 / H)): TC0 = TC
CALL FindTA(TC, pH, K(), TA): TA0 = TA
,
LOCATE 10, 1
PRINT USING "TA = #####.# "; TA0 * 10 ^ 6
PRINT USING "TC = #####.# "; TC0 * 10 ^ 6
TA = TA0: TC = TC0
,
END SELECT
,
LOCATE 24, 1: INPUT "ANOTHER? (<cr> = Y) ", A$
IF LEN(A$) = 0 OR A$ = "y" OR A$ = "Y" THEN GOTO Start:
,
END
*****
ErrorHandler:
CLS
LOCATE 3, 1: BEEP: PRINT "ERROR,START AGAIN ": SLEEP 2
GOTO Start:

SUB ChooseWhich (ICASE%)
' THIS PRINTS OUT THE CHOICES AND TAKES AS INPUT THE DESIRED ONE
,
CLS
LOCATE 3, 1
PRINT "CHOOSE ONE OF THE FOLLOWING: "
PRINT
PRINT "    GIVEN          CALCULATE "
PRINT "    -----          -"
PRINT "  1) TA, TC          pH, pCO2 "
PRINT "  2) TA, pH          TC, pCO2 "

```

```

PRINT " 3) TA, pCO2    TC, pH "
PRINT " 4) TC, pH     TA, pCO2 "
PRINT " 5) TC, pCO2    TA, pH "
PRINT " 6) pH, pCO2    TA, TC "
,
MakeChoice:
LOCATE 3, 30: INPUT "", ICASE$
IF LEN(ICASE$) = 0 THEN
    LOCATE 3, 30: PRINT USING "#"; ICASE%
ELSE
    ICASE% = VAL(ICASE$)
END IF
IF ICASE% < 1 OR ICASE% > 6 THEN
    BEEP
    LOCATE 3, 29: PRINT " "
    GOTO MakeChoice:
END IF
END SUB

SUB Constants (TempC, D, K0, K(), NERNST, FugFac)
,
    TempK = TempC + 273.15
,
*****
CalculateDH20:
D0 = .999842594# + 6.793952E-05 * TempC - 9.09529E-06 * TempC ^ 2
D0 = D0 + 1.001685E-07 * TempC ^ 3 - 1.120083E-09 * TempC ^ 4
D0 = D0 + 6.536332E-12 * TempC ^ 5
D = D0
,
*****
CalculateKs:
' NOTE: K0 = Henry's Law Constant

    K0 = EXP(-60.2409 + 93.4517 * (100 / TempK) + 23.3585 * LOG(TempK / 100))
,
    K1 = 10 ^ (-(6320.81 / TempK - 126.3405 + 19.568 * LOG(TempK)))
,
    K2 = 10 ^ (-(5143.69 / TempK - 90.1833 + 14.613 * LOG(TempK)))
,
    KW = 10 ^ ((-4470.99 / TempK + 6.0875 - .01706 * TempK))
,
*****
' The constants below are those used in the "SaltH2O.Bas" program.

```

```

'   LNK0 = -60.2409 + 93.4517 * (100! / TempK) + 23.3585 * LOG(TempK / 100!)
'   K0 = EXP(LNK0)
'
'   LNK1 = -2307.1266# / TempK + 2.83655 - 1.5529413# * LOG(TempK)
'   K1 = EXP(LNK1)
'
'   LNK2 = -3351.6106# / TempK - 9.226508 - .2005743 * LOG(TempK)
'   K2 = EXP(LNK2)
'
'   LNKW = -13847.26 / TempK + 148.96502# - 23.6521 * LOG(TempK)
'   KW = EXP(LNKW)
'
'*****
MakeKMatrix:
'   NOW PUT EQUILIBRIUM CONSTANTS IN K MATRIX
'   K(1) = K1
'   K(2) = K2
'   K(3) = KW
'
'*****
CalculateOtherConstants:
'   R = 8.31441: ' IN N-m/(mol-K)
'   F = 96.485309#: ' IN N-m/(mol-mV)
'   NERNST = R * TempK * LOG(10) / F
'
'*****
CalculateFugacityConstants:
'   pressure = 87.14 * 10 ^ 3: ' IN Pa THIS IS 0.86 ATM (Placid Lake).
'   'PRESSURE = 101.325 * 10 ^ 3: ' IN Pa = N/m^2 THIS IS 1 ATM.
'   '!!!! CONVERT: IF P IN ATM, THEN 1 Atm = 1.01325 * 10^5 N / m^2
'
'   DELTA = (57.7 - .118 * TempK) * 10 ^ (-6): ' IN m^3 / mol
'
'   B = -1636.75 + 12.0408 * TempK - .0327957 * TempK ^ 2
'   B = B + 3.16528 * 10 ^ (-5) * TempK ^ 3
'   B = B * 10 ^ (-6): ' IN m3 / mol
'
'   FOR A MIXTURE OF CO2 AND AIR:
'   EXPONENT = (B + 2! * DELTA) * pressure / (R * TempK)
'   FugFac = EXP(EXPONENT)
'
END SUB

SUB FindfCO2 (TC, pH, K0, K1, K2, fCO2)

```



```

' THIS FINDS THE VALUE OF fCO2 FROM TC AND pH, USING K0, K1, AND K2
'
  H = 10 ^ (-pH)
  HCO3 = TC * K1 * H / (H * H + K1 * H + K1 * K2)
  CO2Star = H * HCO3 / K1
  fCO2 = CO2Star / K0
END SUB

SUB FindH1 (TA, TC, K0, pH)
' THIS FINDS THE pH FROM TA AND TC USING K1 AND K2
' FOR FIRST GUESS, IT IS ASSUMED THAT ALL Alk IS CAlk
' THIS WILL ALWAYS PUT pH HIGH, WHICH IS BETTER FOR CONVERGENCE
' NEWTON'S METHOD IS USED
'
*****
' NOW GET EQUILIBRIUM CONSTANTS FROM K MATRIX
  K1 = K(1)
  K2 = K(2)
  KW = K(3)
'
*****
InitializeH1:
  BB = (1! - TC / TA) * K1
  CC = (1! - 2! * TC / TA) * K1 * K2
  HGUESS = -.5 * BB + .5 * SQR(BB ^ 2 - 4! * CC)
  DELTAH = 10 ^ (-9)
  HSTART = HGUESS + DELTAH
  TOL = 10 ^ (-4): ' THIS IS 10^(-4) / LOG(10) pH UNITS
'
  H = HSTART
  CAlk = TC * K1 * (H + 2! * K2) / (H * H + K1 * H + K1 * K2)
  OH = KW / H
  RESIDUAL = TA - CAlk - OH
'
  H = HGUESS
NEWTON1:
  RESIDUALPLUS = RESIDUAL
  CAlk = TC * K1 * (H + 2! * K2) / (H * H + K1 * H + K1 * K2)
  OH = KW / H
  RESIDUAL = TA - CAlk - OH
'
  SLOPE = (RESIDUALPLUS - RESIDUAL) / DELTAH
  DELTAH = RESIDUAL / SLOPE
  H = H - DELTAH
  IF (ABS(DELTAH) > TOL * H) GOTO NEWTON1

```

```

    pH = LOG(H) / LOG(.1)
END SUB

```

```

SUB FindH2 (TA, fCO2, K0, K1, K2)
'   THIS FINDS THE VALUE OF [H+] FROM TA AND fCO2 USING K0, K1, K2
'   FOR A STARTING GUESS, IT IS ASSUMED THAT ALL Alk IS CAlk
'   THIS WILL ALWAYS PUT pH HIGH, WHICH IS BETTER FOR CONVERGENCE
'   NEWTON'S METHOD IS USED
'
'*****
'   NOW GET EQUILIBRIUM CONSTANTS FROM K MATRIX
    K1 = K(1)
    K2 = K(2)
    KW = K(3)
'
'*****
InitializeH2:
    BB = -K0 * K1 * fCO2 / TA
    CC = -2! * K0 * K1 * K2 * fCO2 / TA
    HGUESS = -.5 * BB + .5 * SQR(BB ^ 2 - 4! * CC)
    DELTAH = 10 ^ (-9)
    HSTART = HGUESS + DELTAH
    TOL = 10 ^ (-4): ' THIS IS 10^(-4) / LOG(10) pH UNITS
'
'*****
    H = HSTART
    HCO3 = K0 * K1 * fCO2 / H
    CO3 = K0 * K1 * K2 * fCO2 / (H * H)
    CAlk = HCO3 + 2! * CO3
    OH = KW / H
    RESIDUAL = TA - CAlk - OH
'
'*****
    H = HGUESS
Newton2:
    RESIDUALPLUS = RESIDUAL
    HCO3 = K0 * K1 * fCO2 / H
    CO3 = K0 * K1 * K2 * fCO2 / (H * H)
    CAlk = HCO3 + 2! * CO3
    OH = KW / H
    RESIDUAL = TA - CAlk - OH
'
    SLOPE = (RESIDUALPLUS - RESIDUAL) / DELTAH
    DELTAH = RESIDUAL / SLOPE
    H = H - DELTAH

```

```

      IF ABS(DELTAH) > TOL * H THEN GOTO Newton2:
    ,
      pH = LOG(H) / LOG(.1)
    END SUB

SUB FindH3 (TC, fCO2, K0, K1, K2, pH)
'   THIS FINDS pH FROM TC AND fCO2, USING K0, K1, AND K2
,
      CO2Star = K0 * fCO2
      K = K1 / K2
      TERM1 = K * K0 * fCO2
      HCO3 = -.5 * TERM1 + SQR(TERM1 * TERM1 - 4! * TERM1 * (K0 * fCO2 -
        TC)) / 2!
      CO3 = TC - CO2Star - HCO3
      H = K1 * CO2Star / HCO3
      pH = LOG(H) / LOG(.1)
    END SUB

SUB FindTA (TC, pH, K(), TA)
'   THIS FINDS TA GIVEN TC AND pH
,
*****
'   NOW GET EQUILIBRIUM CONSTANTS FROM K MATRIX
      K1 = K(1)
      K2 = K(2)
      KW = K(3)
,
*****
      H = 10 ^ (-pH)
      CAIk = TC * K1 * (H + 2! * K2) / (H * H + K1 * H + K1 * K2)
      OH = KW / H
      TA = CAIk + OH
    END SUB

SUB FindTC (TA, pH, K(), TC)
'   THIS FINDS THE TC FROM TA AND pH
,
*****
'   NOW GET EQUILIBRIUM CONSTANTS FROM K MATRIX
      K1 = K(1)
      K2 = K(2)
      KW = K(3)
,

```

```
*****
```

```

H = 10 ^ (-pH)
OH = KW / H
CAIk = TA - OH
,
CO2Star = CAIk * H * H / (K1 * (H + 2! * K2))
HCO3 = CAIk * H / (H + 2! * K2)
CO3 = CAIk * K2 / (H + 2! * K2)
TC = CO2Star + HCO3 + CO3
END SUB

```

```
SUB InputStuff (TempC)
```

```

,
LOCATE 3, 1: INPUT "ENTER TempC: ", TempC$
IF LEN(TempC$) <> 0 THEN TempC = VAL(TempC$)
LOCATE 3, 1: PRINT USING "TempC = ##.## "; TempC
END SUB

```

```
SUB PrintHeader
```

```

CLS
PRINT
PRINT
PRINT "All results and calculations are "
PRINT " 1) in umol/kg-soln and uatm "
PRINT " 2) on the TOTAL pH scale "
PRINT
PRINT : PRINT
PRINT "PLEASE USE CARE IN THE INTERPRETATION OF THE RESULTS
      FROM THIS PROGRAM: "
PRINT "1) If TA and TC are used, the result is not very accurate, "
PRINT " and is very dependent on the choice of the constants. "
PRINT "2) If TA and pCO2 are used, recall that TA was calculated "
PRINT " in the determination of pCO2. "
PRINT "3) If pH and pCO2 are used, the results are not very accurate. "
,
LOCATE 22, 1: PRINT "HIT ANY KEY TO CONTINUE "
WHILE INKEY$ = "": WEND
END SUB

```

Appendix 4

The following is the meteorological station control software written in Tattletale BASIC.

DIM(32,19206)

```
5 REM *****
10 REM ***** WIND SPEED/DIRECTION AND ATM CO2 SENSOR *****
15 REM ***** MATTHEW M. BAEHR *****
20 REM ***** REV. 30 March 1999 *****
25 REM *****
30 REM GOTO 2000 (DATA DUMP), 3000 (SET CLOCK, DATA COUNTER)
34 REM I/O(0) = AIR PUMP POWER
38 REM I/O(1) = LICOR POWER SUPPLY
42 REM I/O(7) = SHUT OFF SAFETY VALVE CONTROL
46 REM I/O(14) = WIND SPEED/DIRECTION CIRCUIT POWER
48 REM I/O(5,9,10,11) USED FOR CLOCK CONTROL
50 REM CHAN(0) = WIND DIRECTION CHAN(1) = LICOR CO2 (mV)
52 REM CHAN(2) = LICOR TEMP CHAN(3) = WIND SPEED
54 REM CHAN(4) = BATTERY INPUT CHAN(7) = TEMPERATURE
56 REM WIND SPEED & DIRECTION ONLY ON 1/2 HR: ALL ON 1 HR CYCLE
58 REM BATTERY VOLTAGE NOT COLLECTED ON THE 1/2 HOUR
60 REM *****
65 ONERR 8000: REM ERROR TRAP FOR CLOCK DATA TRANSFER ERROR
70 ASM &H9A, DW 8 :REM 512K MEMORY EXPANSION
75 FOR C = 0 TO 15: PCLR C: NEXT C: REM SHUT DOWN ALL DEVICES
80 GOSUB 4000: REM GET TIME FROM RTC, RELOAD TATTLETALE
90 GOTO 200: REM START MEASUREMENT
95 REM *****CTRL-C DESTINATION*****
100 FOR C = 0 TO 15: PCLR C: NEXT C: REM SHUT DOWN ALL DEVICES
110 ASM &HBB, DB &H0A: C = CHAN(0): REM SHUT OFF A/D CONVERTER
120 STOP
125 REM *****
200 REM ***** START OF MEASUREMENT SEQUENCE *****
*****
215 FOR C = 0 TO 15: PCLR C: NEXT C
320 ONERR 9000: REM ERROR TRAP FOR MEMORY OVER FLOW
325 ASM &HBB,DB &H0E: REM SET A/D CONVERTER POWER TO STAY ON
330 C = CHAN(0): REM ENABLE A/D CONVERTER
335 GOSUB 1000: REM GOTO MEASUREMENT SEQUENCE
```

```

340 GOSUB 5000: REM SET NEXT WAKE TIME
350 DONE
360 REM *****
1000     REM             *****             MEASUREMENT             SEQUENCE
*****
1002 PSET14: REM *POWER THE WIND SPEED/DIRECTION CIRCUIT*
1004 RTIME: REM *GET TIME*
1006 PRINT #02, "CURRENT TIME = ",?(2),":",?(1),":",?(0);
1008 PRINT #02, " ON ",?(4),"/",?(3),"/",?(5)
1010 FOR C= 1 TO 20: REM WAIT 20 SECONDS BEFORE DATA ACQS
1012 SLEEP 0: SLEEP 100
1014 NEXT C
1015 B = 0: D = 0
1016 FOR R = 1 TO 100
1018 SLEEP 0: SLEEP 10: REM 0.1 SEC DELAY BETWEEN DATA ACQS
1020 B = B + CHAN(3): D = D + CHAN(0)
1022 NEXT R
1024 B = B/100: D = D/100
1025 PRINT #5, "WIND SPEED = ",B," WIND DIRECTION = ",D
1026 STORE X,#2,?(2),?(1),?(0): REM *STORE TIME AND INTEGER VALUES*
1028 STORE X,#2,?(4),?(3),?(5)
1030 STORE X,#2,B,D
1035 PCLR14: REM *TURN OFF POWER TO WIND CIRCUIT*
1036 IF ?(1) = 30 GOTO 1220: REM *IF ON 1/2 HR THEN SKIP LICOR*
1040 PSET7: REM *OPEN SAFETY VALVE TO ALLOW PUMPING OF AIR*
1045 PSET0:PSET1: REM *TURN ON LICOR & AIR PUMP*
1050 REM **** WAIT FOR 2 MINUTES ****
1060 FOR C = 1 TO 120: REM 2 MINUTE WARM-UP
1070 SLEEP 0: SLEEP 100
1080 NEXT C
1220 T= CHAN(7): REM *GET TEMPERATURE*
1222 IF ?(1) = 30 GOTO 1245
1225 A = 0: REM *GET BATTERY VOLTAGE*
1230 FOR R = 1 TO 10
1233 A = A + CHAN(4)
1235 NEXT R
1240 A = A/10: GOTO 1250
1245 A = 2222: REM *MARKER TO SHOW BATTERY INPUT SKIPPED*
1250 PRINT #04, "TEMPERATURE = ",TEMP(T);
1252 PRINT #5, " BATTERY INPUT = ",A
1255 STORE X,#2,T,A
1256 IF ?(1) = 30 GOTO 1395: REM *IF ON 1/2 HR THEN SKIP LICOR*
1260 REM **** LICOR SIGNAL AVERAGES ****
1270 F = 0: G = 0: H = 0: I = 0
1280 Q = 12: REM *NUMBER OF PTS TO AVERAGE*
1285 FOR R = 1 TO Q

```

```

1290 U = 0: V = 0
1300 FOR C = 1 TO 65
1310 F = CHAN(1): G = CHAN(2)
1320 U = U + F: V = V + G
1330 SLEEP 0: SLEEP 3: REM *DELAY BETWEEN DATA ACQS*
1340 NEXT C
1350 U = U/65: V = V/65
1355 H = U + H: I = V + I
1360 NEXT R
1370 H = H/Q: I = I/Q: REM *CALC AVERAGE FOR 12 SIGNALS*
1380 PRINT #5, "AVE. LICOR mV = ",H," AVE. LICOR TEMP = ",I
1385 PRINT " "
1387 PRINT " "
1390 STORE X,#2,H,I: GOTO 1400
1395 PRINT " "
1396 PRINT " "
1397 H = 22222: I = 22222: REM *MARKER TO SHOW LICOR MEASUREMENT
SKIPPED*
1398 STORE X,#2,H,I
1400 REM **** SHUT OFF ALL SYSTEMS ****
1425 FOR C = 0 TO 15: PCLR C: NEXT C
1430 ASM &HBB,DB &H0A: REM DISABLE A/D POWER
1435 C = CHAN(0): REM SHUT DOWN A/D CONVERTER
1440 RETURN
1450 REM *****
2000 REM ***** READ DATA FILE *****
2005 FOR J = 1 TO (X/24)
2008 IF J = 1 X = 0
2010 PRINT #02,"SENSOR OUTPUTS @ ",GET(X,#2),":",GET(X,#2),":",GET(X,#2);
2015 PRINT #02," ",GET(X,#2),"/",GET(X,#2),"/",GET(X,#2)
2020 B = GET(X,#2): D = GET(X,#2)
2022 PRINT #05, "WIND SPEED = ",B," WIND DIRECTION = ",D
2024 Y = GET(X,#2): A = GET(X,#2)
2026 PRINT #04, "TEMPERATURE = ",TEMP(Y);
2030 PRINT #5, " BATTERY INPUT = ",A
2040 H = GET(X,#2): I = GET(X,#2)
2042 PRINT #5, "AVE. LICOR mV = ",H," AVE. LICOR TEMP = ",I
2045 PRINT " "
2050 PRINT " "
2055 SLEEP 0:SLEEP 10
2060 NEXT J
2065 STOP
2070 REM *****
3000 REM ***** SET TATTLETALES TIME AND DATE *****
3005 REM
3010 INPUT 'ENTER THE YEAR (0 - 99) '(5)

```

```

3015 INPUT 'ENTER THE MONTH      (1 - 12) '(4)
3020 INPUT 'ENTER THE DAY OF THE MONTH (1 - 31) '(3)
3025 INPUT 'ENTER THE DAY OF THE WEEK (1-7) 'Z
3030 INPUT 'ENTER THE HOUR OF THE DAY (0 - 23) '(2)
3035 INPUT 'ENTER THE MINUTE      (0 - 59) '(1)
3040 INPUT 'ENTER THE SECOND      (0 - 59) '(0)
3045 STIME
3050 REM  TRANSFER TIME AND DATE TO RTC
3055 RTIME
3060 PSET 10
3065 SDO &HB1,8: SDO &HB5,8: SDO &H00,8: REM CCR & ICR SETUP
3070 PCLR 10
3075 GOSUB 6000: REM CONVERT BINARY TIME TO BCD
3080 PSET 10: SDO &HA0,8: SDO ?(0),8: PCLR 10
3085 PSET 10: SDO &HA1,8: SDO ?(1),8: PCLR 10
3090 PSET 10: SDO &HA2,8: SDO ?(2),8: PCLR 10
3095 PSET 10: SDO &HA3,8: SDO Z,8: PCLR 10
3100 PSET 10: SDO &HA4,8: SDO ?(3),8: PCLR 10
3105 PSET 10: SDO &HA5,8: SDO ?(4),8: PCLR 10
3110 PSET 10: SDO &HA6,8: SDO ?(5),8: PCLR 10
3115 X = 0: REM ZERO MEMORY POINTER
3130 GOTO 5
3135 REM *****
4000 REM ***** READ RTC & RELOAD TATTLETALE CLOCK *****
4005 PSET 10: SDO &H20,8: ?(0) = SDI(9): PCLR 10
4010 PSET 10: SDO &H21,8: ?(1) = SDI(9): PCLR 10
4015 PSET 10: SDO &H22,8: ?(2) = SDI(9): PCLR 10
4020 PSET 10: SDO &H23,8: Z = SDI(9): PCLR 10
4025 PSET 10: SDO &H24,8: ?(3) = SDI(9): PCLR 10
4030 PSET 10: SDO &H25,8: ?(4) = SDI(9): PCLR 10
4035 PSET 10: SDO &H26,8: ?(5) = SDI(9): PCLR 10
4040 GOSUB 7000: REM BCD TO BINARY CONVERSION ROUTINE
4045 RETURN
4050 REM *****
5000 REM ***** SET WAKE TIME FOR SYSTEM *****
5005 RTIME
5010 REM *COMMENT OUT 5012 AND 5015 TO RUN ON THE HOUR*
5012 IF ?(1) <= 20  ?(1) = 30: GOTO 5045: REM *SET TO GO ON THE HALF
HOUR*
5015 IF ?(1) >= 50  ?(1) = 30: ?(2) = ?(2) + 1: GOTO 5045
5020 ?(1) = 00: ?(2) = ?(2) + 1: REM *SET TO GO ON THE HOUR*
5045 IF ?(1) > 59 ?(1) = ?(1) - 60: ?(2) = ?(2) + 1
5050 IF ?(2) > 23 ?(2) = ?(2) - 24
5055 ?(0) = 0
5065 GOSUB 6010
5070 PSET 10

```



```

5075 SDO &HA8,8: SDO ?(0),8: SDO ?(1),8: SDO ?(2),8
5080 PCLR 10
5085 PSET 10
5090 SDO &HB2,8: SDO &H10,8
5095 PCLR 10
5100 RETURN
6000 REM ***** CONVERT BINARY TIME TO BCD *****
6005 RTIME
6010 FOR C = 0 TO 5
6015 @(C) = ?(C)/10: @(6) = ?(C)%10
6020 ?(C) = (@(C)*16) + @(6)
6025 NEXT C
6030 RETURN
7000 REM ***** CONVERT BCD TIME TO BINARY *****
7005 FOR C = 0 TO 5
7010 @(C) = ?(C)/16: @(6) = ?(C)%16
7015 ?(C) = (@(C)*10) + @(6)
7020 NEXT C
7025 STIME
7030 RETURN
8000 REM ***** ERROR TRAP FOR CLOCK *****
8010 ?(5) = 94
8015 ?(4) = 1
8020 ?(3) = 1
8025 ?(2) = 0
8030 ?(1) = 0
8035 ?(0) = 0
8040 Z = 7
8045 GOTO 3045 :REM CLOCK HAS BEEN RESET TO 1/1/99
9000 REM ***** ERROR TRAP FOR MEMORY OVERFLOW *****
9005 IF X < 544402 GOTO 1000
9010 PSET 10
9015 SDO &HB2,8: SDO &H00,8: REM ICR MODIFIED, ALARM DISABLED
9020 PCLR 10
9025 FOR C = 0 TO 15: PCLR C: NEXT C
9030 DONE :REM COMPLETE SYSTEM SHUTDOWN

```

References

- Agbeti, M.D. and J.P. Smol. 1995. Winter limnology: a comparison of physical, chemical and biological characteristics in two temperate lakes during ice cover. *Hydrobiologia* 304: 221-234.
- APHA (American Public Health Association). 1992. *Standard Methods for the Examination of Water and Wastewater*, 18th ed., Washington, DC.
- Babin, J. and E.E. Prepas. 1985. Modelling winter oxygen depletion rates in ice-covered temperate zone lakes in Canada. *Can. J. Fish. Aquat. Sci.* 42: 239-249.
- Baird, D.J., T.E. Gates, and R.W. Davies. 1987. Oxygen conditions in two prairie pothole lakes during winter ice cover. *Can. J. Fish. Aquat. Sci.* 44: 1092-1095.
- Bari, S.A. and J. Hallett. 1974. Nucleation and growth of bubbles at an ice-water interface. *J. Glaciol.* 13: 489-520.
- Barica, J. 1984. Empirical models for prediction of algal blooms and collapses, winter oxygen depletion and a freeze-out effect in lakes: Summary and verification. *Verh. Internat. Verein. Limnol.* 22: 309-319.
- Bengtsson, L. 1996. Mixing in ice-covered lakes. *Hydrobiologia* 322: 91-97.
- Bleiker, W. and F. Schanz. 1997. Light climate as the key factor controlling the spring dynamics of phytoplankton in Lake Zurich. *Aquat. Sci.* 59: 135-157.
- Bolsenga, S.J. and H.A. Vanderploeg. 1992. Estimating photosynthetically available radiation into open and ice-covered freshwater lakes from surface characteristics; a high transmittance case study. *Hydrobiologia* 243/244: 95-104.
- Bower, P. and D. McCorkle. 1980. Gas exchange, photosynthetic uptake, and carbon budget for a radiocarbon addition to a small enclosure in a stratified lake. *Can. J. Fish. Aquat. Sci.* 37: 464-471.
- Brezinski, D.P. 1983. Kinetic, static and stirring errors of liquid junction reference electrodes. *Analyst* 108: 425-442.
- Broecker, W.S. and T. H. Peng. 1974. Gas exchange rates between air and sea. *Tellus* 26: 21-35.
- Broecker, W.S., T.H. Peng, G. Mathieu, R. Hesslein, and T. Torgersen. 1980. Gas exchange rate measurements in natural systems. *Radiocarbon* 22: 676-683.

- Byrne, R.H. and J.A. Breland. 1989. High precision multiwavelength pH determinations in seawater using cresol red. *Deep-Sea Res.* 36: 803-810.
- Cai, W., L.R. Pomeroy, M.A. Moran, and Y. Wang. 1999. Oxygen and carbon dioxide mass balance for the estuarine-intertidal marsh complex of five rivers in the southeastern U.S. *Limnol. Oceanogr.* 44: 639-649.
- Carignan, R. 1998. Automated determination of carbon dioxide, oxygen, and nitrogen partial pressures in surface waters. *Limnol. Oceanogr.* 43: 969-975.
- Carignan, R., D. Planas, and C. Vis. 2000. Planktonic production and respiration in oligotrophic Shield lakes. *Limnol. Oceanogr.* 45: 189-199.
- Chapra, S.C. and R.P. Canale. 1991. Long-term phenomenological model of phosphorus and oxygen for stratified lakes. *Wat. Res.* 25: 707-715.
- Chen, C.A. and F.J. Millero. 1986. Precise thermodynamic properties for natural waters covering only the limnological range. *Limnol. Oceanogr.* 31: 657-662.
- Cole, J.J., N.F. Caraco, G.W. Kling, and T.K. Kratz. 1994. Carbon dioxide supersaturation in the surface waters of lakes. *Science* 265: 1568-1570.
- Cole, J.J. and N.F. Caraco. 1998. Atmospheric exchange of carbon dioxide in a low-wind oligotrophic lake measured by the addition of SF₆. *Limnol. Oceanogr.* 43: 647-656.
- Covington, A.K., P.D. Whalley, and W. Davison. 1983. Procedures for the measurement of pH in low ionic strength solutions including freshwater. *Analyst* 108: 1528-1532.
- Coyne, P.I. and J.J. Kelley. 1974. Carbon dioxide partial pressures in arctic surface waters. *Limnol. Oceanogr.* 19: 928-938.
- Craig, H., R.A. Wharton, and C.P. McKay. 1992. Oxygen supersaturation in ice-covered Antarctic lakes: Biological versus physical contributions. *Science* 255: 318-321.
- Darbyshire, J. and A. Edwards. 1972. Seasonal formation and movement of the thermocline in lakes. *Pure and Appl. Geophys.* 93: 141-150.
- DeGrandpre, M.D., T.R. Hammar, S.P. Smith, and F.L. Sayles. 1995. In situ measurements of seawater pCO₂. *Limnol. Oceanogr.* 40: 969-975.
- DeGrandpre, M.D., T.R. Hammar, D.W.R. Wallace, and C.D. Wirick. 1997. Simultaneous mooring-based measurements of seawater CO₂ and O₂ off Cape Hatteras, North Carolina. *Limnol. Oceanogr.* 42: 21-28.
- DeGrandpre, M.D., T.R. Hammar, and C.D. Wirick. 1998. Short-term pCO₂ and O₂ dynamics in California coastal waters. *Deep-Sea Res. II* 45: 1557-1575.

- DeGrandpre, M.D., M.M. Baehr, and T.R. Hammar. 1999. Calibration-free optical chemical sensors. *Anal. Chem.* 71: 1152-1159.
- del Giorgio, P.A. and R.H. Peters. 1993. Balance between phytoplankton production and plankton respiration in lakes. *Can. J. Fish. Aquat. Sci.* 50: 282-289.
- Dickson, A.G. and J.P. Riley. 1978. The effect of analytical error on the evaluation of the components of the aquatic carbon-dioxide system. *Mar. Chem.* 6: 77-85.
- Edmond, J.M. 1970. High precision determination of titration alkalinity and total carbon dioxide content of sea water by potentiometric titration. *Deep-Sea Res.* 17: 737-750.
- Effler, S.W. and M.G. Perkins. 1987. Failure of spring turnover in Onondaga lake, NY, U.S.A. *Water, Air, and Soil Pollut.* 34: 285-291.
- Emerson, S. 1975. Gas exchange rates in small Canadian Shield lakes. *Limnol. Oceanogr.* 20: 754-761.
- Farmer, D.M. 1975. Penetrative convection in the absence of mean shear. *Quart. J. R. Met. Soc.* 101: 869-891.
- Fee, E.J., J.A. Shearer, E.R. DeBruyn, and D.W. Schindler. 1992. Effects of lake size on phytoplankton photosynthesis. *Can. J. Fish. Aquat. Sci.* 49: 2445-2459.
- Fogg, G.E. 1980. Phytoplankton primary production. In: Barnes, R.S.K. and K.H. Mann (Editors), *Fundamentals of Aquatic Ecosystems*. Blackwell Scientific Publications, Oxford, pp. 24-45.
- French, C.R., M.D. DeGrandpre, J.J. Carr, E. Dougherty, L.A.K. Eidson, and J. Reynolds. 2000. Spectrophotometric pH measurements of freshwater. Submitted to *Anal. Chim. Acta*.
- Geider, R.J. 1992. Respiration: Taxation without representation? In Falkowski, P.G. and A.D. Woodhead (eds.), *Primary Productivity and Biogeochemical Cycles in the Sea*, Plenum Press, New York, pp. 333-360.
- Ginot, V. and J.C. Hervé. 1994. Estimating the parameters of dissolved oxygen dynamics in shallow ponds. *Ecol. Model.* 73: 169-187.
- Gnanadesikan, A. 1996. Modeling the diurnal cycle of carbon monoxide: Sensitivity to physics, chemistry, biology, and optics. *J. Geophys. Res.* 101: 12,177-12,191.
- Granéli, W., M. Lindell, and L. Tranvik. 1996. Photo-oxidative production of dissolved inorganic carbon in lakes of different humic content. *Limnol. Oceanogr.* 41: 698-706.

- Green, S.A. and N.V. Blough. 1994. Optical absorption and fluorescence properties of chromophoric dissolved organic matter in natural waters. *Limnol. Oceanogr.* 39: 1903-1916.
- Hamilton, D.P. and S.G. Schladow. 1997. Prediction of water quality in lakes and reservoirs. Part I – Model description. *Ecol. Modelling* 96: 91-110.
- Hanna, M. 1990. Evaluation of models predicting mixing depth. *Can. J. Fish. Aquat. Sci.* 47: 940-947.
- Henderson-Sellers, B. 1984. A new formula for latent heat of vaporization of water as a function of temperature. *Quart. J. R. Met. Soc.* 110: 1186-1190.
- Henderson-Sellers, B. 1986. Calculating the surface energy balance for lake and reservoir modeling: A review. *Rev. Geophys.* 24: 625-649.
- Henderson-Sellers, B. and A.M. Davies. 1989. Thermal stratification modeling for oceans and lakes. In: Tien, C.L. and T.C. Chawla (Editors), *Annual Review of Numerical Fluid Mechanics and Heat Transfer, Vol. II*, Hemisphere, New York, pp. 86-156.
- Herczeg, A.L. and R.H. Hesslein. 1984. Determination of hydrogen ion concentration in softwater lakes using carbon dioxide equilibria. *Geochim. Cosmochim. Acta* 48: 837-845.
- Hesslein, R.H., W.S. Broecker, P.D. Quay, and D.W. Schindler. 1980. Whole-lake radiocarbon experiment in an oligotrophic lake at the Experimental Lakes Area, Northwestern Ontario. *Can. J. Fish. Aquat. Sci.* 37: 454-463.
- Hesslein, R.H., J.W.M. Rudd, C. Kelly, P. Ramlal, and K.A. Hallard. 1991. Carbon dioxide pressure in surface waters of Canadian lakes, p. 413-431. In: Wilhelms, S.C. and J.S. Gulliver (Editors), *Air-water mass transfer*. Am. Soc. Civ. Eng.
- Hostetler, S.W. and P.J. Bartlein. 1990. Simulation of lake evaporation with application to modeling lake level variations of Harney-Malheur Lake, Oregon. *Water Resour. Res.* 26: 2603-2612.
- Hostetler, S.W. 1995. Hydrological and thermal response of lakes to climate: Description and modeling. In: Lerman, A., D.M. Imboden, and J.R. Gat (Editors), *Physics and Chemistry of Lakes*, 2nd ed. Springer-Verlag, New York, pp. 63-82.
- Ivey, G.N. and J.C. Patterson. 1984. A model of the vertical mixing in Lake Erie in summer. *Limnol. Oceanogr.* 29: 553-563.
- Jacobson, R.L. and D. Langmuir. 1974. Dissociation constants of calcite and CaHCO_3^+ from 0 to 50 °C. *Geochim. Cosmochim. Acta* 38: 301-318.

Jähne, B., K.O. Münnich, R. Bösinger, A. Dutzi, W. Huber, and P. Libner. 1987. On the parameters influencing air-water gas exchange. *J. Geophys. Res.* 92: 1937-1949.

Jensen, M.E., R.D. Burman, and R.G. Allen (Editors). 1990. *Evapotranspiration and Irrigation Water Requirements*, ASCE Manuals and Reports on Engineering Practice No. 70, New York.

Jewell, P.W. 1995. A simple surface water biogeochemical model. 1. Description, sensitivity analyses, and idealized simulations. *Water Resour. Res.* 31: 2047-2057.

Juday, R.E. and E.J. Keller. 1980. A water quality study of Placid Lake and its drainages. MWRRC Report No. 110. Montana State University, Bozeman, Montana.

Juday, R.E. and E.J. Keller. 1984. The effect of ash fallout on water quality in western Montana. The University of Montana, Missoula, Montana.

Karagounis, I., J. Trosch, and F. Zamboni. 1993. A coupled physical-biochemical lake model for forecasting water quality. *Aquat. Sci.* 55: 87-102.

Kelly, M.G., N. Thyssen, and B. Moeslund. 1983. Light and the annual variation of oxygen- and carbon based measurement of productivity in a macrophyte-dominated river. *Limnol. Oceanogr.* 28: 503-515.

Kemp, P.F., P.G. Falkowski, C.N. Flagg, W.C. Phoel, S.L. Smith, D.W.R. Wallace, and C.D. Wirick. 1994. Modeling vertical oxygen and carbon flux during stratified spring and summer conditions on the continental shelf, Middle Atlantic Bight, eastern U.S.A. *Deep-Sea Res. II* 41: 629-655.

Kiefer, D.A. and R.A. Reynolds. 1992. Advances in understanding phytoplankton fluorescence and photosynthesis. In: Falkowski, P.G. and A.D. Woodhead (Editors), *Primary Productivity and Biogeochemical Cycles in the Sea*, Plenum Press, New York, pp. 155-174.

Kirk, J.T.O. 1994. *Light and Photosynthesis in Aquatic Ecosystems*, 2nd ed. Cambridge University Press, New York, 509 pp.

Kling, G.W., A.E. Giblin, B. Fry, and B.J. Peterson. 1991. The role of seasonal turnover in lake alkalinity dynamics. *Limnol. Oceanogr.* 36: 106-122.

Kling, G.W., G.W. Kipphut, and M.C. Miller. 1992. The flux of CO₂ and CH₄ from lakes and rivers in arctic Alaska. *Hydrobiologia* 240: 23-36.

Kraines, S., Y. Suzuki, K. Yamada, and H. Komiyama. 1996. Separating biological and physical changes in dissolved oxygen concentration in a coral reef. *Limnol. Oceanogr.* 41: 1790-1799.

Kratz, T.K., R.B. Cook, C.J. Bowser, and P.L. Brezonik. 1987. Winter and spring pH depressions in northern Wisconsin lakes caused by increases in pCO₂. *Can. J. Fish. Aquat. Sci.* 44: 1082-1088.

Large, W.G. and S. Pond. 1981. Open ocean momentum flux measurements in moderate to strong winds. *J. Phys. Oceanogr.* 11: 324-336.

Leenheer, J.A. 1994. Chemistry of dissolved organic matter in rivers, lakes, and reservoirs. In: Baker, L.A. (Editor), *Environmental Chemistry of Lakes and Reservoirs, Advances in Chemistry Series 237*, American Chemical Society, pp. 195-221.

Lehman, J.T. and D.K. Branstrator. 1994. Nutrient dynamics and turnover rates of phosphate and sulfate in Lake Victoria, East Africa. *Limnol. Oceanogr.* 39: 227-233.

Lemmin, U. 1987. The structure and dynamics of internal waves in Baldeggersee. *Limnol. Oceanogr.* 32: 43-61.

Lewis, E. and D.W.R. Wallace. 1998. Program developed for CO₂ system calculations. ORNL/CDIAC-105. Carbon Dioxide Information Analysis Center, Oak Ridge National Laboratory, U.S. Department of Energy, Oak Ridge, Tennessee.

Livingstone, D.M. 1993. Lake oxygenation: Application of a one-box model with ice cover. *Int. Revue ges. Hydrobiol.* 78: 465-480.

Maberly, S.C. 1996. Diel, episodic, and seasonal changes in pH and concentrations of inorganic carbon in a productive lake. *Freshwater Biology* 35: 579-598.

Malm, J., L. Bengtsson, A. Terzhevik, P. Boyarinov, A. Glinsky, N. Palshin, and M. Petrov. 1998. Field study on currents in a shallow, ice-covered lake. *Limnol. Oceanogr.* 43: 1669-1679.

Marra, J. 1997. Analysis of diel variability in chlorophyll fluorescence. *J. Mar. Res.* 55: 767-784.

Mathias, J.A. and J. Barica. 1980. Factors controlling oxygen depletion in ice-covered lakes. *Can. J. Fish. Aquat. Sci.* 37: 185-194.

Matthews, P.C. and S.I. Heaney. 1987. Solar heating and its influence on mixing in ice-covered lakes. *Freshwat. Biol.* 18: 135-149.

McConnaughey, T.A., J.W. LaBaugh, D.O. Rosenberry, R.G. Striegl, M.M. Reddy, P.F. Schuster, and V. Carter. 1994. Carbon budget for a groundwater-fed lake: Calcification supports summer photosynthesis. *Limnol. Oceanogr.* 39: 1319-1332.

McNeil, C.L. and D.M. Farmer. 1995. Observations of the influence of diurnal convection on upper ocean dissolved gas measurements. *J. Mar. Res.* 53: 151-169.

- Millero, F.J. 1979. The thermodynamics of the carbonate system in seawater. *Geochim. Cosmochim. Acta* 43: 1651-1661.
- Naumoski, T. and J.T. Lehman. 1984. Nitrogen loading: Influence on dissolved inorganic carbon in natural waters. *Verh. Internat. Verein. Limnol.* 22: 244-249.
- Nebaeus, M. 1984. Algal water-blooms under ice-cover. *Verh. Internat. Verein. Limnol.* 22: 719-724.
- Oudot, C. 1989. O₂ and CO₂ balances approach for estimating biological production in the mixed layer of the tropical Atlantic Ocean (Guinea Dome area). *J. Mar. Res.* 47: 385-409.
- Parkhill, K.L. and J.S. Gulliver. 1999. Modeling the effect of light on whole-stream respiration. *Ecol. Modelling* 117: 333-342.
- Platt, T., C.L. Gallegos, and W.G. Harrison. 1980. Photoinhibition of photosynthesis in natural assemblages of marine phytoplankton. *J. Mar. Res.* 38: 687-701.
- Platt, T., W.G. Harrison, M.R. Lewis, W.K.W. Li, S. Sathyendranath, R.E. Smith, and A.F. Vezina. 1989. Biological production of the oceans: the case for a consensus. *Mar. Ecol. Prog. Ser.* 52: 77-88.
- Portielje, R., K. Kersting, and L. Lijklema. 1996. Primary production estimates from continuous oxygen measurements in relation to external nutrient input. *Wat. Res.* 30: 625-643.
- Prézelin, B.B., M.M. Tilzer, O. Schofield, and C. Haese. 1991. The control of the production process of phytoplankton by the physical structure of the aquatic environment with special reference to its optical properties. *Aquat. Sci.* 53: 136-186.
- Price, J.F., C.N.K. Mooers, and J.C. Van Leer. 1978. Observation and simulation of storm-induced mixed-layer deepening. *J. Phys. Oceanogr.* 8: 582-599.
- Price, J.F., R.A. Weller, and R. Pinkel. 1986. Diurnal cycling: observations and models of the upper ocean response to diurnal heating, cooling, and wind mixing. *J. Geophys. Res.* 91: 8411-8427.
- Quay, P.D., W.S. Broecker, R.H. Hesslein, and D.W. Schindler. 1980. Vertical diffusion rates determined by tritium tracer experiments in the thermocline and hypolimnion of two lakes. *Limnol. Oceanogr.* 25: 201-218.
- Raymond, P.A., N.F. Caraco, and J.J. Cole. 1997. Carbon dioxide concentration and atmospheric flux in the Hudson River. *Estuaries* 20: 381-390.

Riley, M.J. and H.G. Stefan. 1988. MINLAKE: A dynamic lake water quality simulation model. *Ecol. Modelling* 43: 155-182.

Sellers, P., R.H. Hesslein, and C.A. Kelly. 1995. Continuous measurement of CO₂ for estimation of air-water fluxes in lakes: an in situ technique. *Limnol. Oceanogr.* 40: 575-581.

Sill, B.L. 1983. Free and forced convection effects on evaporation. *J. Hydraul. Eng., ASCE*, 109: 1216-1231.

Stanford, J.A. 2000. Director and Bierman Professor of Ecology - Ecosystem Science, The University of Montana Flathead Lake Biological Station.

Stefan, H.G. and X. Fang. 1994. Dissolved oxygen model for regional lake analysis. *Ecol. Modelling* 71: 37-68.

Stefan, H.G., X. Fang, D. Wright, J.G. Eaton, and J.H. McCormick. 1995. Simulation of dissolved oxygen profiles in a transparent, dimictic lake. *Limnol. Oceanogr.* 40: 105-118.

Stigebrandt, A. 1978. Dynamics of an ice covered lake with through-flow. *Nordic Hydrol.* 9: 219-244.

Streebin, L.E., J.M. Robertson, S.M. Allen, W.B. Heller, and J. Westhoff. 1973. Water quality study of the Clearwater River and selected tributaries. Lolo National Forest, USDA Forest Service, Missoula, MT.

Striegl, R.G. and C.M. Michmerhuizen. 1998. Hydrologic influence on methane and carbon dioxide dynamics at two north-central Minnesota lakes. *Limnol. Oceanogr.* 43: 1519-1529.

Stull R.B. 1988. *An Introduction to Boundary Layer Meteorology*, Kluwer Academic Publishers, Dordrecht, The Netherlands, 666 pp.

Stumm, W. and J.J. Morgan. 1996. *Aquatic Chemistry: Chemical Equilibria and Rates in Natural Waters*, 3rd ed. Wiley-Interscience, New York, 1022 pp.

Talling, J.F. 1971. The underwater light climate as a controlling factor in the production ecology of freshwater phytoplankton. *Mitt. Int. Verein. Limnol.* 19: 214-243.

Vadeboncoeur, Y.M. 1988. Longitudinal dynamics of seston concentration and composition in a western Montana lake outlet. Masters Thesis, The University of Montana, Missoula, Montana.

Van Duin, E.H.S. and L. Lijklema. 1989. Modelling photosynthesis and oxygen in a shallow, hypertrophic lake. *Ecol. Model.* 45: 243-260.

- van Senden, D.C., R. Portielje, A. Borer, H. Ambuhl, and D.M. Imboden. 1990. Vertical exchange due to horizontal density gradients in lakes; the case of Lake Lucerne. *Aquat. Sci.* 52: 381-398.
- Wallace, D.W.R. and C.D. Wirick. 1992. Large air-sea gas fluxes associated with breaking waves. *Nature* 356: 694-696.
- Wanninkhof, R., J. Ledwell, and J. Crusius. 1991. Gas transfer velocities on lakes measured with sulfur hexafluoride. In: Wilhelms, S.C. and J.S. Gulliver (Editors), *Air-Water Mass Transfer*. Am. Soc. Civ. Eng., New York, pp. 441-455.
- Wanninkhof, R. 1992. Relationship between wind speed and gas exchange over the ocean. *J. Geophys. Res.* 97: 7373-7382.
- Weiss, R.F. 1970. The solubility of nitrogen, oxygen and argon in water and seawater. *Deep-Sea Res.* 17: 721-735.
- Weiss, R.F. 1974. Carbon dioxide in water and seawater: The solubility of a non-ideal gas. *Mar. Chem.* 2: 203-215.
- Welch, H.E. and M.A. Bergmann. 1985. Water circulation in small arctic lakes in winter. *Can. J. Fish. Aquat. Sci.* 42: 506-520.
- Welschmeyer, N.A. 1994. Fluorometric analysis of chlorophyll *a* in the presence of chlorophyll *b* and pheopigments. *Limnol. Oceanogr.* 39: 1985-1992.
- Wetzel, R.G. 1983. *Limnology*, 2nd ed. Saunders College, Orlando, FL, 767 pp.
- Wetzel, R.G. and G.E. Likens. 1991. *Limnological Analyses*, 2nd ed. Springer-Verlag, New York, 391 pp.
- Wharton, R.A. and G.M. Simmons. 1986. Oxygen budget of a perennially ice-covered Antarctic lake. *Limnol. Oceanogr.* 31: 437-443.
- Wright, R.T. 1964. Dynamics of a phytoplankton community in an ice-covered lake. *Limnol. Oceanogr.* 9: 163-178.